RESEARCH ARTICLE

COI1 F-box proteins regulate DELLA protein levels, growth, and photosynthetic efficiency in maize

Leila Feiz[1,*], Christine Shyu[2], Shan Wu[1], Kevin R. Ahern[1,3], Iram Gull[1,7], Ying Rong[6], Caroline J. Artymowicz[1,8], Miguel A. Piñeros[4], Zhangjun Fei[1,4], Thomas P. Brutnell[5], and Georg Jander[1,*]

[1]Boyce Thompson Institute, Ithaca, NY 14853, USA
[2]Bayer Crop Science, Chesterfield, MO 63017, USA
[3]Plant Breeding and Genetics Section, School of Integrative Plant Science, Cornell University, Ithaca, NY 14853, USA
[4]Robert W. Holley Center for Agriculture and Health, USDA-ARS, Ithaca, NY 14853, USA
[5]McClintock LLC, St. Louis, MO 63110, USA
[6]KWS Gateway Research Center, St. Louis, MO 63132, USA
[7]Present address: School of Biochemistry and Biotechnology, University of the Punjab, Lahore, Pakistan
[8]Present address: Rowan University, Glassboro, NJ 08028, USA

Short title: F-box protein regulation of growth in maize

One-sentence summary: Hormonal regulation of maize stalk height is influenced by four members of a gene family that has similarity to genes previously associated with insect defense induction in numerous other plant species.

* Corresponding authors: Leila Feiz (lf259@cornell.edu), Georg Jander (gj32@cornell.edu)

The authors responsible for distribution of materials integral to the findings presented in this article in accordance with the policy described in the Instructions for Authors (https://academic.oup.com/plcell/pages/General-Instructions) are: Leila Feiz (lf259@cornell.edu) and Georg Jander (gj32@cornell.edu).

Abstract
The F-box protein Coronatine Insensitive (COI) is a receptor for the jasmonic acid signaling pathway in plants. To investigate the functions of the six maize (*Zea mays*) COI proteins (COI1a, COI1b, COI1c, COI1d, COI2a, and COI2b), we generated single, double, and quadruple loss-of-function mutants. The pollen of the *coi2a coi2b* double mutant was inviable. The *coi1* quadruple mutant (*coi1-4x*) exhibited shorter internodes, decreased photosynthesis, leaf discoloration, microelement deficiencies, and accumulation of DWARF8 and/or DWARF9, two DELLA family proteins that repress the gibberellic acid signaling pathway. Co-expression of COI and DELLA in *Nicotiana benthamiana* showed that the COI proteins trigger proteasome-dependent DELLA degradation. Many genes that are downregulated in the *coi1-4x* mutant are gibberellic acid-inducible. In addition, most of the proteins encoded by the downregulated genes are predicted to be bundle sheath- or mesophyll-enriched, including those encoding C_4-specific photosynthetic enzymes. Heterologous expression of maize *Coi* genes in *N. benthamiana* showed that COI2a is nucleus-localized and interacts with maize jasmonate ZIM (zinc-finger inflorescence meristem) domain (JAZ) proteins, the canonical COI repressor partners. However, maize COI1a and COI1c showed only partial nuclear localization and reduced binding efficiency to the tested JAZ proteins. Together, these results show the divergent functions of the six COI proteins in regulating maize growth and defense pathways.

Introduction

Jasmonic acid (JA) is a lipid-derived plant hormone that regulates a wide range of biological processes, including reproductive development, vegetative growth, and responses to biotic and abiotic stresses (Feys et al. 1994; McConn et al. 1997; Vijayan et al. 1998; Stintzi and Browse 2000; Wang et al. 2020; He et al. 2021; Qi et al. 2022; Shikha et al. 2022). Methyl JA (MeJA) is a volatile compound readily taken up and converted to JA by plants (Chuang et al. 2014). In Arabidopsis (*Arabidopsis thaliana*), tomato (*Solanum lycopersicum*), rice (*Oryza sativa*) and other plants, JA is conjugated to isoleucine to produce JA-isoleucine (JA-Ile). This compound is perceived by a receptor, CORONATINE INSENSITIVE1 (COI1) (Xie et al. 1998; Xu et al. 2002), which is the F-box domain protein component of an E3-ligase complex that polyubiquitinates jasmonate ZIM (zinc-finger inflorescence meristem) domain (JAZ) repressors (Chini et al. 2007; Thines et al. 2007; Sheard et al. 2010). JAZ is a large family of proteins that interact with MYC transcription factors (Zhang et al. 2015; Zander et al. 2020) and thereby prevent the induced expression of a cohort of defense, stress, and development-related genes. Binding of JA-Ile to the COI1 receptor promotes COI1-JAZ protein-protein interactions, which in turn leads to the formation of the E3 ubiquitin ligase SCF^{COI1} complex and the subsequent degradation of the JAZ by the 26S proteasome (Fonseca et al. 2009). The de-repression of MYC transcription factors by JAZ degradation initiates transcription of the targeted genes (Dombrecht et al. 2007).

Experiments with several plant species show that JA-Ile perception and the resulting induced defense responses antagonistically modulate gibberellic acid (GA)-mediated growth (Yang et al. 2012; Campos et al. 2016; Machado et al. 2017). This reciprocal relationship between defense and growth is not due to a carbohydrate-resource trade-off (Campos et al. 2016; Machado et al. 2017) but instead results from the fact that JAZ repressors of the JA-responsive genes bind to and entrap DELLA proteins, repressors of GA-responsive growth genes, thereby preventing their repressive effect on the growth-promoting PIF transcription factors (Hou et al. 2010; Yang et al. 2012). In Arabidopsis, JA-Ile perception by COI1 leads to JAZ degradation, which releases DELLA and inhibits growth while inducing the transcription of defense genes by MYC transcription factors. Interruption of JA signaling in both the Arabidopsis *coi1* and the rice *coi1a coi1b* mutants results in a continuous DELLA entrapment by JAZ and a positive growth response. DELLA also is essential for enhancing JA-mediated responses in Arabidopsis (Wild et

al. 2012; de Vleesschauwer et al. 2016). The constitutively active, dominant DELLA mutant *gibberellic acid insensitive* (*gai*) is hypersensitive to JA-mediated gene induction. A quadruple *della* mutant (which lacks four of the five Arabidopsis DELLA proteins) was partially insensitive to JA perception (Navarro et al. 2008).

More recent research has demonstrated varied COI interactions in species other than Arabidopsis. Interaction between COI and the single JAZ repressor in *Marchantia polymorpha* involves dinor-cis-oxophytodienoic acid and dinor-iso-oxophytodienoic acid instead of JA-Ile (Monte et al. 2018). A phylogenetic analysis indicated that JA-Ile biosynthesis is present in angiosperms, ferns, horsetails, and *Selaginella*, though rapid wound-induced accumulation of JA-Ile was found only in angiosperms (Pratiwi et al. 2017; Chini et al. 2023). Ligand specificity of COI proteins also depends in part on the specific JAZ proteins with which they are interacting (Monte et al. 2022). Whereas Arabidopsis and tomato have only one *COI* gene, multiple copies of *COI* genes in rice (Inagaki et al. 2022) and other monocot species also suggest that the encoded proteins may have acquired different functions in the course of evolution.

Maize (*Zea mays*) is one of the main staple crops and a model monocot. However, both the mechanisms of JA signaling and the functions of individual maize COI receptors remain under-investigated. Gene duplication events led to the evolution of three clades, two *Coi1* and one *Coi2*, in Poaceae (grasses) (Figure 1). Modern maize has six *Coi* genes (*Coi1a*, *Coi1b*, *Coi1c*, *Coi1d*, *Coi2a*, and *Coi2b*; Supplementary Dataset S1), which may be due to an ancestral genome duplication event that occurred between 8.5 and 13 million years ago. Genome duplication was followed by genome reduction of the tetraploid maize to a diploid state, with uneven gene losses and residual duplication of many genes, including the JA synthesizing enzymes (reviewed in (Borrego and Kolomiets 2016)). CRISPR/Cas9-mediated knockouts of *Coi2a* and *Coi2b* showed that these genes are essential for jasmonate signaling and pollen formation in maize (Qi et al. 2022). When transformed into an Arabidopsis *coi1* mutant, maize *Coi1a*, *Coi1b*, and *Coi1c*, but not *Coi2a*, complemented the defects in fertility and induced changes in gene expression after JA treatment (An et al. 2019). Maize COI1a interacts with JAZ15, and *coi1a* mutant plants showed elevated resistance to *Fusarium graminearum* (Gibberella stem rot) (Ma et al. 2021). Yeast two-hybrid assays showed interactions of maize COI1 but not COI2 with several maize JAZ proteins (Qi et al. 2022).

Rice has three *COI* genes and, similar to maize, rice COI2 has essential roles in pollen vitality and male fertility (Inagaki et al., 2022; Trang Nguyen et al., 2022; Wang et al., 2023; Yang et al., 2012). One study showed that rice COI2 is the essential receptor in JA-mediated signaling, whereas COI1a and COI1b play redundant roles with COI2 in plant growth regulation. (Inagaki et al. 2022). In another study, rice COI2, COI1a and COI1b were all essential for JA-mediated defense against *Nilaparvata lugens*, the brown planthopper (Wang et al. 2023). In both of these studies, the rice COI2 protein showed interaction with more members of the rice JAZ family than COI1.

Here, we present a functional analysis of the maize COI proteins using transposon mutagenesis. *Dissociation* (*Ds*) and *Mutator* (*Mu*) transposon insertion mutations in each of the six *COI* genes were isolated and single and higher order mutants characterized through insect bioassays, measurement of morphological changes, quantification of gene expression profiles, subcellular localization, and protein-protein interaction studies. Together, our results show that, whereas the two maize COI2 proteins have a function similar to what has been observed for Arabidopsis COI1, the four maize COI1 proteins function primarily in regulating GA-mediated growth responses. This reveals a molecular model where subfunctionalization of COI gene family members in maize enables growth responses to be uncoupled from plant defense pathways.

Results

COI gene duplication in monocots and maize

There are six paralogous *Coi* genes in maize, which are derived from gene duplication events in the course of monocot evolution (Figure 1, protein sequences in Supplementary Dataset S2, machine-readable tree in Supplementary File S1). These six proteins share 55% to 58% sequence identity with Arabidopsis COI1 (Figure S1A). The two members of each protein pair, COI1a and COI1d, COI1b and COI1c, and COI2a and COI2b, respectively, shared 94%, 93%, and 95% amino acid sequence identity, respectively (Figure S1B). COI1a and COI1d showed about 80% identity with COI1c and COI1b, whereas the four COI1 proteins only share about 60% identical amino acids with the two COI2 proteins. An alignment of COI protein sequences shows that phenylalanine 89 of Arabidopsis COI, which is essential for the insertion of JA-Ile between COI and JAZ (Sheard et al. 2010) is modified to tyrosine in four maize COI1 proteins (red arrow in Figure S2). The other amino acids in the active site of Arabidopsis COI were not different from

their corresponding amino acids in the Poaceae COI proteins (Figure S2, black arrows). Several other amino acids that are not located in the active site differ between Arabidopsis and maize COI proteins. For instance, alanine 63 of Arabidopsis COI is changed to valine in C_4 plant COI1 proteins and *M. polymorpha*, and to tyrosine in maize COI2 proteins (Figure S2, green arrow). However, based on the amino acid sequence alone, we cannot predict the function of each individual COI protein in the Poaceae.

COI sub-cellular localization and interactions with JAZ proteins

To investigate the subcellular locations of maize COI proteins, one gene of each closely related pair (*Coi1a*, *Coi1c*, and *Coi2a*) was fused to *GFP* and transiently expressed in *Nicotiana benthamiana*. We observed that COI2a was predominantly localized in the nucleus (Figure 2), similar to what is observed with COI in Arabidopsis (Withers et al. 2012). This subcellular localization was not changed by spraying plants with 0.02% MeJA. By contrast, COI1a and COI1c showed nucleo-cytosolic partitioning and appeared to be partly in subcellular structures in the cytosol (Figure 2), though this could be an artefact of overexpression in *N. benthamiana* and may not necessarily reflect localization in maize. Nucleo-cytosolic partitioning of transcription factors and their regulators, an emerging field in developmental biology, has essential functions in hormonal regulation of plant physiology (Powers et al. 2019; Jing et al. 2022).

The canonical functions of COI proteins include binding to JAZ repressors. Using a bimolecular fluorescence complementation (BiFC) vector system, we co-expressed *Coi1a*, *Coi1c*, and *Coi2a*, fused to the C-terminal half of the *YFP*, together with fifteen members of the maize *JAZ* gene family (Han and Luthe 2021) fused to the N-terminal half of the *YFP*. This showed that, whereas COI2a strongly interacted with almost half of the maize JAZ proteins in *N. benthamiana* leaf nuclei, neither COI1a nor COI1c showed a consistent, reproducible interaction with any JAZ proteins after induction by treatment with 0.02% MeJA (Figures 3, and S3). An independent repeat of this experiment showed similar results (Figure S4).

As further confirmation of these BiFC results, we used JAZ1a, which showed the highest affinity for all three COIs by BiFC, in reciprocal pulldown experiments with COI1a, COI1c, COI2a. All three tested COI proteins showed interaction with JAZ1a (Figure S5). Applying exogenous JA-Ile substantially increased the COI1a and COI1ca/JAZ interactions when the corresponding COI protein was the bait (Figure S5A). Together, both BIFC and reciprocal pulldown experiments indicate that JAZ1a binds to all three COI proteins. However, BIFC

experiments show that COI1a and COI1b bind less efficiently than COI2a to the rest of the tested maize JAZ proteins.

Generation of higher-order mutants of the maize *COI* genes

To investigate the *in vivo* functions of the maize COI proteins, we identified *Ds* and *Mu* transposon insertions in the genetic background of maize inbred line W22 (Springer et al. 2018). There was a pre-existing *Ds* transposon insertion mutation in the *COI1d* gene (Ahern et al. 2009; Vollbrecht et al. 2010), and we remobilized other *Ds* transposon insertions to create mutations in *COI1a*, *COI1c*, and *COI1b*. We obtained *Mu* transposon-insertion mutations of the *COI2* genes from the UniformMu Transposon Resource (Settles et al. 2007; Liu et al. 2016a). Genotyping of the mutants by PCR identified the position of each transposon insertion (Figure 4A; Supplementary Dataset S3). The transposon insertions are in the coding regions of their respective genes, causing loss-of-function mutations due to in-frame stop codons in the transposon sequences or aberrant splicing (Simon and Starlinger 1987). As the observed mutant phenotypes are recessive in crosses, it is unlikely that they are caused by dominant negative effects of the truncated or improperly spliced proteins.

Homozygous *coi* mutants were intercrossed to generate a set of higher-order mutants. This included a homozygous *coi1a coi1d* double mutant, a homozygous *coi1b coi1c* double mutant, and a homozygous quadruple mutant of all four *Coi1* genes, hereafter called *coi1-4x*. The *Coi2* combinations included a *coi2a coi2b* double mutant that was homozygous for *coi2a* and heterozygous for the *coi2b* (*coi2a/coi2a COI2b/coi2b*) and a double mutant that was heterozygous for *coi2a* and homozygous for *coi2b* (*COI2a/coi2a coi2b/coi2b*).

Knockout of both *COI2* genes leads to pollen lethality

As has been reported previously for CRISPR/Cas9 mutants of these genes (Qi et al. 2022), a *coi2a coi2b* double knockout is pollen lethal. We were not able to obtain a homozygous double mutant by self-pollination of *coi2a/coi2a COI2b/coi2b* or *COI2a/coi2a coi2b/coi2b.* Genotyping of the progeny from these self-pollinations showed a 1:1 ratio of the parental genotype and homozygous single mutants. This ratio is expected if a double knockout of *COI2* genes results in gametophyte lethality rather than embryo lethality (Figure S6). To investigate whether *coi2a coi2b* is lethal to pollen or egg cells, we performed test crosses between the *coi2a/coi2a Coi2b/coi2b* and *Coi2a/coi2a coi2b/coi2b* and wildtype W22, with the wildtype being either the pollen or the egg donor. Genotyping of the progeny indicated that, whereas *coi2a coi2b* eggs are

viable and can be transmitted to the next generation, the *coi2a coi2b* pollen genotype is lethal (Figure S7). The tissue-specific abundance of the *Coi2a* transcripts in anthers and the *Coi2b* gene in mature pollen (Figure S8, plotted using the Maize Genome Database, www.maizegdb.org) and the COI2a protein in pollen (Figure S9; data from (Walley et al. 2016)) further suggested that the COI2 proteins contribute to pollen development.

Resistance to lepidopteran herbivory is not compromised in *coi* mutants

Perception of JA-Ile by COI proteins is associated with the induction of herbivore defenses in other plant species. However, *Spodoptera frugiperda* (fall armyworm) did not grow larger on *coi1-4x* (Figure 4B), and *Spodoptera exigua* (beet armyworm) grew less well on *coi-4x* than on wildtype W22 plants (Figure 4C). This suggested that the COI1 proteins by themselves do not play a major role in maize defense against insect herbivores. On *coi2a/coi2a Coi2b/coi2b* and *Coi2a/coi2a coi2b/coi2b* mutant lines, *S. frugiperda* growth was not significantly improved relative to wildtype parental lines (Figure 4D). However, as it was not possible to obtain homozygous *coi2a coi2b* double mutants, and a single functional *Coi2* gene may allow defense induction, residual COI activity may be sufficient to limit herbivory.

***COI1* quadruple mutants have shortened internodes**

When growing the *coi1-4x* mutant line, we noticed that the plants were shorter than wildtype W22 and the *coi1* double mutants (*coi1a coi1d* and *coi1b coi1c*) derived from the same crosses. At ten days post-germination, the *coi1-4x* mutants were similar in size to wildtype (Figure S10A). However, whereas the first two leaves were longer in *coi1-4x* mutants than in wildtype, the third leaves were significantly shorter, marking the onset of a developmental delay in the mutant (Figure 5A,B). The *coi1-4x* mutants were almost half of the size of wildtype W22 and both of the *coi1-2x* mutants at 20 days (Figure S10B, C) and 60 days (Figure 5C,D) post-germination. The reduced height at 60 days post-germination was primarily due to shortened internodes in the *coi1-4x* plants relative to the corresponding internode lengths in *coi1a coi1d* and *coi1b coi1c*, and wildtype lines derived from the same crosses (Figure 5E,F).

The *coi1-4x* mutant has reduced leaf micronutrients and photosynthetic activity

The consistently shorter growth of the *coi1-4x* mutant (Figure 5) was accompanied by a striped-leaf phenotype that persisted throughout the life of the plant (Figure 6A). As striped leaves can indicate a mineral nutrient deficiency (Foy and Barber 1958; Thoiron et al. 1997; Curie et al. 2001; Mattiello et al. 2015), we measured macro- and microelements in the leaves of *coi1-4x*,

coi1a coi1d, *coi1b coi1c*, and wildtype W22 using inductively coupled plasma atomic absorption emission spectroscopy (ICP-MS). This showed a decrease in leaf iron, manganese, copper, and zinc in the *coi1-4x* mutant relative to the double mutants and wildtype 20-day-old plants (Figure 6B). Similar reductions in iron, manganese, copper, and boron in *coi1-4x* were seen in 13-day-old plants in a separate experiment (Figure S11A). The levels of leaf macroelements showed only a few differences between the *coi1-4x* mutants and the other lines, a decrease in phosphorous at 20 days (Figure 6C) and an increase in potassium at 13 days (Figure S11B) after germination.

Because the striped leaf phenotype can also indicate photosynthetic deficiency, we compared the carbon assimilation efficiency and photosynthesis quantum yields between *coi1-4x* and wildtype. This showed a decrease in both carbon assimilation and quantum yield in the *coi1-4x* mutant at 20 days after germination (Figure 6D, E). In a separate experiment, a similar photosynthetic defect was observed in 28-day-old plants (Figure S11C, D).

Differential gene expression in *coi* mutants, with or without MeJA elicitation

We used transcript profiling to identify differentially expressed genes in the *coi* mutants compared to wildtype plants, with and without MeJA elicitation. The 13 tested genotypes consisted of six *coi* single mutants, *coi1a coi1d*, *coi1b coi1c*, *coi1-4x*, double homozygote-heterozygote combinations of the *coi2* mutations, and two corresponding inbred line W22 wildtype lines (for the *Ds* and *Mu* insertion line crosses, respectively). Leaf tissue for gene expression assays was taken from 5-9 biological replicates of the thirteen genotypes, each sprayed with 0.02% MeJA in water or water alone as a control for 12 hours in one-hour intervals. Leaves were harvested after the last treatment. Reads per million mapped reads (RPM) were calculated for each gene, and *P* values for each between-genotype or between-treatment pairwise comparison were calculated for 40,690 annotated genes in the maize W22 genome (Springer et al. 2018). In one or more of 73 pairwise comparisons that were quantified among the 26 tested conditions (13 genotypes +/- MeJA; Supplementary Datasets S4 and S5), there were 13,365 genes with differential expression (adjusted $P < 0.05$; Supplementary Dataset S6). A heatmap based on this list of differentially expressed genes showed that most expression differences were due to induction or repression by MeJA (Figure 7).

Transcripts accumulating to lower levels in *coi1-4x* encode components of photosynthetic machinery and cell wall metabolism

As we were interested in the short stature and photosynthetic defects that differentiate the *coi1-4x* mutant from wildtype W22 and other *coi* mutant lines (Figures 5 and 6), we searched specifically for genes that were differentially expressed in *coi1-4x* relative to *coi1a coi1d*, *coi1b coi1c*, *coi2a/coi2a Coi2b/coi2b*, *Coi2a/coi2a coi2b/coi2b*, and wildtype W22, with or without MeJA treatment. This identified 25 genes that were expressed at a significantly downregulated (Figure 8A and Supplementary Datasets S4 and S7) and 68 genes that were significantly upregulated (Figure 9A and Supplementary Datasets S4 and S8) in *coi1-4x* relative to the other genotypes.

The downregulated genes in the *coi1-4x* mutant are clustered in two groups in the heatmap dendrogram (Figure 8A), based on whether they are upregulated (top half) or downregulated (bottom half) by MeJA in the other twelve maize lines. Genes that were repressed by MeJA treatment were expressed at a low level in *coi1-4x*, even prior to MeJA elicitation. Conversely, genes that were induced by MeJA in other lines were still expressed at a relatively low level in *coi1-4x* after MeJA.

Among the downregulated genes in the *coi1-4x* mutant, 72% encode bundle sheath or mesophyll-abundant transcripts (Supplementary Dataset S9), based on previously published cell-type-specific transcriptome data (Li et al. 2010). We grouped the downregulated gene list (Figure 8B and Supplementary Data Set S7) based on functional annotations in the Maize Genome Database (www.maizegdb.org) and homologs in The Arabidopsis Information Resource (TAIR, www.arabidopsis.org). Genes involved in photosynthesis, carbon fixation, and cyclic electron transport constituted almost one-third of the downregulated genes in the *coi1-4x* mutant, consistent with this mutant's decrease in carbon assimilation and photosystem II quantum yield (Figure 6D, E). These included genes encoding Calvin cycle enzymes (Rubisco small subunit and phosphoribulokinase1 (PRK1)), C_4 photosynthesis enzymes (phosphoenolpyruvate carboxykinase1 (PEPCK1)), alpha carbonic anhydrase, orthophosphate dikinase 2 (PPDK2), and NAD(P)H-quinone oxidoreductase subunit U (NadhU)), fibrillin 4, which is associated with the photosystem II light-harvesting complex, thylakoids, and plastoglobules (Singh et al. 2010), and a chloroplast co-chaperonin. NadhU is an essential part of the NAD(P)H dehydrogenase complex (NDH), which performs cyclic electron transport in chloroplasts by transferring electrons from ferredoxin to plastoquinone (Yamamoto et al. 2011), and fibrilins have essential roles in the

biosynthesis of plastoquinone, light acclimation, and sulfur metabolism (Kim et al. 2015; Lee et al. 2020).

Another group of downregulated genes encoded proteins involved in cell wall metabolism, carbohydrate breakdown, and reactive oxygen species (ROS) scavenging. This group included those encoding peroxidase 52 and a cinnamyl alcohol dehydrogenase (CAD), which are both involved in lignin biosynthesis, a copper/zinc superoxide dismutase 1 (CSD1), Sugary 1 (SU1, a pectin methylesterase inhibitor), which has a role in amylopectin biosynthesis, and an invertase involved in sucrose breakdown.

A small group of transcription factors, including the HAP5-transcription factor (*NF-YC4*), which is involved in GA and abscisic acid (ABA)-activated signaling pathways (Liu et al., 2016b), *MYC70*, a bHLH-transcription factor, and a cell growth defect protein with unknown function, were among the genes that were downregulated in the *coi1-4x* mutant. We did not find any downregulated genes with a known role in homeostasis, regulation, or transport of the micronutrients that could explain the specific deficiency of these elements in the *coi1-4x* mutant (Figure 6B). However, it is possible that the downregulation of some of the cell wall and lignin-related proteins, such as *CAD*, which have been implicated in zinc and iron homeostasis, might be the underlying cause of the microelement deficiency in the *coi1-4x* mutant (Van De Mortel et al. 2006; Reyt et al. 2021).

Only a few defense-associated genes were downregulated in the *coi1-4x* mutant (Figure 8), including those encoding terpene synthase 19 (TPS19), halotolerant determinant 3-like protein (HAL3A, a heme-binding protein with a putative role in terpenoid metabolism), a ras-group-related LRR protein, an isoflavone reductase, and a serine-type endopeptidase. Expression of well-studied JA-induced maize defense genes, including benzoxazinoid biosynthesis genes (Figure S12 and Supplementary Dataset S10), terpene synthase genes with detectable expression (other than *Tps19*) (Figure S13 and Supplementary Dataset S11), and *Jaz* genes (Figure S14 and Supplementary Dataset S12), was not altered in the *coi1-4x* mutant relative to the other genotypes. Moreover, the expression of most defense-related and lipoxygenase (LOX)-encoding genes, which were previously studied in maize (Christensen et al. 2015), remained unchanged in the *coi1-4x* mutant relative to the other genotypes (Figure S15 and Supplementary Dataset S13). This is consistent with the observation that resistance to lepidopteran herbivory was not compromised in the *coi1-4x* mutant compared to W22. There was no significant increase in the

expression of *COI2* genes in the *coi1-4x* mutant compared to W22 (Supplementary Dataset S14), ruling out the possibility that the observed effects are due to a compensatory rise in *COI2* genes.

Genes with higher transcript abundance in *coi1-4x* are mainly involved in phosphate metabolism, cell wall modification, and transcription regulation

A dendrogram and heatmap of genes that are expressed at a higher level in the *coi1-4x* mutant than in the other genotypes (Figure 9A and Supplementary Dataset S8) also had two clusters, genes that are induced (top part) or repressed (bottom part) by MeJA. These genes were expressed at a higher level in *coi1*-4x, with or without MeJA treatment. Altogether, 29% of the genes encode bundle sheath or mesophyll-abundant transcripts (Supplementary Dataset S15) (Li et al. 2010). When these upregulated genes were grouped by their functional annotations, the most abundant group comprised those encoding kinases, phosphatases, and a few transporters involved in the transport of phosphate and other molecules, some of which are implicated in phosphate homeostasis (Figure 9B and Supplementary Dataset S8).

A smaller group of upregulated genes had roles in lipid and phospholipid or glycolipid metabolism. Noticeably in this group, *Glycerophosphodiester phosphodiesterase 2* (*Gpx2*) and *Monogalactosyldiacylglycerol synthase type c* (*Mgd3*) catalyze lipid metabolism during phosphate starvation. Another relatively large group of upregulated transcripts included genes that were shown to be hormone-regulated in prior research. Most of these genes, including two PP2C phosphatase genes, were induced by abscisic acid. This group also included those encoding *Friendly mitochondria* (*Fmt*), *Non-responding to oxylipins 38* (*Noxy38*), and *Lipoxygenase 12* (*Lox12*), a 9-LOX that is the main enzyme involved in the biosynthesis of the JA stereoisomers called death acids (Christensen et al. 2015). FMT is an RNA binding protein associated with cytosolic ribosomes (Kirschner 2022), which regulates mitochondrial distribution, fusion, and quality control in Arabidopsis (El Zawily et al. 2014). Friendly Mitochondria has also been shown to perceive 9-LOX-derived oxylipins (Vellosillo et al. 2007, 2013), but the exact mechanism of this perception is not known.

COI1 proteins function in GA signaling

The two main downregulated gene groups (photosynthesis and cell wall metabolism) in the *coi1-4x* mutant are induced by the GA signaling pathway (Ranwala and Miller 2008; Falcioni et al. 2018; Chen et al. 2020). Moreover, the short stature and shortened internodes of the *coi1-4x* mutant are similar to what is observed in constitutively active, dominant *DELLA* mutants, which

also have a dwarf phenotype (Gale and Marshall 1973; Fujioka et al. 1988; Strader et al. 2004; Ueguchi-Tanaka et al. 2008; Cassani et al. 2009; Lawit et al. 2010). Therefore, we hypothesized that, unlike Arabidopsis and rice *coi* mutants, which are elongated relative to the respective wildtype plants (Xu et al. 2002; Yang et al. 2012; Machado et al. 2017; Inagaki et al. 2022), the maize *coi1-4x* mutant is hyposensitive to GA signaling.

To test this hypothesis, we used an antibody against rice DELLA (SLENDER RICE 1 (SLR1)) (Ueguchi-Tanaka et al. 2008) to detect the maize DELLA protein and compare its abundance in the leaves of 20-day-old *coi1-4x* mutant and wildtype W22 maize seedlings. A protein band migrated at the predicted size of DELLA, over-accumulated in the mutant plants, suggesting that DELLA is more stable in the *coi1-4x* mutant (Figure 10). As transcription of *Dwarf9* but not *Dwarf8* is detected in our dataset (Supplementary Dataset 16), it is likely that the rice DELLA antibodies are detecting DWARF8. To confirm that the detected protein band is DELLA, we treated the 5-day-old *coi1-4x* and wildtype seedlings germinated in water-filled pouches, with 0.02% GA or 0.02% MeJA for two days. Immunoblot analysis of the leaves from these seedlings showed that DELLA was reduced and increased after GA and MeJA treatments, respectively (Figure S16). The level of DELLA, however, was not different between the *coi1-4x* and wildtype seedlings in this experiment. This was expected because the wildtype and *coi1-4x* seedlings at this early age and after germination in water, show height and leaf phenotypes that are similar to wildtype plants.

To further investigate the effect of COI1 on DELLA, we examined protein-protein interactions. We did not observe any interaction between COI proteins and DELLA using BiFC. However, co-expression of *DELLA-RFP* with *COI-GFP* in *N. benthamiana* is consistent with the hypothesis that these proteins may interact directly or indirectly through a larger protein complex. While DELLA-RFP was highly expressed and fully localized in the nuclei when expressed alone or with GFP, it disappeared from nuclei upon co-expression with any of the three tested COI proteins, COI1a, COI1c, or COI2a (Figure 11). Overall, less than 1% of the nuclei contained DELLA-RFP in the presence of COI. However, we could still detect DELLA-RFP outside of the nuclei, colocalized with the COI1-GFP in the unknown cytosolic structures (Figure S17). We previously observed these structures with COI1-GFP alone (red arrow in Figure 2).

COI is the F-box domain protein component of an E3-ligase complex that

polyubiquitinates JAZ repressors and sends them for degradation by the 26S proteasome. We hypothesized that the maize COI proteins also participate directly or indirectly in the assembly of E3-ligase complexes that degrade DELLA. Therefore, we infiltrated leaves co-expressing DELLA-RFP and COI1a-GFP with the proteasome inhibitor bortezomib (BTZ) to test this hypothesis. BTZ treatment restored DELLA in 60% of the nuclei (Figure 12A). Immunoblotting of the total proteins extracted from the leaves with SLR1 antibody, showed that BTZ treatment of the leaves that co-expressed DELLA-RFP with COI1a, restored the level of DELLA-RFP from 25% to more than 50% of the controls (expressing DELLA-RFP alone or with GFP) (Figure 12B). The similar BTZ-mediated restoration for the COI1c was from more than 50% to 100%. Together, these experiments indicate that COI directly or indirectly targets DELLA for degradation by proteasomes.

Effects of Exogenous Hormones on the *coi1-4x* Growth Phenotypes

To further investigate the effects of JA and GA signaling on the *coi1-4x* and wildtype maize, one-week-old seedlings of both genotypes were watered with either 0.02% MeJA or 0.02% GA for three weeks. Three weeks after MeJA treatment, *coi1-4x* leaves were chlorotic, with a yellow color (Figure 13A). By contrast, wildtype leaves only showed some stripes during the first week of treatment but then became green again. After two weeks, the height of MeJA-treated wildtype plants was reduced by 53% relative to mock-treated controls (Figure 13B, D). Growth reduction of the *coi1-4x* mutant was less severe (35%), suggesting that the mutant line was less sensitive to the growth-inhibitory effect of the MeJA. We attributed this continued MeJA sensitivity to the presence of the two functional *COI2* genes in the *coi1-4x* mutant. GA treatment increased the height of wildtype and *coi1-4x* plants by 46% and 74%, respectively (Figure 13B and D). It did not, however, rescue the developmental delay of the third leaf in the mutant. Three weeks after MeJA treatment, wildtype plants grew out of the juvenile stage and restored their green leaves, but the *coi1-4x* failed to transition from the juvenile to adult growth phase (Figure 13C and D). The plant height of wildtype and *coi1-4x* treated with MeJA for three weeks showed a 41% and 55% decrease, respectively (Figure 13C, D), relative to the corresponding mock-treated control plants.

Discussion

The shortened internode length and reduced plant height exhibited by the *coi1-4x* mutant are reminiscent of the constitutively-active dominant *DELLA* mutants or GA suppression mutants, which have been characterized in Arabidopsis (Strader et al. 2004), rice (Ueguchi-Tanaka et al. 2008), wheat (Gale and Marshall 1973) and maize (Fujioka et al. 1988; Cassani et al. 2009; Lawit et al. 2010; Paciorek et al. 2022). The increased DELLA abundance in *coi1-4x* relative to wildtype (Figure 10) and the degradation of DELLA when co-expressed with COI in *N. benthamiana* (Figure 11) confirmed that the underlying cause of the growth deficiency in the *coi1-4x* mutant is likely increased DELLA stability. Several studies have demonstrated crosstalk between DELLA and plant defense responses (Navarro et al. 2008; Hou et al. 2010; Wild et al. 2012; Yang et al. 2012; Qi et al. 2014; de Vleesschauwer et al. 2016; Machado et al. 2017; Dong and Hudson 2022). In Arabidopsis and rice, the JAZ repressors of the JA signaling pathway bind to and entrap DELLA to hinder its repression of the growth-related genes (Hou et al. 2010; Yang et al. 2012). As a result of JAZ stability and DELLA entrapment in the Arabidopsis *coi1* and the rice *coi1a coi1b* mutants, these plants are hypersensitive to GA and grow taller than corresponding wildtype plants (Xu et al. 2002; Yang et al. 2012; Machado et al. 2017). Thus, the increased DELLA abundance and decreased growth in the maize *coi1-4x* mutant is a notable contrast to the corresponding Arabidopsis and rice *coi* knockout mutants, which are taller than the corresponding wildtype plants.

One possible explanation for the short stature of *coi1-4x* is that maize COI1 proteins have lost affinity for JAZ but not for the rest of the E3-ligase complex, thereby functioning as competitive inhibitors of COI2. The resulting enrichment of COI2 in the E3-ligase complexes, which results from COI1 depletion in *coi1-4x*, may lead to JA hypersensitivity, increased stabilization of DELLA proteins, and growth inhibition. However, expression of most canonical JA-responsive genes (Figure S15 and Supplementary Dataset S13), as well as those encoding enzymes for the biosynthesis of benzoxazinoids and terpenes (Figures S12 and S13; Supplementary Datasets S10 and S11), was not significantly changed in the *coi1-4x* mutant relative to wildtype.

The lack of a significant change in the defense response at the gene expression level was in accordance with a lack of improved caterpillar growth on the *coi1-4x* mutant relative to wildtype plants (Figure 4B, C). In fact, *S. exigua* caterpillars were significantly smaller on the *coi1-4x* mutant, which could be due to lower nutritional quality of the dwarf plants, which also

have photosynthetic and mineral deficiencies (Figure 6). Prior experiments with *S. exigua* on maize have shown MeJA accumulation in response to insect feeding (Al-Zahrani et al. 2020) and increased caterpillar growth on mutant lines that are JA-deficient (Yan et al. 2012). This suggests that maize COI1 proteins are not involved in the jasmonate signaling pathway and that COI2 proteins may have this canonical defensive function. Consistent with this hypothesis, maize *coi2a coi2b* homozygous knockouts of are male sterile (Qi et al. 2022), a phenotype that also has been associated with Arabidopsis *coi1* mutants.

Rice COI2 showed stronger interactions with JAZ proteins than either of the two rice COI1 proteins (Inagaki et al. 2022; Wang et al. 2023). Similar to these rice experiments, our BiFC experiments show that maize COI2 has more consistent interactions with eight of the tested JAZ proteins than either COI1a or COI1c (Figures 3, S3, and S4). This effect was recapitulated in co-immunoprecipitation and pulldown experiments (Figure S5), where COI2a showed stronger interactions with JAZ1a in the presence of JA-Ile than either COI1a or COI1c. Our results (Supplementary Dataset S12) differ from those of Qi et al (2022) who investigated a partially overlapping set of JAZ proteins using yeast 2-hybrid assays and found that, whereas some maize JAZ proteins showed interactions with maize COI1 proteins, none showed interactions with maize COI2 proteins. The differences between our observations and those of Qi et al (2022) may be related to the different assay systems. It may be that the protein milieu of plant cells (*N. benthamiana* in our experiments) promotes different COI-JAZ interactions than those that occur when maize proteins are expressed in yeast.

In Arabidopsis, co-immunoprecipitation experiments show that JA-Ile elicits COI-mediated ubiquitination of JAZ, degradation by the 26S proteasome, and activation of defense-related gene expression (Fonseca et al. 2009; Sheard et al. 2010). We propose that COI2 in maize has a similar function in regulating defense responses (Figure 14A). However, although maize *coi2a coi2b* double mutants are male sterile, maize COI2b failed to restore fertility in an Arabidopsis *coi* mutant (An et al. 2019), suggesting that the maize COI2 proteins are somewhat diverged from the Arabidopsis COI function, or at least don't interact properly with other members of Arabidopsis protein complexes.

The results that we have presented are consistent with the hypothesis that maize COI1 proteins, interacting with an as yet unknown ligand, have acquired a new function that leads to DELLA instead of JAZ polyubiquitination and degradation (Figure 14B). In the absence of direct

interactions between COI1 and DELLA, it is possible that the COI1 proteins lead to the activation of some other E3 ubiquitin ligase that triggers DELLA degradation. DELLA-RFP disappeared from the nuclei when co-expressed with COI1a, COI1c, and even COI2a in *N. benthamiana* leaves. The proteasome inhibitor BTZ restored DELLA in 60% of the nuclei, consistent with the hypothesis that maize COI proteins directly or indirectly target DELLA for degradation by the proteasome (Figures 11 and 12).

DELLA is polyubiquitinated by SLEEPY1 (SLY1; AT4G24210) in Arabidopsis (Dill et al. 2004) and by GIBBERELIN INSENSITIVE DWARF 2 (GID2; Gene bank: AB100246) in rice (Gomi et al. 2004). These two F-box domain E3 ligases have only 41% sequence identity with one another, suggesting that functional diversification of the DELLA-targeting E3 ligases in the course of plant evolution. In Arabidopsis and rice, E3 ligases polyubiquitinate DELLA proteins after they interact with the corresponding GID1 receptors bound to GA. Maize has two uncharacterized putative GID2 orthologs (www.maizegdb.org) which may function in the canonical GA-mediated DELLA degradation. However, the corresponding maize E3 ligases have not been identified. DELLA in maize and perhaps other C_4 plants may have become a direct or indirect target of COI1 leading to E3-ligase activity that can polyubiquitinate DELLA for proteasome-dependent degradation (Figure 14B).

DELLA is at the nexus of several signaling pathways and not limited to regulating the crosstalk between GA and JA. In Arabidopsis, ABA inhibits GA-mediated seed germination, and overaccumulation of DELLA upregulates ABA-mediated responses. This antagonistic crosstalk was shown to be mediated through the formation of a module between the DELLA protein RGL2 and one of the three NF-YC3, 4, or 9 homologs, which subsequently binds to the promoter of the *ABI5* transcription factor and modulates the ABA-responsive genes, regardless of the ABA level (Liu et al. 2016b). In our data, one prominent group of genes that are more highly expressed in the *coi1-4x* mutant relative to all other genotypes consisted of ABA-regulated and drought-responsive genes (Figure 9 and Supplementary Dataset S8), which is consistent with over-accumulated DELLA (Figure 10) upregulating the ABA pathway in the *coi1-4x* mutant. Downregulation of *NF-YC4* in the *coi1-4x* mutant relative to all other genotypes (Figure 8 and Supplementary Dataset S7) may indicate a compensatory or regulatory feedback reaction to alleviate the effects of the DELLA-mediated ABA induction.

Both GA and JA signaling pathways have crosstalk with the auxin pathway. The interactive modules between DELLA, ARF activators, and AUX-IAA repressors play crucial roles in fruit ripening and vascular development (Hu et al. 2018, 2022). Moreover, JA and auxin signaling complexes are structurally similar (Pérez and Goossens 2013; Tal et al. 2020). Cullin1 is a scaffolding module and a shared component of the SCF ubiquitin ligase complexes involved in mediating responses to auxin and JA (Ren et al. 2005). An overabundance of Cullin1 derived from the depletion of the SCF^{coi1} complex from the four COI proteins may lead to an increased formation and activity of the SCF^{TIR1}, the auxin-inducible SCF ubiquitin ligase complex (Gray et al. 2001), and hypersensitivity to auxin, assuming that the unique components of the auxin-inducible complex are not limiting. It is known that auxin inhibits seed germination in an ABA-dependent manner (Liu et al. 2013). It remains to be determined whether the auxin-related symptoms in the *coi1-4x* mutant are a consequence of auxin or other hormonal imbalances.

Our results show that 72% of the downregulated and 29% of the upregulated genes in the *coi1-4x* mutant encode proteins are related to C_4 metabolism, exhibiting bundle sheath or mesophyll-specific expression (Supplementary Dataset S9 and S15) (Li et al. 2010). C_4 species have evolved more than 60 times independently in the plant kingdom in response to selective pressures from the environment (Christin et al. 2013; Zhou et al. 2018; Blätke and Bräutigam 2019). We propose that in maize, and perhaps other C_4 species, COI-regulated DELLA degradation might be part of the plant adaptation strategies to maintain growth in response to biotic stresses and severe environmental conditions (*e.g.*, drought, high light, and elevated temperatures), which are the driving forces in C_4 evolution. It has long been speculated that C_4 characteristics were pre-existing in C_3 plants and were only modified in C_4 species in response to their environmental needs (Hibberd and Quick 2002; Burgess et al. 2016; Wasilewska-Dębowska et al. 2022). A recent study, which aimed to identify the genes associated with the onset of the bundle sheath specificity in C_3 plants, showed that bundle sheath cells of rice and Arabidopsis are conditioned to synthesize proteins involved in water transport, sulfur assimilation, and JA synthesis (Hua et al. 2021).

Most downregulated genes in the *coi1-4x* mutant, which are GA-inducible and growth-related, are also C_4 genes with cell-specific-expression patterns (Figure 8 and Supplementary Datasets S7 and S9). These genes encode bundle sheath-abundant photosynthetic proteins, including NadhU, which is an essential part of the NAD(P)H dehydrogenase (NDH) complex

that performs cyclic electron transport in chloroplasts (Yamamoto et al. 2011). NDH levels increased from 4% of the total photosystem I (PSI) in C_3 plants to 40% in the bundle sheath chloroplasts of C_4 to provide the high demand of ATP in the bundle sheath chloroplasts of NADP-ME C_4 plants, including maize, sorghum, and *Flaveria* C_4 species (Takabayashi et al. 2005; Wasilewska-Dębowska et al. 2022). Studies on the genus *Flaveria,* which includes both C_3, C_4, and intermediate species, showed that this protein complex increases up to fourteen times in the bundle sheath chloroplasts of the C_4 *Flaveria* species compared to the C_3 species (Nakamura et al. 2013). The NDH cyclic electron transport also protects plastoquinone, the electron receiver of cyclic electron transport, and photosystem I against excessive reduction and high light-derived reactive oxygen species, which can cause photoinhibition.

Interestingly, fibrillin 4, another photosynthetic protein that is downregulated in the *coi1-4x*, is a photosystem II (PSII) and light harvesting complex II (LHCII) associated member (Singh et al. 2010) of the fibrillin family, which plays essential roles in the biosynthesis of plastoquinone, light acclimation, and sulfur metabolism (Kim et al. 2015; Lee et al. 2020). Phosphorylation of PSII and LHCII play essential roles in the acclimation of photosynthesis to high light intensity, and this role becomes more essential in maize (Drozak and Romanowska 2006) and other C_4 plants (Reviewed in (Wasilewska-Dębowska et al. 2022)). Upregulation of genes encoding kinases, phosphatases, and phosphate transporters, including the sulfur transporter 3:4 (SULTR 3:4), a protein involved in the transport of sulfur (Takahashi et al. 1997) and phosphorus (Ding et al. 2020), in the *coi1-4x* mutant (Figure 9 and Supplementary Dataset S8), might be a compensatory response. Phosphorus deficiency in the leaves of the 20-day-old *coi1-4x* seedlings (Figure 6C), strengthens this hypothesis.

In conclusion, we propose that a non-classical crosstalk between the JA and GA pathways, which is disrupted in the *coi1-4x* mutant, plays a role in the evolution of maize and perhaps other C_4 plants. By regulating growth responses, maize COI1 proteins compensate for the canonical growth penalty associated with JA-Ile induction of plant defense responses. Future research will define the exact mechanisms of this compensatory response.

Materials and Methods

Plant materials and growth conditions

Experiments were done with maize (*Zea mays*) inbred line W22 (Springer et al. 2018) and derived transposon insertion lines. Seedlings were grown in Conviron (Winnipeg, Canada) growth chambers under a light intensity of 500 μmol/m^2/sec from actinic bulbs, a 16:8 h light:dark cycle, 25 °C light, 22 °C dark, and 50% relative humidity, and in a soil mix containing 35% peat moss, 10% vermiculite, 35% baked clay, 10% sand, 10% sterilized topsoil. One-month-old plants were transplanted into pots and moved to greenhouse rooms with a temperature of 27 °C (day) and 22 °C (night), with a 16:8 h light:dark cycle and high pressure sodium light bulbs supplying additional light when the ambient photosynthetically active radiation dropped below 350 μE. Methyl jasmonate (MeJA) and gibberellic acid (GA) treatments were done on plants that were germinated in soil or germination pouches. In the latter case, seeds were germinated in CYG germination pouches (Mega-International.com).

Nicotiana benthamiana plants were grown in a temperature-controlled growth room with a 16:8 h light:dark cycle under a light intensity of 500 μmol/m^2/sec from actinic bulbs, 25 °C light, 22 °C dark, and 50% relative humidity, in Cornell Mix Cornell Mix [by weight 56% peat moss, 35% vermiculite, 4% lime, 4% Osmocote slow-release fertilizer (Scotts, Marysville, OH), and 1% Unimix (Scotts, Marysville, OH)].

Protein alignment and phylogenetic tree

The accession numbers and sequences for the maize six COI proteins were obtained from the maizeGDB (https://www.maizegdb.org/). Blastp (protein-protein BLAST; https://blast.ncbi.nlm.nih.gov/) was used for pairwise alignments and calculating the percentage identity between COI proteins. The paralogous COI sequences from other organisms were obtained from Phytozome (https://phytozome-next.jgi.doe.gov/) and were aligned with the maize proteins using Clustal Omega (Sievers et al. 2011). A maximum likelihood, midpoint-rooted tree was created using IQ-Tree and 1,000 replicates for calculating bootstrap values (Hoang et al. 2018; Minh et al. 2020). A machine-readable (Newick Format) version of the tree is in Supplementary File S1. The tree in Figure 1 was visualized using MEGA11 (Tamura et al. 2021).

Transposon insertion lines and genotyping

The *coi2 Mu* transposon insertion alleles were identified from the UniformMu Transposon Resource (https://curation.maizegdb.org/documentation/uniformmu/index.php) (Settles et al. 2007). The *coi1a, coi1b,* and *coi1c* mutants were created by remobilizing nearby *Ds* transposon

insertions. *Ds* transposon insertions that were tightly linked to maize *Coi1a, Coi1b,* and *Coi1c* genes (I.S07.1293, I.W06.0524B, and I.S07.1819, respectively) were identified through the MaizeGDB webpage (https://www.maizegdb.org/). The identities of these lines were verified with primers designed to specifically amplify a *Ds* junction fragment. Verified lines were crossed with *Activator* (*Ac*) to induce *Ds* transposition. F1 seeds from these crosses were planted and screened within two weeks after germination using primers designed to the *Ds* end sequence and the *Coi* sequence of interest (Supplementary Dataset S17). A total of 4,004 (*Coi1a*), 6,160 (*Coi1b*), and 1,800 (*Coi1c*) maize seedlings were screened by PCR to find transposon insertions in each *Coi* gene. Amplification fragments indicated a potential insertion in a *Coi* gene, and genotypes were verified through successive PCR validation screens using different primer sets that amplified *Ds* and *Coi*, followed by Sanger sequencing to identify the insertion site (Supplementary Dataset S2). Seedlings carrying *Coi::Ds* alleles were transplanted and grown to maturity in a greenhouse and self-pollinated to recover progeny. Seeds from these *Coi::Ds* insertion lines were harvested and planted for screening of homozygous *Ds* insertions. Homozygous *Coi::Ds* insertion lines were then further characterized in this study. Detailed methodology of *Ac*/*Ds* tagging has been described previously, and the *coi1d* mutant was identified from this maize *Ds* transposon insertion collection (Ahern et al. 2009; Vollbrecht et al. 2010). Genotyping of the mutant and wildtype alleles of each *Coi* gene was performed using the PCR primer pairs listed in Supplementary Dataset S17.

Insect bioassays

Eggs of fall armyworm (*Spodoptera frugiperda*) and beet armyworm (*Spodoptera exigua*) were purchased from Benzon Research (www.benzonresearch.com) and were hatched at 28 ºC on fall armyworm diet and beet armyworm diet (Southland Products, www.southlandproducts.net), respectively. Neonate larvae were confined on three-week-old maize plants using micro-perforated plastic bread bags (www.amazon.com) that were sealed around the base of the plants with wire twist ties. After ten days, caterpillars were harvested and weighed.

COI and DELLA construct preparation, plant infiltration, and imaging

To prepare the BiFC assay, the coding regions of *CoiA1*, *Coi1c*, and *Coi2a* (W22 accession numbers in Supplementary Dataset S1), 15 *Jaz* genes (W22 accession numbers in Supplementary Dataset S12), and the *Dwarf9* (*DELLA*) gene (accession number: Zm00004b011408 in Supplementary Dataset S16), were either amplified by PCR or synthesized by Twist Bioscience

(https://www.twistbioscience.com/) and cloned by restriction cloning using *Pac*I and *Spe*I or *Asc*I into the BiFC vectors p2YC and p2YN (Kong et al. 2014) to generate *Coi-cYFP*, and *JAZ-nYFP*, respectively. The primers used for vector construction are listed in Supplementary Dataset S17.

To prepare constructs for the subcellular localization, the open reading frames of *Coi1a, Coi1c*, *Coi2a,* and *DELLA* (*Dwarf9*) were amplified and cloned into pDONR 207 using BP clonase recombination (Invitrogen, Carlsbad, CA, USA), before being transferred with a second recombination reaction (LR, Invitrogen) into the vector pEAQ-EGgW (Berthold et al. 2019). The primers used for vector construction are listed in Supplementary Dataset S17. The recombinant vectors were transformed into *Agrobacterium tumefaciens* strain GV3101 and grown in LB medium with 50 mg l^{-1} kanamycin and 50 mg l^{-1} rifampicin for 1 d. After centrifugation for 10 min at 2000 x *g*, the bacteria were collected and resuspended in an infection solution (10 mM MES, 10 mM $MgCl_2$ and 200 μM acetosyringone). The prepared suspensions (A600 nm = 0.5) were infiltrated into young but fully expanded *N. benthamiana* leaves using a needleless syringe. Two to three days later, leaves were sprayed with 0.02% (v/v) MeJA in water. Two hours after the MeJA spraying, yellow fluorescent protein (YFP, for BiFC) and enhanced green fluorescent protein (EGFP) for subcellular localization were monitored using a laser confocal scanning microscope (LSM 800, Zeiss) with an argon laser and DSS561 diode lasers. GFP was excited at 488-nm by the argon laser and observed using a detection window from 497 to 526 nm. RFP was excited at 561 nm using the laser diode and detected in the 600 to 638 nm range. YFP was excited at 514 nm by the argon laser and detected from 528 to 603 nm. Red channels in the original images were changed to magenta for improved visibility using Fiji (https://imagej.net/software/fiji/). All areas of the images received equivalent treatment.

Co-immunoprecipitation and pulldown assays

The coding sequence for full-length *Jaz1a* was synthesized by Twist Bioscience (https://www.twistbioscience.com/) and cloned into the pMAL-TEV vector (Kroeger et al. 2009) via restriction enzymes *Bam*H1 and *Sal*1. The recombinant maltose binding protein fusion, MBP-JAZ1a, was purified using amylose magnetic beads (New England Biolabs.), eluted from the beads using 25 mM HCl, neutralized with one sixth volume of 1 M Tris pH 8, and used in the JAZ/COI interaction studies. Three grams of *N. benthamiana* leaves infiltrated with each construct expressing COI1a, COI1c, COI2a fused to GFP, were ground in liquid nitrogen, and

homogenized in extraction buffer containing 50 mM Tris-HCl pH 7.4, 100 mM NaCl, 10% (v/v) glycerol, 1% (v/v) Tween-20, 0.1% Sodium Deoxycholate, 1 mM dithiothreitol (DTT), complete protease inhibitor (Roche) and 50 mM MG132 (Sigma). After cleaning plant particles using Micro-Spin filters (Pierce) and centrifugation (16,000g, 4 °C), the supernatant was collected. For the co-immunoprecipitation experiment shown in Figure S5A, 30 µl of the ChromoTek GFP-Trap® Magnetic Particles M-270 (proteintech) was added to 2 ml of the cleared leaf lysate mixed with 6 µg of the purified MBP-JAZ, supplemented with JA-Ile or mock, and incubated for 1 h at 4 °C. After washing, samples were eluted with 40µl of the 2x Laemmli sample buffer, boiled for 5 minutes, and 15 µl was loaded on SDS-PAGE gels, transferred to PVDF membranes and incubated with monoclonal anti-GFP antibody (BioLegend, Cat:902605) (1:10000 dilution) and anti-MBP antibody (Santa Cruz Biotechnology, Cat: sc-13564). Pulldown assay shown in Figures S5B, was done the same with the exception that 6 µg of the MBP-JAZ1a bound amylose resin was added to 2 ml of the cleared leaf lysates.

Expression analysis by RNA sequencing

Tissue was collected from the sixth leaf, 20 days after germination, at the end of the light period. Leaves were sprayed with either 0.02% MeJA in water or water alone for 12 hours, in one-hour intervals. Roughly 100 mg of leaf tissue from the middle of the leaf without the midrib was placed into collection tubes. RNA extraction and 3' RNA sequencing were performed at the Cornell Institute of Biotechnology Genomic Facility (https://www.biotech.cornell.edu/core-facilities-brc/facilities/genomics-facility), as described previously (Kremling et al. 2018).

Single-end Illumina reads generated from 3' RNA-Seq libraries were processed to remove adaptor and low-quality sequences using Trimmomatic (v0.38) (Bolger et al. 2014) and to trim polyA/T tails using PRINSEQ++ (Cantu et al. 2019). The resulting reads were aligned to the SILVA rRNA database (Quast et al. 2013) using Bowtie (Langmead et al. 2009) to remove ribosomal RNA contamination. The cleaned high-quality RNA-Seq reads were aligned to the maize W22 reference genome (Springer et al. 2018) using HISAT2 (v2.1) (Kim et al. 2019) with default parameters. Based on these alignments, raw read counts were derived for each gene and normalized to reads per million mapped reads (RPM). Differential gene expression analyses were performed using DESeq2 (Love et al. 2014).

To prepare heat maps, the RPM data were transformed by log(1+RPM) prior to clustering. The color gradient in the heatmap reflects the Z scores, with red colors indicating

higher-than-average expression levels (Z score > 0) and blue colors indicating lower-than-average expression levels (Z score < 0). The pairwise comparative *p* values (<0.05) were used for the sequential sorting to make the gene lists used in heatmaps. Heatmaps were produced in R (https://www.r-project.org/) and Venn diagrams were made using FunRich (http://www.funrich.org/).

Inductively coupled plasma atomic absorption emission spectroscopy

Elemental analysis determinations were performed using ICP-MS. Less than 200 milligrams of leaf tissue were digested with a cocktail of HNO_3 and perchloric acid (1:1 ratio), diluted in 10 ml of 5% HNO_3, and analyzed using Sciex Inductively coupled argon plasma (AB Sciex LLC, Framingham, MA), as described previously (Cobb et al. 2021).

Photosynthetic measurements

Photosynthetic efficiency was assessed by measuring gas exchange at a fixed CO_2 concentration of 400 μmol mol^{-1} (GasExA), using an LI-6800 portable photosynthesis system (Li-Cor Inc., Lincoln, NE, USA). The efficiency of the photosystem II photochemistry and other light response parameters was assessed at a fixed light intensity of 2000 μmol $m^{-2}s^{-1}$.

Protein extraction, and immunoblotting

Total protein was extracted from 60 mg of leaf material (Figures 10, 12, and S15) as described previously (Feiz et al. 2012). For maize grown in soil, the fourth leaf was harvested 20 days after germination. For *N. benthamiana* experiments, samples were collected 48 hours after co-infiltration. For maize grown in germination pouches, seedlings were harvested after 5 days. Briefly, the ground leaf material was mixed with 250 μl of the extraction buffer (50 mM Tris-HCl, pH 7.5, 150 mM NaCl, 1% Triton X-100, 1 mM ethylene glycol-bis(β-aminoethyl ether)-N,N,N′,N′-tetraacetic acid (EGTA), and 1 mM DTT) with 1% protease inhibitor cocktail (04693116001, Roche) and diluted 1x with the 2x loading buffer (65.8 mM Tris-HCl, pH 6.8, 2.1% SDS, 26.3% (w/v) glycerol, 0.01% bromophenol blue). A volume corresponding to 150 μg of tissue was analyzed using 10% SDS-polyacrylamide gels. Proteins were analyzed by transfer to polyvinylidene difluoride (PVDF) membranes. Immunodetection of the maize DELLA proteins was performed using anti-SLR1 primary antibody (Cosmo Bio USA, Carlsbad, California) (2:10,000 dilution) and anti-rabbit IgG, horseradish peroxidase conjugated secondary antibody (www.promega.com) (1:10,000 dilution). The corresponding molecular weight for the band in immunoblotting (70 kDa) was consistent with the expected size of maize DELLA

proteins (65-66 kDa). The chemiluminescence signal was detected with the Pierce™ ECL Plus immunoblotting substrate on a GelDoc Go Imaging (BIO-RAD). Bortezomib (BTZ, Selleckchem.com) at 20 μM concentration was infiltrated into the *N. benthamiana* leaves 24 hours after leaf infiltration with the plasmids expressing the DELLA-RFP, and COI1a-EGFP or COI1c-EGFP proteins. Sixteen hours after BTZ treatments, leaves were used for confocal microscopy or immunoblot analyses.

Statistical analysis

Statistical comparisons (*t*-tests and ANOVA) were conducted using Microsoft Excel. Raw data and statistical analyses for all bar graphs and line graphs are presented in Supplementary Dataset S18.

Accession numbers

Raw RNA-Seq reads have been deposited in the NCBI BioProject database under accession PRJNA951759. MaizeGDB (www.maizegdb.org) accession numbers for maize inbred line W22 alleles of key genes described in this work: Zm00004b018438 (*Coi1a*); Zm00004b027897 (*Coi1d*); Zm00004b030639 (*Coi1c*); Zm00004b026046 (*Coi1b*); Zm00004b001065 (*Coi2a*); Zm00004b033978 (*Coi2b*); Zm00004b036097 (*Jaz1a*); Zm00004b009062 (*Jaz1b*); Zm00004b040435 (*Jaz2a*); Zm00004b006088 (*Jaz2b*); Zm00004b037309 (*Jaz3-1a*); Zm00004b009908 (*Jaz3-1b*); Zm00004b001750 (*Jaz3-2*); Zm00004b034344 (*Jaz4-1b*); Zm00004b008980 (*Jaz5-1b*); Zm00004b021513 (*Jaz5-2*); Zm00004b006410 (*Jaz4-3*); Zm00004b036592 (*Jaz4-5*); Zm00004b004884 (*Dwarf8*); Zm00004b011408 (*Dwarf9*).

Supplementary Data

Supplementary Figure S1. Amino acid identity of Arabidopsis and maize COI proteins.

Supplementary Figure S2. Alignment of COI proteins from different plant species .

Supplementary Figure S3. BiFC between maize COI1A, COI1B or COI2a and seven JAZ proteins.

Supplementary Figure S4. Independent repeat of the COI–JAZ BiFC experiment.

Supplementary Figure S5. Interactions between each maize COI and JAZ1a detected via coimmunoprecipitation and pulldown assays.

Supplementary Figure S6. Segregation patterns of selfed *coi2a/coi2a Coi2b/coi2b* and *Coi2a/coi2a coi2b/coi2b* mutants.

Supplementary Figure S7. Test crosses between *coi2a/coi2a Coi2b/coi2b* and *Coi2a/coi2a coi2b/coi2b* and the wildtype W22 maize.

Supplementary Figure S8. Expression of maize *Coi2* genes.

Supplementary Figure S9. Proteomics data show pollen-specific abundance of maize COI2a protein.

Supplementary Figure S10. Growth phenotypes of *coi1-4x* compared to wild type and double mutants.

Supplementary Figure S11. Microelements, macroelements, and photosynthesis assays.

Supplementary Figure S12. Heatmap showing expression of maize benzoxazinoid biosynthesis genes.

Supplementary Figure S13. Heatmap showing expression of the maize terpene synthase genes.

Supplementary Figure S14. Heatmap showing expression of the maize *JAZ* genes.

Supplementary Figure S15. Heatmap showing expression of maize defense-related genes and *LOX* genes.

Supplementary Figure S16. DELLA protein levels decrease and increase after treatment of five-day-old seedlings with GA and MeJA, respectively.

Supplementary Figure S17. Co-localization of DELLA-RFP and COI1a-EGFP.

Supplementary Dataset S1. Cross-reference of maize *Coi* gene names.

Supplementary Dataset S2. COI protein sequences included in the phylogenetic tree in Figure 1.

Supplementary Dataset S3. Flanking sequences of transposon insertion sites in maize *Coi* genes.

Supplementary Dataset S4. RNA-Seq data for all annotated genes.

Supplementary Dataset S5. Pairwise comparisons of RNA-Seq data.

Supplementary Dataset S6. Expression levels of differentially expressed genes.

Supplementary Dataset S7. List of genes that are downregulated in *coi1-4x.*

Supplementary Dataset S8. List of genes that are upregulated in *coi1-4x.*

Supplementary Dataset S9. List of downregulated genes that are bundle sheath and mesophyll specific.

Supplementary Dataset S10. Expression levels of benzoxazinoid biosynthesis genes, with and without MeJA treatment.

Supplementary Dataset S11. Expression levels of terpene synthases, with and without MeJA treatment.

Supplementary Dataset S12. Expression levels of maize *JAZ* genes, with and without MeJA treatment.

Supplementary Dataset S13. Expression levels of maize defense-related genes and *LOX* genes, with and without MeJA treatment.

Supplementary Dataset S14. Expression levels of maize *Coi* genes, with and without MeJA treatment.

Supplementary Dataset S15. List of upregulated genes that are bundle sheath and mesophyll specific.

Supplementary Dataset S16. Expression levels of maize *Dwarf8* and *Dwarf9* genes, with and without MeJA treatment.

Supplementary Dataset S17. Primers used for genotyping and gene amplification .

Supplementary Dataset S18. Summary of statistical analyses.

Supplementary File S1. Machine-readable tree file of COI protein phylogeny, in support of Figure 1.

Supplementary File S2. Protein sequences included in the phylogeny, FASTA format, in support of Figure 1.

Funding information

This project was supported by NSF award 2019516 and USDA award 2021-67014-342237 to GJ, an International Postdoc Scholarship from the Punjab Higher Education Commission to IG, and USDA-AFRI NIFA Postdoctoral Fellowship 2014-67012-22269 to CS.

Acknowledgments

We thank Shree Giri at the USDA, Robert W. Holly Center for Agriculture and Health, Plant Soil and Nutrition Research for ICP atomic absorption emission spectroscopy; Filipe Aiura Namorato (USDA, Ithaca), Eric Craft (USDA, Ithaca), Eric Schmelz (UC San Diego), Brad Nelms (University of Georgia), Honghe Sun (BTI), Judith Kolkman (Cornell University), Fay

Wei Li (BTI), Venkatesh Thirumalaikumar (BTI), Cynthia Holland (Williams College), Amber Hotto (BTI) for their conceptual and/or technical advice; Dong-Lei Yang and Mingzhu Wang (Nanjing Agricultural University) for kindly providing the SLR1 antibody; and Miyanko Ueguchi-Tanaka from Nagoya University for the helpful information regarding the process to purchase their SLR1 antibody #2 from Cosmo Bio USA; and Corinne Schmitt-Keichinger (Université de Strasbourg) for kindly providing the modified and tagged versions of the pEAQ vectors.

Author contributions

LF, CS, TPB, and GJ designed the research. CS, YR, and KRA generated three of the maize *coi* mutants. LF generated the higher-order mutants and performed the experiments, and analyzed the data. CJA. and IG contributed to insect bioassays. LF, SW, and ZF analyzed the RNA sequencing data. MAP provided the plant elemental analysis tool and expertise. LF and GJ wrote the manuscript with input from all authors.

Figure legends

Figure 1. The maize genome encodes six coronatine insensitive (COI) proteins. The sequences of six maize COI proteins, along with their paralogs from other species, were obtained from Phytozome (https://phytozome-next.jgi.doe.gov/). Two predicted duplication events are marked. Four maize COI1 proteins are marked with green boxes. Two maize COI2 proteins are marked with blue boxes. The species in the Poaceae have three COI protein clades, two containing COI1 proteins (exemplified by maize COI1a and COI1d, and COI1b and COI1c, respectively) and one containing COI2 proteins (exemplified by maize COI2a and COI2b). The protein sequence alignment and species names are presented in Supplementary Dataset S2. A machine-readable (Newick Format) version of the tree is in Supplementary File S1. FASTA sequences of all proteins are in Supplementary File S2. The maximum likelihood, midpoint-rooted tree was produced with IQ-Tree and visualized with MEGA11. Bootstrap values are based on 1000 replicates. Scale bar indicates substitutions per site.

Figure 2. Subcellular locations of the maize coronatine insensitive (COI) proteins. COI1a, COI1c, and COI2a proteins were fused to enhanced green fluorescent protein (EGFP), showing

that COI2a is more targeted to the nuclei than the two COI1 proteins. Confocal images were taken at 48 h after infiltrating plasmids expressing the COI-EGFP fusion proteins into the *Nicotiana benthamiana*. Leaves were sprayed with water (mock) or 0.02% methyl jasmonate (MeJA) two hours before imaging. White arrows indicate the nuclei, and red arrow represents a cytosolic condensate. Scale bars = 25 μm.

Figure 3. Bimolecular fluorescence complementation (BIFC) between the maize coronatine insensitive (COI) proteins fused to the carboxy-terminus of yellow fluorescent protein (cYFP) and jasmonate-ZIM domain (JAZ) proteins fused to the amino-terminus of yellow fluorescent protein (nYFP). BIFC indicating co-localization is shown as white spots in the images. Magenta represents chlorophyll fluorescence. Maize JAZ proteins have a higher affinity for COI2a than COI1a or COI1c. Leaves were sprayed with 0.02% methyl jasmonate (MeJA) two hours before imaging. Scale bars = 50 μm. These experiments were repeated independently with similar results (Figure S4). JAZ protein names are as in Han and Luthe (2022).

Figure 4. Fall armyworm (*Spodoptera exigua*) and beet armyworm (*Spodoptera exigua*) caterpillar growth on *coronatine insensitive* (*Coi*) mutant and wildtype maize. (A) Locations of *Dissociation* (*Ds*) transposon insertions in *COI1* genes and *Mutator* (*Mu*) transposon insertions in *COI2* genes are marked with triangles. Insertions are located at 140, 2682, 344, 2342, -8, and 198 bp from the start codons of *COI1a*, *COI1d*, *COI1c*, *COI1b*, *COI2a*, and *COI2b*, respectively. Black bars represent exons, thin lines are introns, and white bars are non-coding regions of the genes. (B) Mass of ten-day-old *S. frugiperda* caterpillars on wildtype and *coi1-4x* maize. No significant difference ($P > 0.05$, *t*-test). (C) Mass of ten-day-old *S. exigua* caterpillars on wildtype and *coi1-4x*. *$P < 0.05$, *t*-test. (D) Mass of ten-day-old *S. frugiperda* on wildtype and *coi2* mutants. No significant difference (NS, $P > 0.05$), Dunnett's test relative to wildtype-*Mu*. All data are mean +/− s.e., numbers in bars indicate the number of caterpillars for each treatment. Raw data and statistical calculations are in Supplementary Dataset S18.

Figure 5. Plants with mutations in four maize *coronatine insensitive* (*Coi*) genes (*coi1-4x*) have impaired growth relative to the corresponding double mutants, *coi1a coi1d* and *coi1b coi1c*, and wildtype inbred line W22 maize. (A,B) Lengths of the third leaf (dashed arrows in Panel A) of

coi-4x and wildtype (WT) ten days after germination, N = 4 plants, mean ± se, two-tailed Student's *t*-test, *P < 0.05, **P < 0.01. Scale bar in Panel A = 10 cm. (C,D) Plant heights at 60 days after germination. Numbers in bars = number of plants of each genotype, mean +/− s.e., letters indicate significant differences, P < 0.05, ANOVA followed by Tukey's HSD test. Scale bar in Panel C = 22 cm. (E,F) Internode lengths were compared between four genotypes at 60 days post-germination. Positions of stem nodes are marked with white arrows in Panel B. *coi1-4x* N = 13 plants, wildtype N = 6 plants, *coi1a coi1d* and *coi1b coi1c* N = 5 plants, mean +/− s.e., ***P < 0.01, Dunnett's test relative to wildtype. Scale bar in Panel E = 22 cm. Raw data and statistical calculations are in Supplementary Dataset S18.

Figure 6. Plants with mutations in four maize *coronatine insensitive* (*Coi*) genes (*coi1-4x*) have striped leaves, decreased microelement levels, and reduced photosynthesis. (A) The striped leaf phenotype of the *coi1-4x* at 20 days post-germination compared to corresponding leaves from the double mutants and wildtype W22. Scale bar = 5 cm. (B) Microelements and (C) macroelements in 20-day-old seedlings, N = 7 plants, mean +/− s.e., letters indicate differences (P < 0.05) using Tukey's HSD test. (D) Leaf CO_2 assimilation rate (GasEX A) at 400 µmol mol^{-1} CO_2 and (E) the quantum yield of the photosystem II phytochemistry (*øPSII*) at 2000 µmol m^{-2} s^{-1} of actinic light were measured at 20 days after germination, respectively. Mean +/− s.e., n = 20 plants, two-tailed Student's *t*-test, **$P < 0.01$, ***$P < 0.001$. Raw data and statistical calculations are in Supplementary Dataset S18.

Figure 7. Heatmap of gene expression for 13,365 genes that were differentially regulated between two or more genotypes or between mock and methyl jasmonate (MeJA) induction. Color ranges from blue (minimum) to red (maximum) reads per million bp for each gene. The color key represents the normalized log(1+expression) ranging from blue (indicating low values) to red (indicating high values). Reads per million (RPM) data were transformed by log(1+RPM) prior to clustering. The color gradient in the heatmap reflects the Z scores, with red colors indicating higher-than-average expression levels (Z score > 0) and blue colors indicating lower-than-average expression levels (Z score < 0). Numerical data underlying the heatmap are in Supplementary Dataset S6.

Figure 8. Genes down-regulated in maize plants with mutations in four *coronatine insensitive* (*Coi*) genes (*coi1-4x*) encode two main groups of proteins, involved in C_4 photosynthesis and carbohydrate and cell wall metabolism. (A) Heatmap showing downregulated genes in *coi1-4x* relative to other genotypes, with or without methyl jasmonate (MeJA) treatment. Reads per million (RPM) data were transformed by log(1+RPM) prior to clustering. The color gradient in the heatmap reflects the Z scores, with red colors indicating higher-than-average expression levels (Z score > 0) and blue colors indicating lower-than-average expression levels (Z score < 0). (B) Down-regulated genes in *coi1-4x* were categorized into five functional groups. The list of the genes, color-coded by their functional group, as well as ordered based on their position in the heatmap, is presented in Supplementary Dataset S7.

Figure 9. Genes up-regulated in maize plants with mutations in four *coronatine insensitive* (*Coi*) genes (*coi1-4x*) encode proteins involved in phosphate regulation, lipid and carbohydrate metabolism, hormone regulation, and transcription. (A) Heatmap showing upregulated genes in *coi1-4x* relative to other genotypes, with or without methyl jasmonate (MeJA) treatment. The reads are transformed by log(1+expression) prior to clustering. (B) Up-regulated genes in *coi1-4x* were categorized into six functional groups. The list of the genes, color-coded by their functional group, as well as ordered based on their position in the heatmap, is presented in Supplementary Dataset S8.

Figure 10. Immunoblot analyses of maize DELLA proteins. The leaf total proteins from equal surface area (similar weight) leaves (fourth leaf, 20 days after germination) of wildtype maize inbred line W22 and a line with mutations in four *coronatine insensitive* (*Coi*) genes (*coi1-4x*) were analyzed by probing with antibodies that react with rice DELLA (SLENDER RICE 1 (SLR1)). The membrane was stained with Ponceau S as the loading control.

Figure 11. Maize DELLA (DWARF9) disappears from the nuclei upon coexpression with the maize coronatine insensitive (COI) proteins. Confocal images were taken after transiently expressing genes in *Nicotiana benthamiana* leaves for 48 hours. Labels on left indicate infiltrated genes for each row of images. GFP = green fluorescent protein, EGFP = enhanced green

fluorescent protein, RFP = red fluorescent protein. Protease inhibitor (bortezomib) was co-infiltrated in the bottom row. Scale bars = 50 μm.

Figure 12. Expression of the maize coronatine insensitive1 (COI1) proteins leads to proteasome-dependent degradation of maize DELLA in *Nicotiana benthamiana***.** (A) Nuclei showing the presence of the COI1a-EGFP (enhanced green fluorescent protein) and or DELLA-RFP (red fluorescent protein) were counted on confocal images from an experiment similar to Figure 11, with and without protease inhibitor. The bars are means +/− s.e. of N = 48 plants for the mock treatment and N = 71 plants treated with the proteasome inhibitor bortezomib (BTZ). Raw data and statistical calculations are in Supplementary Dataset S18. (B) Leaf tissue from the *N. benthamiana* plants expressing DELLA-RFP alone or with EGFP, COI1a-EGFP, or COI1c-EGFP (similar to those used in Figure 11), 48 hours after infiltration, was used for immunoblot analyses. Membranes were probed with antibodies that react with rice DELLA (SLENDER RICE 1 (SLR1)) and antibodies that react with GFP. The first membrane was stained with Ponceau S as the loading control. Non-specific binding of the SLR1 antibody to an unrelated protein was used as an extra loading control.

Figure 13. Effect of exogenous methyl jasmonate (MeJA) and gibberellic acid (GA) on growth of wildtype maize inbred line W22 and Plants with mutations in four maize *coronatine insensitive* (*Coi*) genes (*coi1-4x*). (A) Leaf discoloration symptoms at 30 days post-germination and after three weeks of JA treatment. Scale bar = 5 cm. (B) Plant heights at 23 days post-germination, with mock, MeJA, or GA treatments. Scale bar = 10 cm. (C) Plant heights at 30 days post-germination, with or without MeJA treatment. WT = wildtype. Scale bar = 10 cm. (D) Bar chart showing percent change in height relative to the mock-treated controls for the MeJA and GA treatments shown in panels B and C. N = 4, mean +/− s.e., two-tailed Student's *t*-test, $*P < 0.05$. Raw data and statistical calculations are in Supplementary Dataset S18.

Figure 14. Model for differential functions of maize coronatine insensitive (COI) proteins in regulating growth and defense. **(**A) Maize COI2 proteins are proposed to have the classical F-box domain protein function of Arabidopsis and tomato COIs. At low jasmonate-isoleucine (JA-Ile) concentrations (black arrow pointing down), jasmonate ZIM-domain (JAZ) proteins prevent activation of JA-Ile-responsive genes by MYC transcription factor (black right-angle arrow with

a red X). Higher abundance of JA-Ile (black arrow pointing up) leads to interactions between COI2 and JAZ proteins (arched gray arrow), causing addition of ubiquitin (U) to JAZ and degradation (blue arrow) by the 16S proteasome (red triangles). The absence of JAZ proteins leads to activation of transcription by MYC proteins and expression of defense-related genes (black right-angle arrow). (B) At low gibberellic acid (GA) levels (black arrow pointing down), DELLA is bound to PIF transcription factors, preventing transcription of GA-responsive genes (black right-angle arrow with a red X). At high GA levels, an as yet unknown maize F-box protein contributes to an E3 ligase complex (dashed blue arrow) that causes addition of ubiquitin (U) to DELLA and degradation (blue arrow) by the 16S proteasome, leading to activation of GA-responsive genes (black right-angle arrow). Based on the results that are presented, we propose that maize COI1 proteins directly or indirectly cause DELLA degradation (green triangles). In the *coi1-4x* mutant, there is no COI1, resulting in less DELLA degradation, less growth, and shorter stature of the maize plants.

References

Ahern KR, Deewatthanawong P, Schares J, Muszynski M, Weeks R, Vollbrecht E, Duvick J, Brendel VP, and Brutnell TP. Regional mutagenesis using *Dissociation* in maize. Methods. 2009:**49**(3):248–254. https://doi.org/10.1016/j.ymeth.2009.04.009

Al-Zahrani W, Bafeel SO, and El-Zohri M. Jasmonates mediate plant defense responses to *Spodoptera exigua* herbivory in tomato and maize foliage. Plant Signal Behav. 2020:**15**(5):1746898. https://doi.org/10.1080/15592324.2020.1746898

An L, Ahmad RM, Ren H, Qin J, and Yan Y. Jasmonate signal receptor gene family *ZmCOIs* restore male fertility and defense response of *Arabidopsis* mutant *coi1-1*. J Plant Growth Regul. 2019:**38**(2):479–493. https://doi.org/10.1007/s00344-018-9863-2

Berthold F, Roujol D, Hemmer C, Jamet E, Ritzenthaler C, Hoffmann L, and Schmitt-Keichinger C. Inside or outside? A new collection of Gateway vectors allowing plant protein subcellular localization or over-expression. Plasmid. 2019:**105**. https://doi.org/10.1016/j.plasmid.2019.102436

Blätke MA and Bräutigam A. Evolution of C4 photosynthesis predicted by constraint-based modelling. eLife. 2019:**8**:e49305. https://doi.org/10.7554/eLife.49305

Bolger A, Scossa F, Bolger ME, Lanz C, Maumus F, Tohge T, Quesneville H, Alseekh S, Sørensen I, Lichtenstein G, et al. The genome of the stress-tolerant wild tomato species Solanum pennellii. Nature Genetics. 2014:**46**(9):1034–1038. https://doi.org/10.1038/ng.3046

Borrego EJ and Kolomiets MV. Synthesis and functions of jasmonates in maize. Plants. 2016:**5**(4):41. https://doi.org/10.3390/plants5040041

Burgess SJ, Granero-Moya I, Grangé-Guermente MJ, Boursnell C, Terry MJ, and Hibberd JM. Ancestral light and chloroplast regulation form the foundations for C4 gene expression. Nature Plants. 2016:**2**:16161. https://doi.org/10.1038/nplants.2016.161

Campos ML, Yoshida Y, Major IT, Ferreira D de O, Weraduwage SM, Froehlich JE, Johnson BF, Kramer DM, Jander G, Sharkey TD, et al. Rewiring of jasmonate and phytochrome B signalling uncouples plant growth-defense tradeoffs. Nature Communications. 2016:**7**:12570. https://doi.org/10.1038/ncomms12570

Cantu VA, Sadural J, and Edwards R. PRINSEQ++, a multi-threaded tool for fast 1 and efficient quality control and 2 preprocessing of sequencing datasets. PeerJ. 2019:**7**:e27553v1. https://doi.org/10.7287/peerj.preprints.27553v1

Cassani E, Bertolini E, Badone FC, Landoni M, Gavina D, Sirizzotti A, and Pilu R. Characterization of the first dominant dwarf maize mutant carrying a single amino acid insertion in the VHYNP domain of the *dwarf8* gene. Molecular Breeding. 2009:**24**(4):375–385. https://doi.org/10.1007/s11032-009-9298-3

Chen R, Fan Y, Yan H, Zhou H, Zhou Z, Weng M, Huang X, Lakshmanan P, Li Y, Qiu L, et al. Enhanced activity ofgenes associated with photosynthesis, phytohormone metabolism and cell wall

synthesis Is involved in gibberellin-mediated sugarcane internode growth. Frontiers in Genetics. 2020:**11**:570094. https://doi.org/10.3389/fgene.2020.570094

Chini A, Fonseca S, Fernández G, Adie B, Chico JM, Lorenzo O, García-Casado G, López-Vidriero I, Lozano FM, Ponce MR, et al. The JAZ family of repressors is the missing link in jasmonate signalling. Nature. 2007:**448**(7154):666–671. https://doi.org/10.1038/nature06006

Chini A, Monte I, Zamarreño AM, García-Mina JM, and Solano R. Evolution of the jasmonate ligands and their biosynthetic pathways. New Phytol. 2023:**238**(5):2236–2246. https://doi.org/10.1111/nph.18891

Christensen SA, Huffaker A, Kaplan F, Sims J, Ziemann S, Doehlemann G, Ji L, Schmitz RJ, Kolomiets MV, Alborn HT, et al. Maize death acids, 9-lipoxygenase-derived cyclopente(a)nones, display activity as cytotoxic phytoalexins and transcriptional mediators. Proceedings of the National Academy of Sciences of the United States of America. 2015:**112**(36):11407–11412. https://doi.org/10.1073/pnas.1511131112

Christin P-A, Osborne CP, Chatelet DS, Columbus JT, Besnard G, Hodkinson TR, Garrison LM, Vorontsova MS, and Edwards EJ. Anatomical enablers and the evolution of C4 photosynthesis in grasses. PNAS. 2013:**110**(4):1381–1386. https://doi.org/10.5061/dryad.6j9r7

Chuang WP, Herde M, Ray S, Castano-Duque L, Howe GA, and Luthe DS. Caterpillar attack triggers accumulation of the toxic maize protein RIP2. New Phytologist. 2014:**201**(3):928–939. https://doi.org/10.1111/nph.12581

Cobb JN, Chen C, Shi Y, Maron LG, Liu D, Rutzke M, Greenberg A, Craft E, Shaff J, Paul E, et al. Genetic architecture of root and shoot ionomes in rice (*Oryza sativa* L.). Theoretical and Applied Genetics. 2021:**134**(8):2613–2637. https://doi.org/10.1007/s00122-021-03848-5

Curie C, Panaviene Z, Loulergue C, Dellaporta SL, Briat J-F, and Walker EL. Maize yellow stripe1 encodes a membrane protein directly involved in Fe(III) uptake. Nature. 2001:**409**:346–349.

Dill A, Thomas SG, Hu J, Steber CM, and Sun TP. The arabidopsis F-box protein SLEEPY1 targets gibberellin signaling repressors for gibberellin-induced degradation. Plant Cell. 2004:**16**(6):1392–1405. https://doi.org/10.1105/tpc.020958

Ding G, Lei GJ, Yamaji N, Yokosho K, Mitani-Ueno N, Huang S, and Ma JF. Vascular cambium-localized AtSPDT mediates xylem-to-phloem transfer of phosphorus for its preferential distribution in Arabidopsis. Molecular Plant. 2020:**13**(1):99–111. https://doi.org/10.1016/j.molp.2019.10.002

Dombrecht B, Gang PX, Sprague SJ, Kirkegaard JA, Ross JJ, Reid JB, Fitt GP, Sewelam N, Schenk PM, Manners JM, et al. MYC2 differentially modulates diverse jasmonate-dependent functions in Arabidopsis. Plant Cell. 2007:**19**(7):2225–2245. https://doi.org/10.1105/tpc.106.048017

Dong J and Hudson ME. WI12Rhg1 interacts with DELLAs and mediates soybean cyst nematode resistance through hormone pathways. Plant Biotechnology Journal. 2022:**20**(2):283–296. https://doi.org/10.1111/pbi.13709

Drozak A and Romanowska E. Acclimation of mesophyll and bundle sheath chloroplasts of maize to different irradiances during growth. Biochimica et Biophysica Acta - Bioenergetics. 2006:**1757**(11):1539–1546. https://doi.org/10.1016/j.bbabio.2006.09.001

El Zawily AM, Schwarzländer M, Finkemeier I, Johnston IG, Benamar A, Cao Y, Gissot C, Meyer AJ, Wilson K, Datla R, et al. FRIENDLY regulates mitochondrial distribution, fusion, and quality control in Arabidopsis. Plant Physiology. 2014:**166**(2):808–828. https://doi.org/10.1104/pp.114.243824

Falcioni R, Moriwaki T, de Oliveira DM, Andreotti GC, de Souza LA, dos Santos WD, Bonato CM, and Antunes WC. Increased gibberellins and light levels promotes cell wall thickness and enhance lignin deposition in xylem fibers. Frontiers in Plant Science. 2018:**9**:1391. https://doi.org/10.3389/fpls.2018.01391

Feiz L, Williams-Carrier R, Wostrikoff K, Belcher S, Barkan A, and Stern DB. Ribulose-1,5-bis-phosphate carboxylase/oxygenase accumulation factor1 is required for holoenzyme assembly in maize. Plant Cell. 2012:**24**(8):3435–3446. https://doi.org/10.1105/tpc.112.102012

Feys BJF, Benedetti,' CE, Penfold CN, and Turner2 JG. Arabidopsis mutants selected for resistance to the phytotoxin coronatine are male sterile, insensitive to methyl jasmonate, and resistant to a bacterial pathogen.

Fonseca S, Chini A, Hamberg M, Adie B, Porzel A, Kramell R, Miersch O, Wasternack C, and Solano R. (+)-7-iso-Jasmonoyl-L-isoleucine is the endogenous bioactive jasmonate. Nature Chemical Biology. 2009:**5**(5):344–350. https://doi.org/10.1038/nchembio.161

Foy CD and Barber SA. Magnesium deficiency and corn yield on two acid Indiana soils. Soil Science Society of America Journal. 1958:**22**(2):145–148. https://doi.org/10.2136/sssaj1958.03615995002200020014x

Fujioka S, Yamane H, Spray CR, Katsumit M, Phinney B 0, Gaskin ¶ P, Macmillan ¶ J, and Takahashiii N. The dominant non-gibberellin-responding dwarf mutant (D8) of maize accumulates native gibberellins. PNAS. 1988:**85**:9031–9035.

Gale MD and Marshall GA. Insensitivity to gibberellin in dwarf wheats. Annals of Botany. 1973:**4**:729–764.

Gomi K, Sasaki A, Itoh H, Ueguchi-Tanaka M, Ashikari M, Kitano H, and Matsuoka M. GID2, an F-box subunit of the SCF E3 complex, specifically interacts with phosphorylated SLR1 protein and regulates the gibberellin-dependent degradation of SLR1 in rice. Plant Journal. 2004:**37**(4):626–634. https://doi.org/10.1111/j.1365-313X.2003.01990.x

Gray WM, Kepinski[23] S, Rouse[3] D, Leyser[3] O, and Estelle M. Auxin regulates SCF TIR1-dependent degradation of AUX/IAA proteins. Nature. 2001:**414**:271–276.

Han Y and Luthe D. Identification and evolution analysis of the JAZ gene family in maize. BMC Genomics. 2021:**22**(1):256. https://doi.org/10.1186/s12864-021-07522-4

He Y, Liu C, Zhu L, Fu M, Sun Y, Zeng H, Brunetti C, Komatsu S, and River Y. Jasmonic acid plays a pivotal role in pollen development and fertility regulation in different types of P(T)GMS rice lines. International Journal of Molecular Sciences. 2021:**22**:7926. https://doi.org/10.3390/ijms

Hibberd JM and Quick WP. Characteristics of C4 photosynthesis in stems and petioles of C3 flowering plants. Nature. 2002:**415**:451–454.

Hoang DT, Chernomor O, von Haeseler A, Minh BQ, and Vinh LS. UFBoot2: Improving the Ultrafast Bootstrap Approximation. Mol Biol Evol. 2018:**35**(2):518–522. https://doi.org/10.1093/molbev/msx281

Hou X, Lee LYC, Xia K, Yan Y, and Yu H. DELLAs modulate jasmonate signaling via competitive binding to JAZs. Developmental Cell. 2010:**19**(6):884–894. https://doi.org/10.1016/j.devcel.2010.10.024

Hu J, Israeli A, Ori N, and Sun TP. The interaction between DELLA and ARF/IAA mediates crosstalk between gibberellin and auxin signaling to control fruit initiation in tomato. Plant Cell. 2018:**30**(8):1710–1728. https://doi.org/10.1105/tpc.18.00363

Hu J, Su H, Cao H, Wei H, Fu X, Jiang X, Song Q, He X, Xu C, and Luo K. AUXIN RESPONSE FACTOR7 integrates gibberellin and auxin signaling via interactions between della and AUX/IAA proteins to regulate cambial activity in poplar. Plant Cell. 2022:**34**(7):2688–2707. https://doi.org/10.1093/plcell/koac107

Hua L, Stevenson SR, Reyna-Llorens I, Xiong H, Kopriva S, and Hibberd JM. The bundle sheath of rice is conditioned to play an active role in water transport as well as sulfur assimilation and jasmonic acid synthesis. Plant Journal. 2021:**107**(1):268–286. https://doi.org/10.1111/tpj.15292

Inagaki H, Hayashi K, Takaoka Y, Ito H, Fukumoto Y, Yajima-Nakagawa A, Chen X, Shimosato-Nonaka M, Hassett E, Hatakeyama K, et al. Genome Editing Reveals Both the Crucial Role of OsCOI2 in Jasmonate Signaling and the Functional Diversity of COI1 Homologs in Rice. Plant and Cell Physiology. 2022. https://doi.org/10.1093/pcp/pcac166

Jing H, Korasick DA, Emenecker RJ, Morffy N, Wilkinson EG, Powers SK, and Strader LC. Regulation of AUXIN RESPONSE FACTOR condensation and nucleo-cytoplasmic partitioning. Nat Commun. 2022:**13**(1):4015. https://doi.org/10.1038/s41467-022-31628-2

Kim D, Paggi JM, Park C, Bennett C, and Salzberg SL. Graph-based genome alignment and genotyping with HISAT2 and HISAT-genotype. Nature Biotechnology. 2019:**37**(8):907–915. https://doi.org/10.1038/s41587-019-0201-4

Kim EH, Lee Y, and Kim HU. Fibrillin 5 Is essential for plastoquinone-9 biosynthesis by binding to solanesyl diphosphate synthases in arabidopsis. Plant Cell. 2015:**27**(10):2956–2971. https://doi.org/10.1105/tpc.15.00707

Kirschner GK. A FRIENDLY connection: how mRNAs get recruited to the mitochondrial surface. Plant Journal. 2022:**112**(2):307–308. https://doi.org/10.1111/tpj.15992

Kong L, Wu J, Lu L, Xu Y, and Zhou X. Interaction between rice stripe virus disease-specific protein and host PsbP enhances virus symptoms. Molecular Plant. 2014:**7**(4):691–708. https://doi.org/10.1093/mp/sst158

Kremling KAG, Chen SY, Su MH, Lepak NK, Romay MC, Swarts KL, Lu F, Lorant A, Bradbury PJ, and Buckler ES. Dysregulation of expression correlates with rare-allele burden and fitness loss in maize. Nature. 2018:**555**(7697):520–523. https://doi.org/10.1038/nature25966

Kroeger TS, Watkins KP, Friso G, Van Wijk KJ, and Barkan A. A plant-specific RNA-binding domain revealed through analysis of chloroplast group II intron splicing. Proceedings of the National Academy of Sciences of the United States of America. 2009:**106**(11):4537–4542. https://doi.org/10.1073/pnas.0812503106

Langmead B, Trapnell C, Pop M, and Salzberg SL. Ultrafast and memory-efficient alignment of short DNA sequences to the human genome. Genome Biology. 2009:**10**(3). https://doi.org/10.1186/gb-2009-10-3-r25

Lawit SJ, Wych HM, Xu D, Kundu S, and Tomes DT. Maize della proteins dwarf plant8 and dwarf plant9 as modulators of plant development. Plant and Cell Physiology. 2010:**51**(11):1854–1868. https://doi.org/10.1093/pcp/pcq153

Lee K, Lehmann M, Paul MV, Wang L, Luckner M, Wanner G, Geigenberger P, Leister D, and Kleine T. Lack of FIBRILLIN6 in *Arabidopsis thaliana* affects light acclimation and sulfate metabolism. New Phytologist. 2020:**225**(4):1715–1731. https://doi.org/10.1111/nph.16246

Li P, Ponnala L, Gandotra N, Wang L, Si Y, Tausta SL, Kebrom TH, Provart N, Patel R, Myers CR, et al. The developmental dynamics of the maize leaf transcriptome. Nature Genetics. 2010:**42**(12):1060–1067. https://doi.org/10.1038/ng.703

Liu P, McCarty DR, and Koch KE. Transposon mutagenesis and analysis of mutants in UniformMu maize (*Zea mays*). Curr Protoc Plant Biol. 2016a:**1**(3):451–465. https://doi.org/10.1002/cppb.20029

Liu X, Hu P, Huang M, Tang Y, Li Y, Li L, and Hou X. The NF-YC-RGL2 module integrates GA and ABA signalling to regulate seed germination in Arabidopsis. Nature Communications. 2016b:**7**:12768. https://doi.org/10.1038/ncomms12768

Liu X, Zhang H, Zhao Y, Feng Z, Li Q, Yang HQ, Luan S, Li J, and He ZH. Auxin controls seed dormancy through stimulation of abscisic acid signaling by inducing ARF-mediated ABI3 activation in Arabidopsis. PNAS. 2013:**110**(38):15485–15490. https://doi.org/10.1073/pnas.1304651110

Love MI, Huber W, and Anders S. Moderated estimation of fold change and dispersion for RNA-seq data with DESeq2. Genome Biology. 2014:**15**(12):550. https://doi.org/10.1186/s13059-014-0550-8

Ma L, Sun Y, Ruan X, Huang P-C, Wang S, Li S, Zhou Y, Wang F, Cao Y, Wang Q, et al. Genome-wide characterization of jasmonates signaling components reveals the essential role of ZmCOI1a-ZmJAZ15 action module in regulating maize immunity to Gibberella stalk rot. International Journal of Molecular Sciences. 2021:**22**(2):870. https://doi.org/10.3390/ijms22020870

Machado RAR, Baldwin IT, and Erb M. Herbivory-induced jasmonates constrain plant sugar accumulation and growth by antagonizing gibberellin signaling and not by promoting secondary metabolite production. New Phytologist. 2017:**215**(2):803–812. https://doi.org/10.1111/nph.14597

Mattiello EM, Ruiz HA, Neves JCL, Ventrella MC, and Araújo WL. Zinc deficiency affects physiological and anatomical characteristics in maize leaves. Journal of Plant Physiology. 2015:**183**:138–143. https://doi.org/10.1016/j.jplph.2015.05.014

McConn M, Creelman RA, Bell E, Mullet JE, and Browse J. Jasmonate is essential for insect defense in Arabidopsis. PNAS. 1997:**94**:5473–5477.

Minh BQ, Schmidt HA, Chernomor O, Schrempf D, Woodhams MD, von Haeseler A, and Lanfear R. IQ-TREE 2: New models and efficient methods for phylogenetic inference in the genomic era. Molecular Biology and Evolution. 2020:**37**(5):1530–1534. https://doi.org/10.1093/molbev/msaa015

Monte I, Caballero J, Zamarreño AM, Fernández-Barbero G, García-Mina JM, and Solano R. JAZ is essential for ligand specificity of the COI1/JAZ co-receptor. Proc Natl Acad Sci U S A. 2022:**119**(49):e2212155119. https://doi.org/10.1073/pnas.2212155119

Monte I, Ishida S, Zamarreño AM, Hamberg M, Franco-Zorrilla JM, García-Casado G, Gouhier-Darimont C, Reymond P, Takahashi K, García-Mina JM, et al. Ligand-receptor co-evolution shaped the jasmonate pathway in land plants. Nat Chem Biol. 2018:**14**(5):480–488. https://doi.org/10.1038/s41589-018-0033-4

Nakamura N, Iwano M, Havaux M, Yokota A, and Munekage YN. Promotion of cyclic electron transport around photosystem I during the evolution of NADP-malic enzyme-type C4 photosynthesis in the genus Flaveria. New Phytologist. 2013:**199**(3):832–842. https://doi.org/10.1111/nph.12296

Navarro L, Bari R, Achard P, Lisón P, Nemri A, Harberd NP, and Jones JDG. DELLAs control plant immune responses by modulating the balance of jasmonic acid and salicylic acid signaling. Current Biology. 2008:**18**(9):650–655. https://doi.org/10.1016/j.cub.2008.03.060

Paciorek T, Chiapelli BJ, Wang JY, Paciorek M, Yang H, Sant A, Val DL, Boddu J, Liu K, Gu C, et al. Targeted suppression of gibberellin biosynthetic genes *ZmGA20ox3* and *ZmGA20ox5* produces a short stature maize ideotype. Plant Biotechnology Journal. 2022:**20**(6):1140–1153. https://doi.org/10.1111/pbi.13797

Pérez AC and Goossens A. Jasmonate signalling: A copycat of auxin signalling? Plant, Cell and Environment. 2013:**36**(12):2071–2084. https://doi.org/10.1111/pce.12121

Powers SK, Holehouse AS, Korasick DA, Schreiber KH, Clark NM, Jing H, Emenecker R, Han S, Tycksen E, Hwang I, et al. Nucleo-cytoplasmic partitioning of ARF proteins controls auxin responses in *Arabidopsis thaliana*. Molecular Cell. 2019:**76**(1):177–190. https://doi.org/10.1016/j.molcel.2019.06.044

Pratiwi P, Tanaka G, Takahashi T, Xie X, Yoneyama K, Matsuura H, and Takahashi K. Identification of jasmonic acid and jasmonoyl-isoleucine, and characterization of AOS, AOC, OPR and JAR1 in the

model lycophyte *Selaginella moellendorffii*. Plant Cell Physiol. 2017:**58**(4):789–801. https://doi.org/10.1093/pcp/pcx031

Qi T, Huang H, Wu D, Yan J, Qi Y, Song S, and Xie D. Arabidopsis DELLA and JAZ proteins bind the WD-Repeat/ bHLH/MYB complex to modulate gibberellin and jasmonate signaling synergy. Plant Cell. 2014:**26**(3):1118–1133. https://doi.org/10.1105/tpc.113.121731

Qi X, Guo S, Wang D, Zhong Y, Chen M, Chen C, Cheng D, Liu Z, An T, Li J, et al. ZmCOI2a and ZmCOI2b redundantly regulate anther dehiscence and gametophytic male fertility in maize. Plant Journal. 2022:**110**(3):849–862. https://doi.org/10.1111/tpj.15708

Quast C, Pruesse E, Yilmaz P, Gerken J, Schweer T, Yarza P, Peplies J, and Glöckner FO. The SILVA ribosomal RNA gene database project: Improved data processing and web-based tools. Nucleic Acids Research. 2013:**41**(D1):D590–D596. https://doi.org/10.1093/nar/gks1219

Ranwala AP and Miller WB. Gibberellin-mediated changes in carbohydrate metabolism during flower stalk elongation in tulips. Plant Growth Regulation. 2008:**55**(3):241–248. https://doi.org/10.1007/s10725-008-9280-9

Ren C, Pan J, Peng W, Genschik P, Hobbie L, Hellmann H, Estelle M, Gao B, Peng J, Sun C, et al. Point mutations in Arabidopsis *Cullin1* reveal its essential role in jasmonate response. Plant Journal. 2005:**42**(4):514–524. https://doi.org/10.1111/j.1365-313X.2005.02394.x

Reyt G, Ramakrishna P, Salas-González I, Fujita S, Love A, Tiemessen D, Lapierre C, Morreel K, Calvo-Polanco M, Flis P, et al. Two chemically distinct root lignin barriers control solute and water balance. Nature Communications. 2021:**12**(1). https://doi.org/10.1038/s41467-021-22550-0

Settles AM, Holding DR, Tan BC, Latshaw SP, Liu J, Suzuki M, Li L, O'Brien BA, Fajardo DS, Wroclawska E, et al. Sequence-indexed mutations in maize using the UniformMu transposon-tagging population. BMC Genomics. 2007:**8**:116. https://doi.org/10.1186/1471-2164-8-116

Sheard LB, Tan X, Mao H, Withers J, Ben-Nissan G, Hinds TR, Kobayashi Y, Hsu FF, Sharon M, Browse J, et al. Jasmonate perception by inositol-phosphate-potentiated COI1-JAZ co-receptor. Nature. 2010:**468**(7322):400–407. https://doi.org/10.1038/nature09430

Shikha D, Jakhar P, and Satbhai SB. Role of jasmonate signaling in the regulation of plant responses to nutrient deficiency. Journal of Experimental Botany. 2022:**74**:1221–1243. https://doi.org/10.1093/jxb/erac387

Sievers F, Wilm A, Dineen D, Gibson TJ, Karplus K, Li W, Lopez R, McWilliam H, Remmert M, Söding J, et al. Fast, scalable generation of high-quality protein multiple sequence alignments using Clustal Omega. Mol Syst Biol. 2011:**7**:539. https://doi.org/10.1038/msb.2011.75

Simon R and Starlinger P. Transposable element *Ds2* of *Zea mays* influences polyadenylation and splice site selection. Mol Gen Genet. 1987:**209**(1):198–199. https://doi.org/10.1007/BF00329859

Singh DK, Maximova SN, Jensen PJ, Lehman BL, Ngugi HK, and McNellis TW. FIBRILLIN4 is required for plastoglobule development and stress resistance in apple and arabidopsis. Plant Physiology. 2010:**154**(3):1281–1293. https://doi.org/10.1104/pp.110.164095

Springer NM, Anderson SN, Andorf CM, Ahern KR, Bai F, Barad O, Barbazuk WB, Bass HW, Baruch K, Ben-Zvi G, et al. The maize W22 genome provides a foundation for functional genomics and transposon biology. Nature Genetics. 2018:**50**(9):1282–1288. https://doi.org/10.1038/s41588-018-0158-0

Stintzi A and Browse J. The *Arabidopsis* male-sterile mutant, *opr3*, lacks the 12-oxophytodienoic acid reductase required for jasmonate synthesis. PNAS. 2000:**97**:10625–10630.

Strader LC, Ritchie S, Soule JD, McGinnis KM, Steber CM, and Ryan CA. Recessive-interfering mutations in the gibberellin signaling gene *SLEEPY1* are rescued by overexpression of its homologue, *SNEEZY*. PNAS. 2004:**101**:12771–12776.

Takabayashi A, Kishine M, Asada K, Endo T, and Sato F. Differential use of two cyclic electron flows around photosystem I for driving CO 2-concentration mechanism in C4 photosynthesis. PNAS. 2005:**102**:16898–16903.

Takahashi H, Yamazaki M, Sasakura N, Watanabe A, Leustek T, De Almeida Engler J, Engler G, Van Montagu M, and Saito K. Regulation of sulfur assimilation in higher plants: A sulfate transporter induced in sulfate-starved roots plays a central role in *Arabidopsis thaliana*. PNAS. 1997:**94**:11102–11107.

Tal L, Gil MXA, Guercio AM, and Shabek N. Structural aspects of plant hormone signal perception and regulation by ubiquitin ligases. Plant Physiology. 2020:**182**(4):1537–1554. https://doi.org/10.1104/PP.19.01282

Tamura K, Stecher G, and Kumar S. MEGA11: Molecular Evolutionary Genetics Analysis Version 11. Mol Biol Evol. 2021:**38**(7):3022–3027. https://doi.org/10.1093/molbev/msab120

Thines B, Katsir L, Melotto M, Niu Y, Mandaokar A, Liu G, Nomura K, He SY, Howe GA, and Browse J. JAZ repressor proteins are targets of the SCFCOI1 complex during jasmonate signalling. Nature. 2007:**448**(7154):661–665. https://doi.org/10.1038/nature05960

Thoiron S, Pascal N, and Briat JF. Impact of iron deficiency and iron re-supply during the early stages of vegetative development in maize (*Zea mays* L.). Plant, Cell and Environment. 1997:**20**(8):1051–1060. https://doi.org/10.1111/j.1365-3040.1997.tb00681.x

Trang Nguyen H, Cheaib M, Fournel M, Rios M, Gantet P, Guyomarc S, Riemann M, Heitz T, and Petitot A-S. Genetic analysis of the rice jasmonate receptors reveals specialized function for OsCOI2. BioRxiv. https://doi.org/10.1101/2022.12.12.520024

Ueguchi-Tanaka M, Hirano K, Hasegawa Y, Kitano H, and Matsuoka M. Release of the repressive activity of rice DELLA protein SLR1 by gibberellin does not require SLR1 degradation in the gid2 mutant. Plant Cell. 2008:**20**(9):2437–2446. https://doi.org/10.1105/tpc.108.061648

Van De Mortel JE, Villanueva LA, Schat H, Kwekkeboom J, Coughlan S, Moerland PD, Van Themaat EVL, Koornneef M, and Aarts MGM. Large expression differences in genes for iron and zinc homeostasis, stress response, and lignin biosynthesis distinguish roots of Arabidopsis thaliana and the related metal hyperaccumulator Thlaspi caerulescens. Plant Physiology. 2006:**142**(3):1127–1147. https://doi.org/10.1104/pp.106.082073

Vellosillo T, Aguilera V, Marcos R, Bartsch M, Vicente J, Cascón T, Hamberg M, and Castresana C. Defense activated by 9-lipoxygenase-derived oxylipins requires specific mitochondrial proteins. Plant Physiology. 2013:**161**(2):617–627. https://doi.org/10.1104/pp.112.207514

Vellosillo T, Martínez M, López MA, Vicente J, Cascón T, Dolan L, Hamberg M, and Castresana C. Oxylipins produced by the 9-lipoxygenase pathway in Arabidopsis regulate lateral root development and defense responses through a specific signaling cascade. Plant Cell. 2007:**19**(3):831–846. https://doi.org/10.1105/tpc.106.046052

Vijayan P, Shockey J, Lévesque CA, Cook RJ, and Browse J. A role for jasmonate in pathogen defense of Arabidopsis. PNAS. 1998:**95**:7209–7214.

de Vleesschauwer D, Seifi HS, Filipe O, Haeck A, Huu SN, Demeestere K, and Höfte M. The DELLA protein SLR1 integrates and amplifies salicylic acid- and jasmonic acid-dependent innate immunity in rice. Plant Physiology. 2016:**170**(3):1831–1847. https://doi.org/10.1104/pp.15.01515

Vollbrecht E, Duvick J, Schares JP, Ahern KR, Deewatthanawong P, Xu L, Conrad LJ, Kikuchi K, Kubinec TA, Hall BD, et al. Genome-wide distribution of transposed *Dissociation* elements in maize. Plant Cell. 2010:**22**(6):1667–1685. https://doi.org/10.1105/tpc.109.073452

Walley JW, Sartor RC, Shen Z, Schmitz RJ, Wu KJ, Urich MA, Nery JR, Smith LG, Schnable JC, Ecker JR, et al. Integration of omic networks in a developmental atlas of maize. Science. 2016:**353**(6301):814–818. https://doi.org/10.1126/science.aag1125

Wang J, Song L, Gong X, Xu J, and Li M. Functions of jasmonic acid in plant regulation and response to abiotic stress. International Journal of Molecular Sciences. 2020:**21**(4):1446. https://doi.org/10.3390/ijms21041446

Wang X, Chen Y, Liu S, Fu W, Zhuang Y, Xu J, Lou Y, Baldwin IT, and Li R. Functional dissection of rice jasmonate receptors involved in development and defense. New Phytologist. 2023. https://doi.org/10.1111/nph.18860

Wasilewska-Dębowska W, Zienkiewicz M, and Drozak A. How Light Reactions of Photosynthesis in C4 Plants Are Optimized and Protected under High Light Conditions. International Journal of Molecular Sciences. 2022:**23**(7):3626. https://doi.org/10.3390/ijms23073626

Wild M, Davière JM, Cheminant S, Regnault T, Baumberger N, Heintz D, Baltz R, Genschik P, and Achard P. The Arabidopsis DELLA RGA-LIKE3 is a direct target of MYC2 and modulates jasmonate signaling responses. Plant Cell. 2012:**24**(8):3307–3319. https://doi.org/10.1105/tpc.112.101428

Withers J, Yao J, Mecey C, Howe GA, Melotto M, and He SY. Transcription factor-dependent nuclear localization of a transcriptional repressor in jasmonate hormone signaling. PNAS. 2012:**109**(49):20148–20153. https://doi.org/10.1073/pnas.1210054109

Xie D-X, Feys B, James S, Nieto-Rostro M, and Turner J. COI1: An Arabidopsis gene required for jasmonate-regulated defense and fertility. Science. 1998:**280**:1091–1094.

Xu L, Liu F, Lechner E, Genschik P, Crosby WL, Ma H, Peng W, Huang D, and Xie D. The SCF COI1 ubiquitin-ligase complexes are required for jasmonate response in Arabidopsis. The Plant Cell. 2002:**14**(8):1919–1935. https://doi.org/10.1105/tpc.003368

Yamamoto H, Peng L, Fukao Y, and Shikanai T. An Src homology 3 domain-like fold protein forms a ferredoxin binding site for the chloroplast NADH dehydrogenase-like complex in Arabidopsis. Plant Cell. 2011:**23**(4):1480–1493. https://doi.org/10.1105/tpc.110.080291

Yan Y, Christensen S, Isakeit T, Engelberth J, Meeley R, Hayward A, Emery RJ, and Kolomiets MV. Disruption of OPR7 and OPR8 reveals the versatile functions of jasmonic acid in maize development and defense. Plant Cell. 2012:**24**(4):1420–1436. https://doi.org/10.1105/tpc.111.094151

Yang DL, Yao J, Mei CS, Tong XH, Zeng LJ, Li Q, Xiao LT, Sun TP, Li J, Deng XW, et al. Plant hormone jasmonate prioritizes defense over growth by interfering with gibberellin signaling cascade. PNAS. 2012:**109**(19):E1192–E1200. https://doi.org/10.1073/pnas.1201616109

Zander M, Lewsey MG, Clark NM, Yin L, Bartlett A, Saldierna Guzmán JP, Hann E, Langford AE, Jow B, Wise A, et al. Integrated multi-omics framework of the plant response to jasmonic acid. Nature Plants. 2020:**6**(3):290–302. https://doi.org/10.1038/s41477-020-0605-7

Zhang F, Yao J, Ke J, Zhang L, Lam VQ, Xin XF, Zhou XE, Chen J, Brunzelle J, Griffin PR, et al. Structural basis of JAZ repression of MYC transcription factors in jasmonate signalling. Nature. 2015:**525**(7568):269–273. https://doi.org/10.1038/nature14661

Zhou H, Helliker BR, Huber M, Dicks A, Akçay E, Designed EA, and Performed EA. C4 photosynthesis and climate through the lens of optimality. PNAS. 2018:**115**(47):12057–12062. https://doi.org/10.4231/R7PR7T75

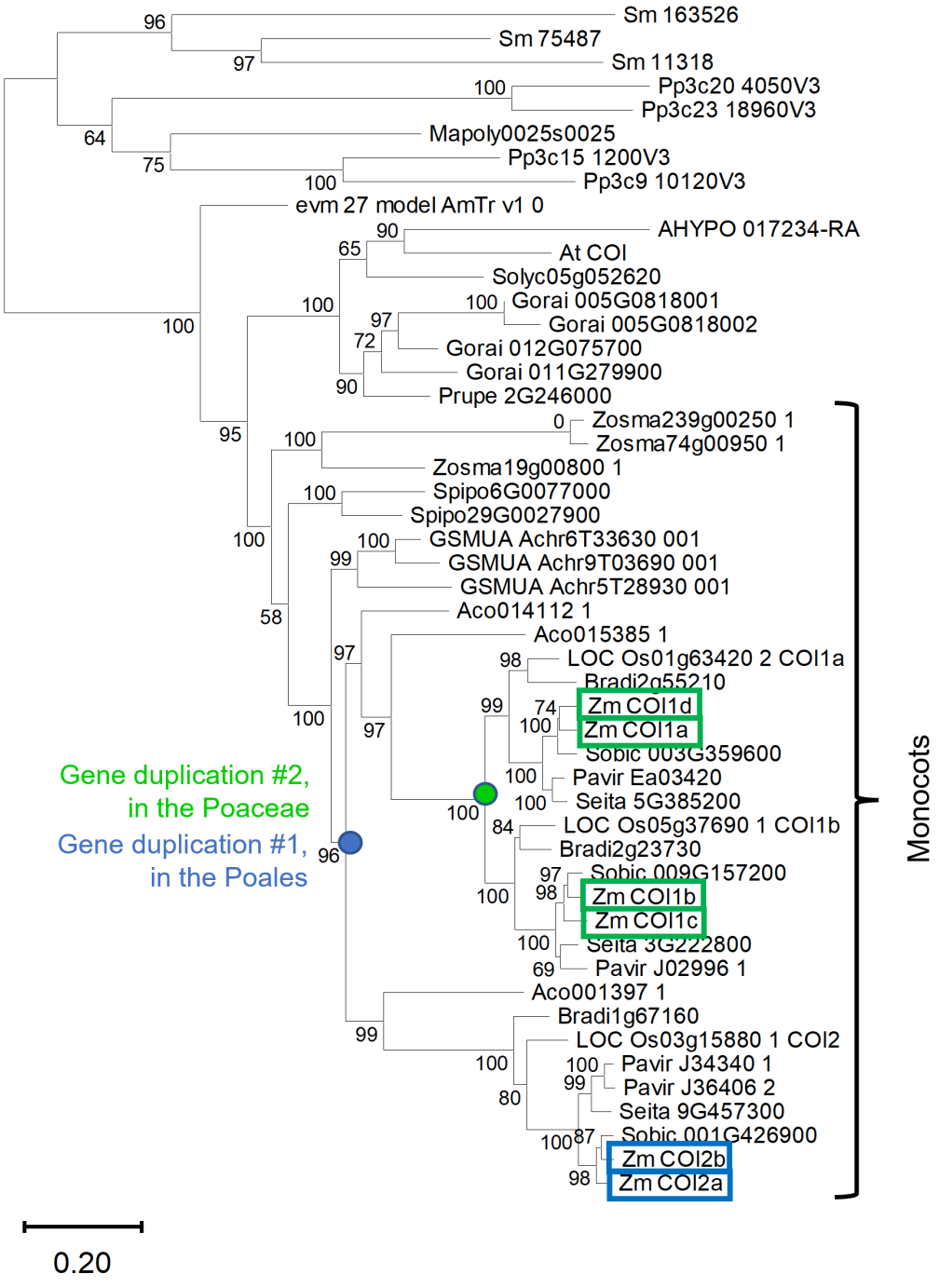

Figure 1. The maize genome encodes six coronatine insensitive (COI) proteins. The sequences of six maize COI proteins, along with their paralogs from other species, were obtained from Phytozome (https://phytozome-next.jgi.doe.gov/). Two predicted duplication events are marked. Four maize COI1 proteins are marked with green boxes. Two maize COI2 proteins are marked with blue boxes. The species in the Poaceae have three COI protein clades, two containing COI1 proteins (exemplified by maize COI1a and COI1d, and COI1b and COI1c, respectively) and one containing COI2 proteins (exemplified by maize COI2a and COI2b). The protein sequence alignment and species names are presented in Supplementary Dataset S2. A machine-readable (Newick Format) version of the tree is in Supplementary File S1. FASTA sequences of all proteins are in Supplementary File S2. The maximum likelihood, midpoint-rooted tree was produced with IQ-Tree and visualized with MEGA11. Bootstrap values are based on 1000 replicates. Scale bar indicates substitutions per site.

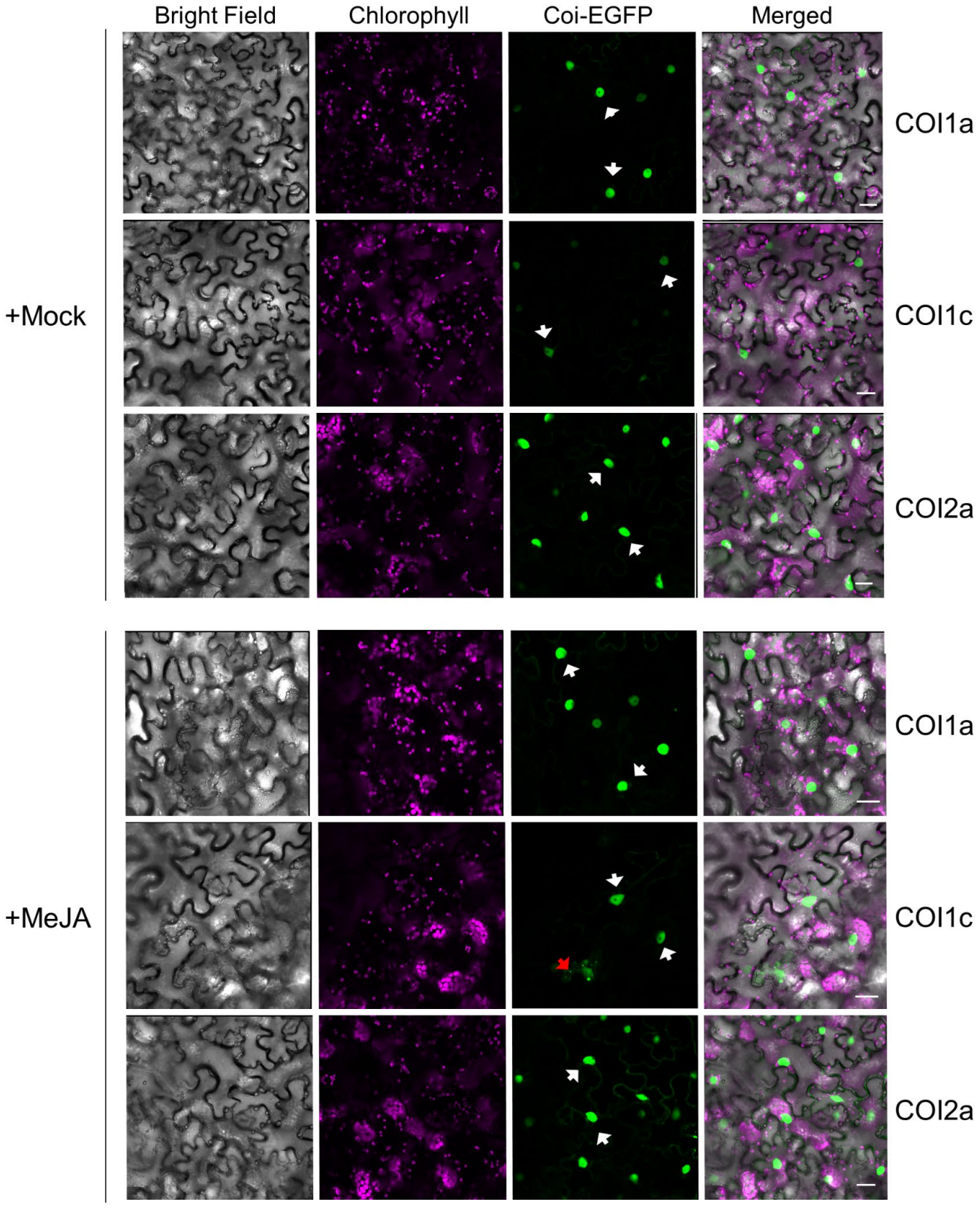

Figure 2. Subcellular locations of the maize coronatine insensitive (COI) proteins. COI1a, COI1c, and COI2a proteins were fused to enhanced green fluorescent protein (EGFP), showing that COI2a is more targeted to the nuclei than the two COI1 proteins. Confocal images were taken at 48 h after infiltrating plasmids expressing the COI-EGFP fusion proteins into the *Nicotiana benthamiana*. Leaves were sprayed with water (mock) or 0.02% methyl jasmonate (MeJA) two hours before imaging. White arrows indicate the nuclei, and red arrow represents a cytosolic condensate. Scale bars = 25 μm.

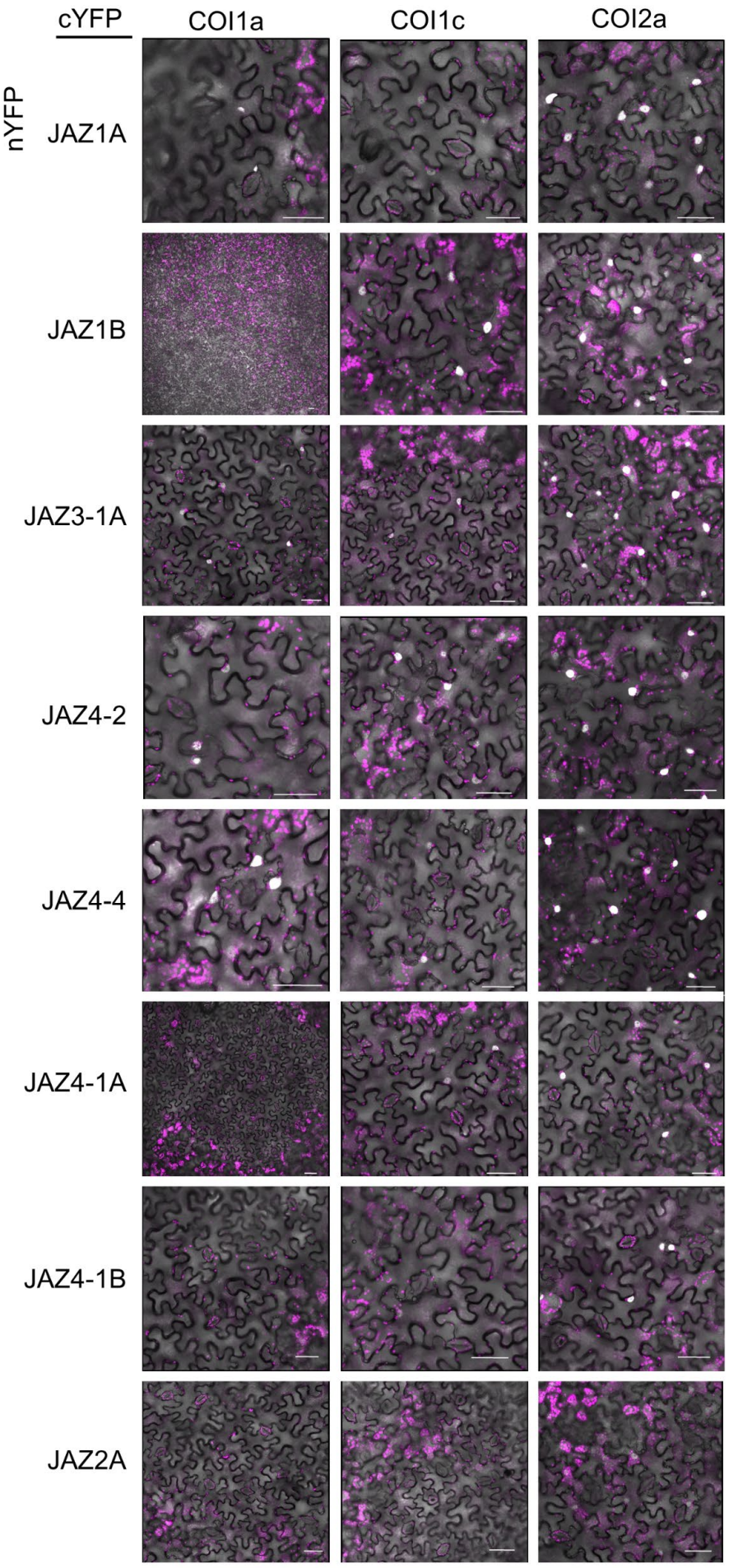

Figure 3. Bimolecular fluorescence complementation (BIFC) between the maize coronatine insensitive (COI) proteins fused to the carboxy-terminus of yellow fluorescent protein (cYFP) and jasmonate-ZIM domain (JAZ) proteins fused to the amino-terminus of yellow fluorescent protein (nYFP). BIFC indicating co-localization is shown as white spots in the images. Magenta represents chlorophyll fluorescence. Maize JAZ proteins have a higher affinity for COI2a than COI1a or COI1c. Leaves were sprayed with 0.02% methyl jasmonate (MeJA) two hours before imaging. Scale bars = 50 µm. These experiments were repeated independently with similar results (Figure S4). JAZ protein names are as in Han and Luthe (2022).

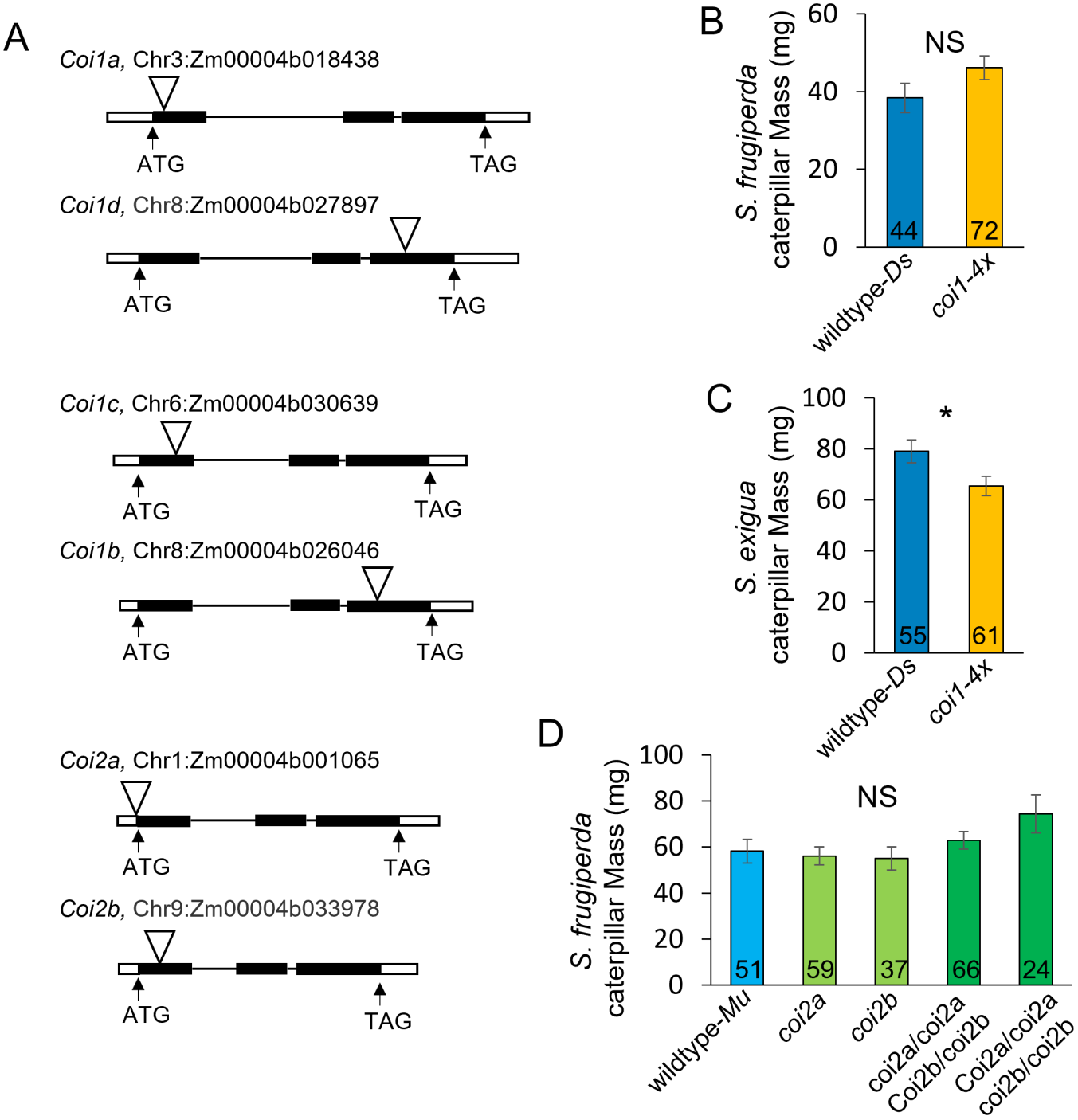

Figure 4. Fall armyworm (*Spodoptera exigua*) and beet armyworm (*Spodoptera exigua*) caterpillar growth on *coronatine insensitive* (*Coi*) mutant and wildtype maize. (A) Locations of *Dissociation* (*Ds*) transposon insertions in *COI1* genes and *Mutator* (*Mu*) transposon insertions in *COI2* genes are marked with triangles. Insertions are located at 140, 2682, 344, 2342, -8, and 198 bp from the start codons of *COI1a*, *COI1d*, *COI1c*, *COI1b*, *COI2a*, and *COI2b*, respectively. Black bars represent exons, thin lines are introns, and white bars are non-coding regions of the genes. (B) Mass of ten-day-old *S. frugiperda* caterpillars on wildtype and *coi1-4x* maize. No significant difference ($P > 0.05$, *t*-test). (C) Mass of ten-day-old *S. exigua* caterpillars on wildtype and *coi1-4x.* *$P < 0.05$, *t*-test. (D) Mass of ten-day-old *S. frugiperda* on wildtype and *coi2* mutants. No significant difference (NS, $P > 0.05$), Dunnett's test relative to wildtype-*Mu*. All data are mean +/− s.e., numbers in bars indicate the number of caterpillars for each treatment. Raw data and statistical calculations are in Supplementary Dataset S18.

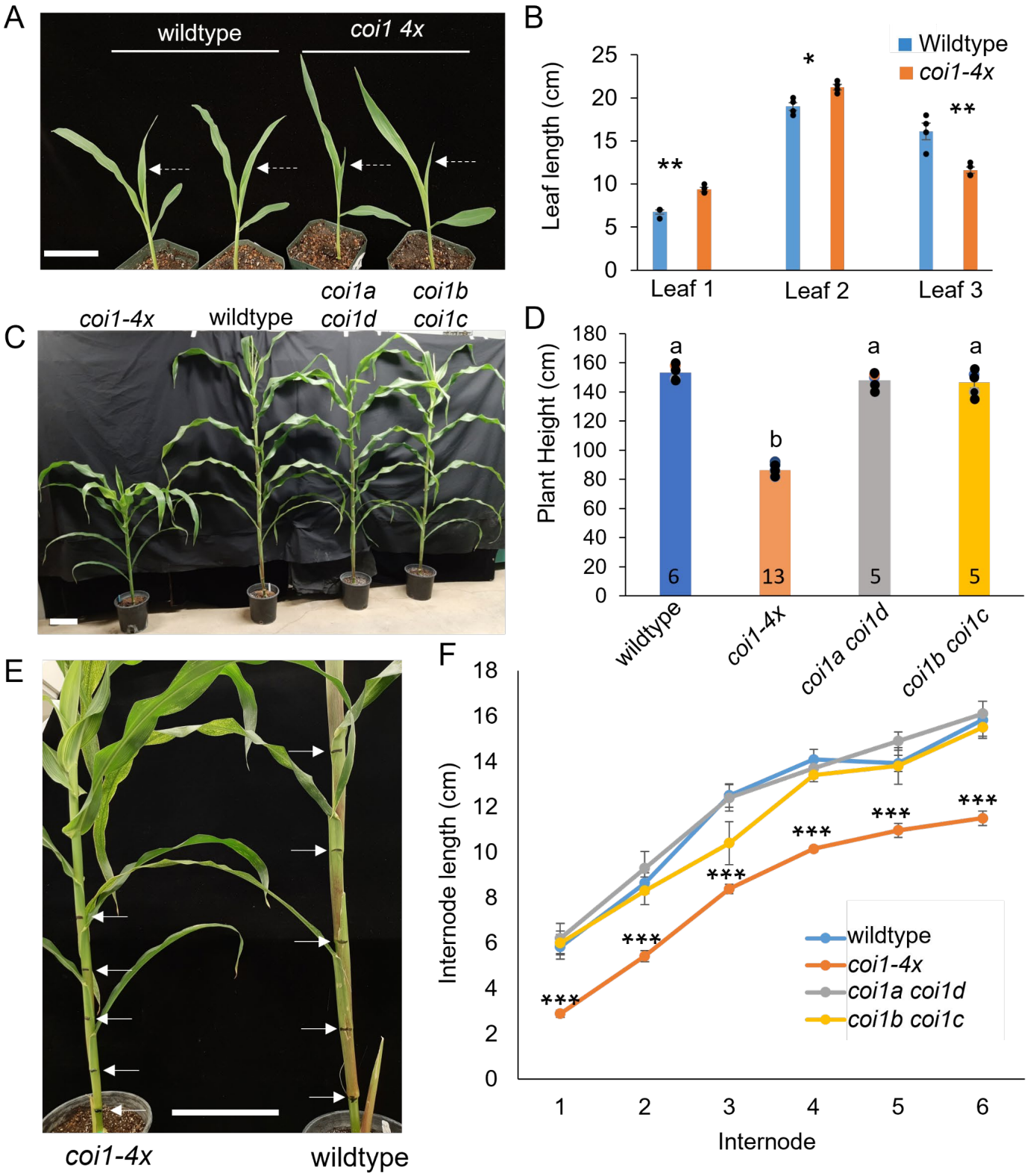

Figure 5. *coi1-4x* has impaired growth relative to the corresponding double mutants, *coi1a coi1d* and *coi1b coi1c*, and wildtype inbred line W22 maize. (A,B) Leaf lengths of *coi-4x* and wildtype (WT) ten days after germination, N = 4, mean ± se, two-tailed Student's *t*-test, *P < 0.05, **P < 0.01. (C,D) Plant heights at 60 days after germination. Numbers in bars = sample sizes, mean +/- s.e., letters indicate significant differences, P < 0.05, ANOVA followed by Tukey-Kramer Post Hoc Test. (E,F) Internode lengths were compared between four genotypes at 60 days post-germination. *coi1-4x* N = 13, wildtype N = 6, *coi1a coi1d* and *coi1b coi1c* N = 5 , mean +/- s.e., ***P < 0.001, Dunnett's test relative to wildtype. Raw data and statistics are presented in Supplemental Dataset S4.

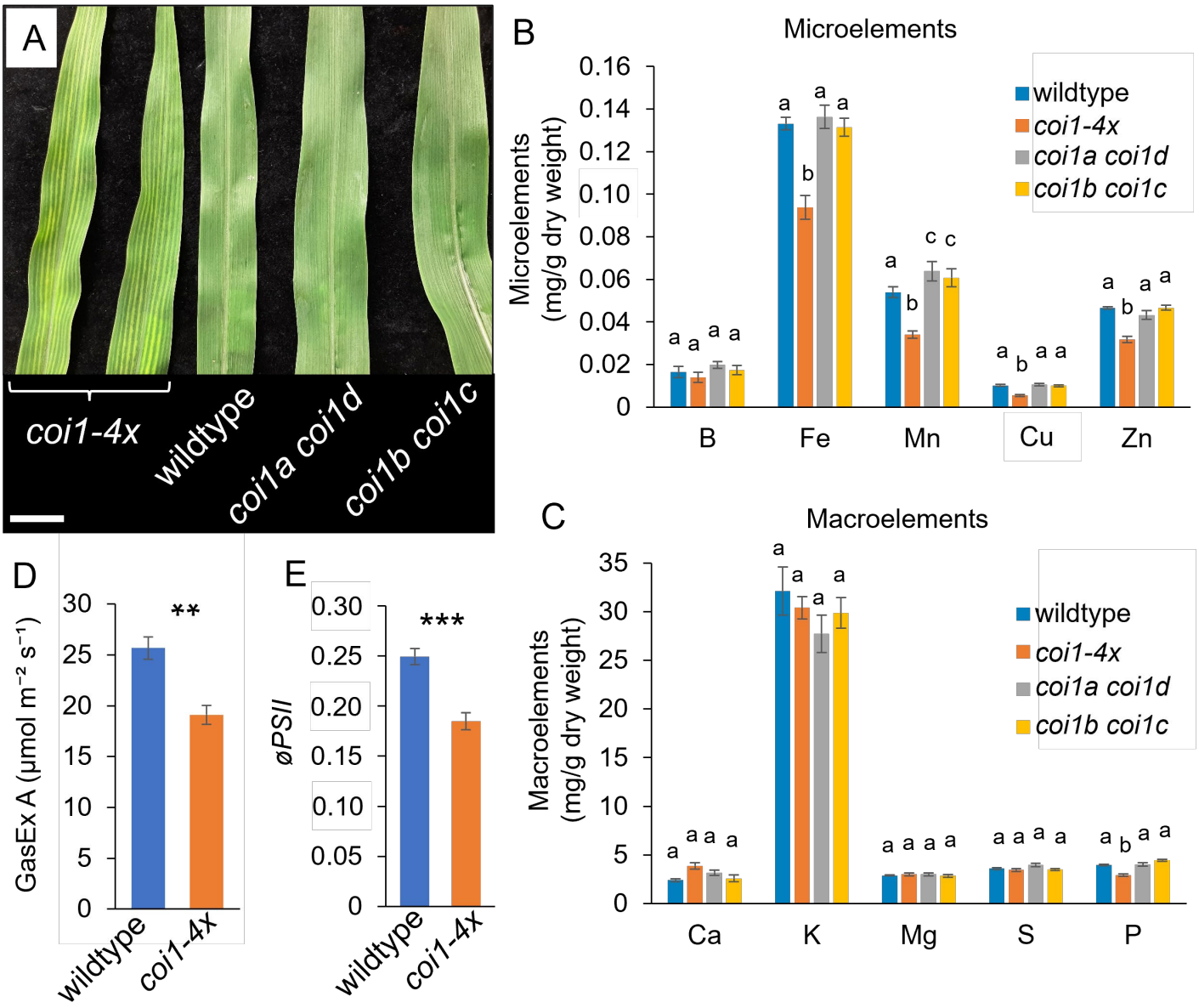

Figure 6. Plants with mutations in four maize *coronatine insensitive* (*Coi*) genes (*coi1-4x*) have striped leaves, decreased microelement levels, and reduced photosynthesis. (A) The striped leaf phenotype of the *coi1-4x* at 20 days post-germination compared to corresponding leaves from the double mutants and wildtype W22. Scale bar = 5 cm. (B) Microelements and (C) macroelements in 20-day-old seedlings, N = 7 plants, mean +/− s.e., letters indicate differences ($P < 0.05$) using Tukey's HSD test. (D) Leaf CO_2 assimilation rate (GasEX A) at 400 µmol mol^{-1} CO_2 and (E) the quantum yield of the photosystem II phytochemistry (*øPSII*) at 2000 µmol m^{-2} s^{-1} of actinic light were measured at 20 days after germination, respectively. Mean +/− s.e., n = 20 plants, two-tailed Student's *t*-test, $^{**}P < 0.01$, $^{***}P < 0.001$. Raw data and statistical calculations are in Supplementary Dataset S18.

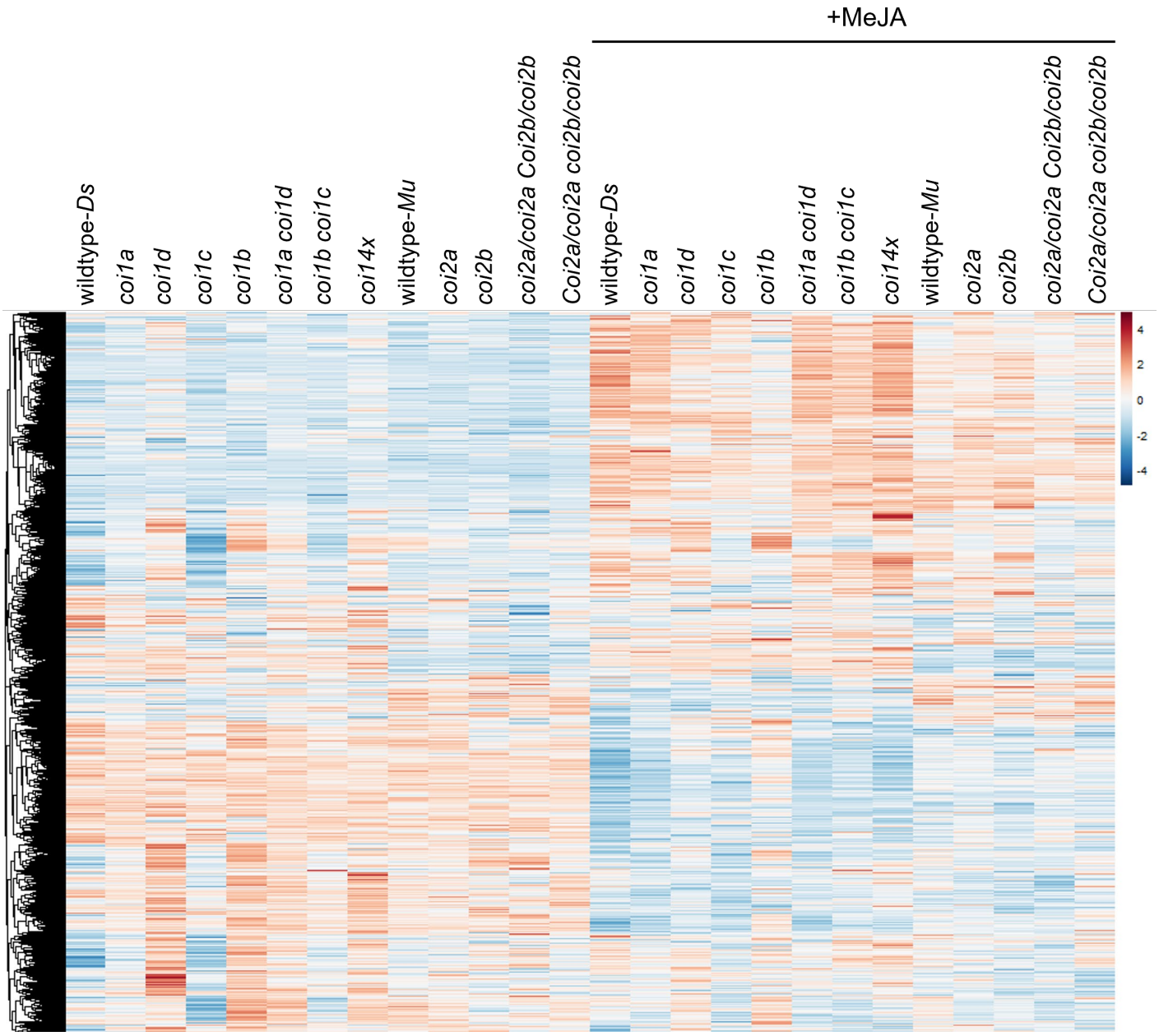

Figure 7. Heatmap of gene expression for 13,365 genes that were differentially regulated between two or more genotypes or between mock and methyl jasmonate (MeJA) induction. Color ranges from blue (minimum) to red (maximum) reads per million bp for each gene.
The color key represents the normalized log(1+expression) ranging from blue (indicating low values) to red (indicating high values). Reads per million (RPM) data were transformed by log(1+RPM) prior to clustering. The color gradient in the heatmap reflects the Z scores, with red colors indicating higher-than-average expression levels (Z score > 0) and blue colors indicating lower-than-average expression levels (Z score < 0). Numerical data underlying the heatmap are in Supplementary Dataset S6.

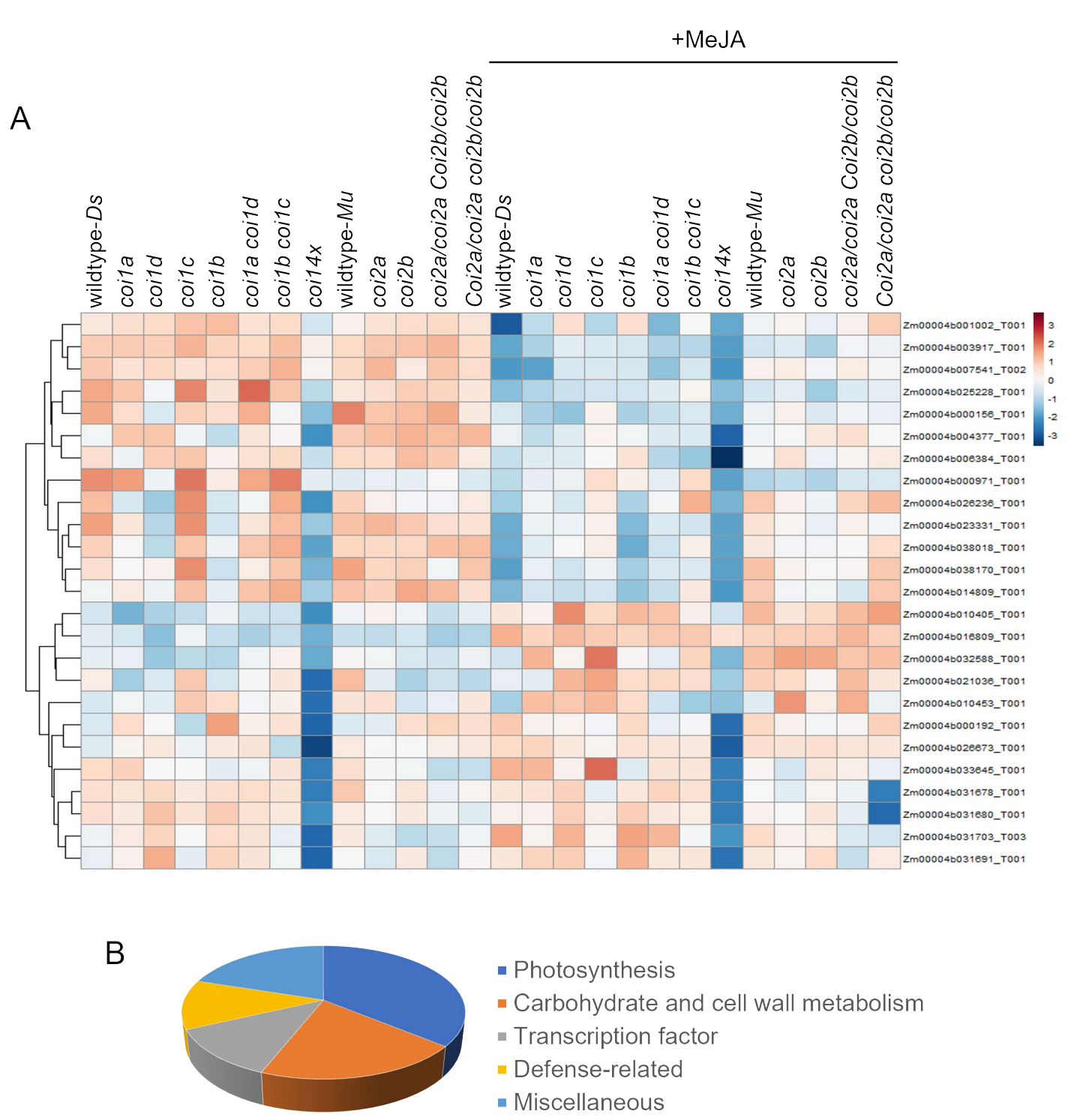

Figure 8. Genes down-regulated in maize plants with mutations in four *coronatine insensitive* (*Coi*) genes (*coi1-4x*) encode two main groups of proteins, involved in C_4 photosynthesis and carbohydrate and cell wall metabolism. (A) Heatmap showing downregulated genes in *coi1-4x* relative to other genotypes, with or without methyl jasmonate (MeJA) treatment. Reads per million (RPM) data were transformed by log(1+RPM) prior to clustering. The color gradient in the heatmap reflects the Z scores, with red colors indicating higher-than-average expression levels (Z score > 0) and blue colors indicating lower-than-average expression levels (Z score < 0). (B) Down-regulated genes in *coi1-4x* were categorized into five functional groups. The list of the genes, color-coded by their functional group, as well as ordered based on their position in the heatmap, is presented in Supplementary Dataset S7.

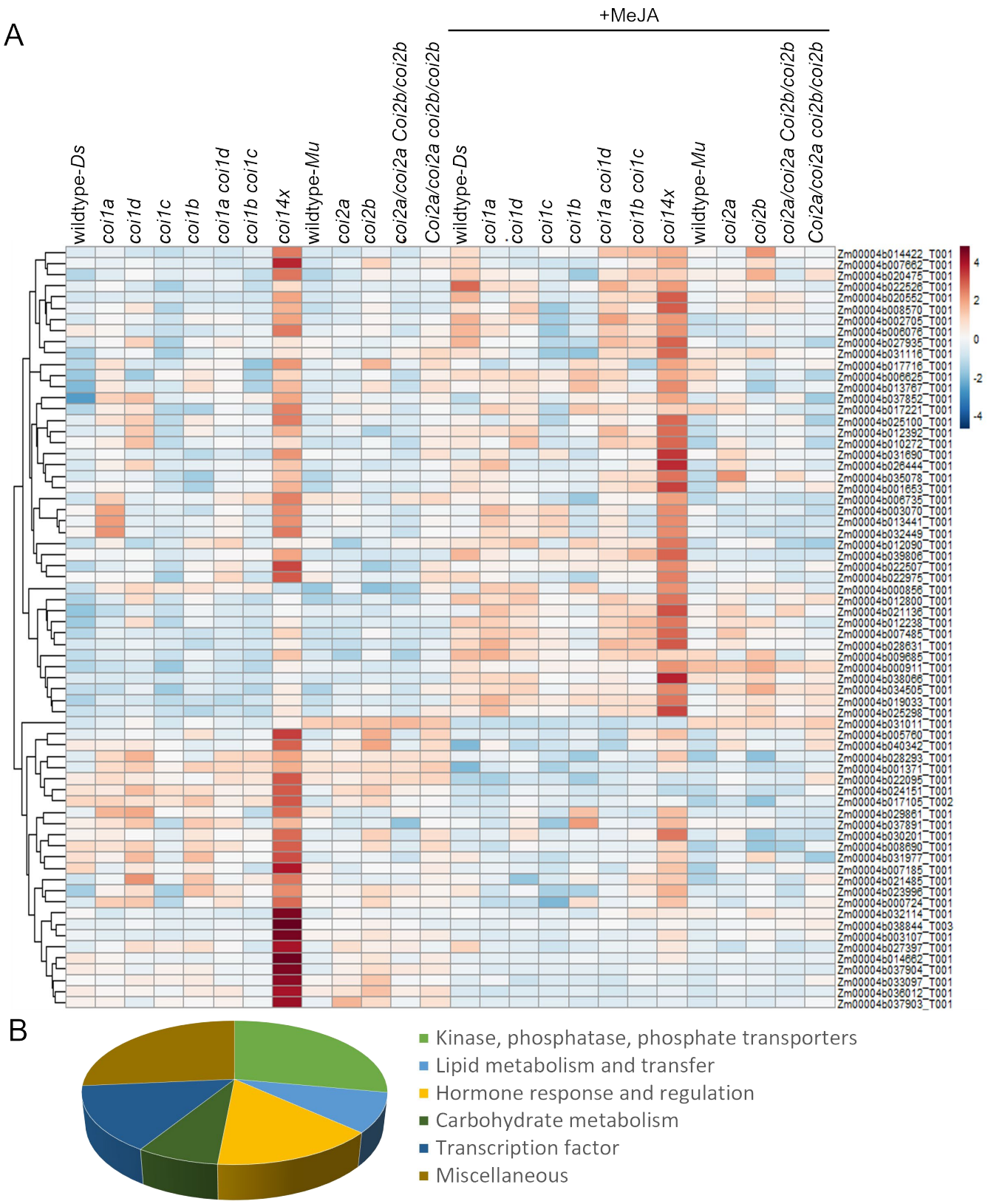

Figure 9. Genes up-regulated in maize plants with mutations in four *coronatine insensitive* (*Coi*) genes (*coi1-4x*) encode proteins involved in phosphate regulation, lipid and carbohydrate metabolism, hormone regulation, and transcription. (A) Heatmap showing upregulated genes in *coi1-4x* relative to other genotypes, with or without methyl jasmonate (MeJA) treatment. The reads are transformed by log(1+expression) prior to clustering. (B) Up-regulated genes in *coi1-4x* were categorized into six functional groups. The list of the genes, color-coded by their functional group, as well as ordered based on their position in the heatmap, is presented in Supplementary Dataset S8.

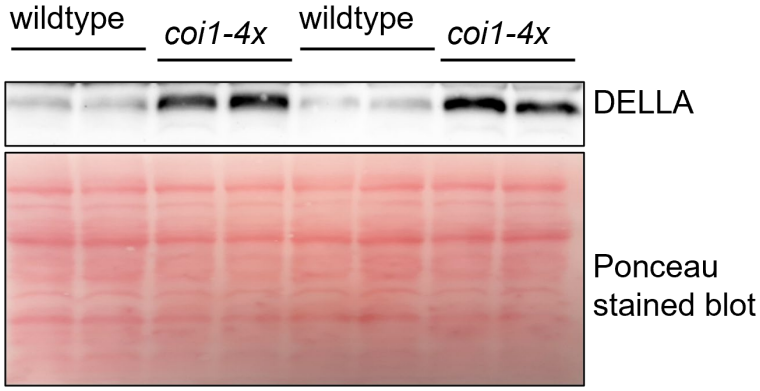

Figure 10. Immunoblot analyses of maize DELLA proteins. The leaf total proteins from equal surface area (similar weight) leaves (fourth leaf, 20 days after germination) of wildtype maize inbred line W22 and a line with mutations in four *coronatine insensitive* (*Coi*) genes (*coi1-4x*) were analyzed by probing with antibodies that react with rice DELLA (SLENDER RICE 1 (SLR1)). The membrane was stained with Ponceau S as the loading control.

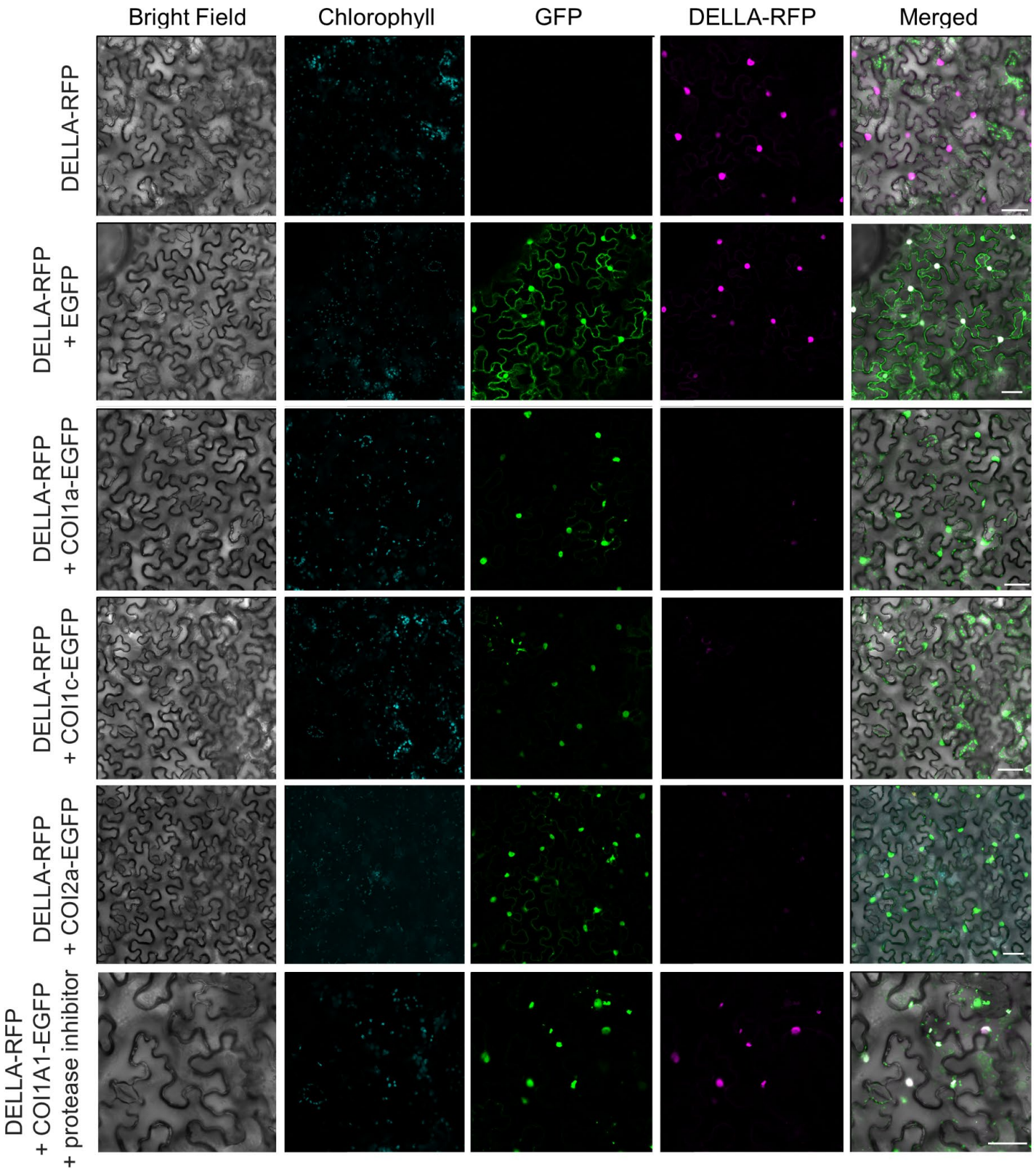

Figure 11. Maize DELLA (DWARF9) disappears from the nuclei upon coexpression with the maize coronatine insensitive (COI) proteins. Confocal images were taken after transiently expressing genes in *Nicotiana benthamiana* leaves for 48 hours. Labels on left indicate infiltrated genes for each row of images. GFP = green fluorescent protein, EGFP = enhanced green fluorescent protein, RFP = red fluorescent protein. Protease inhibitor (bortezomib) was co-infiltrated in the bottom row. Scale bars = 50 µm.

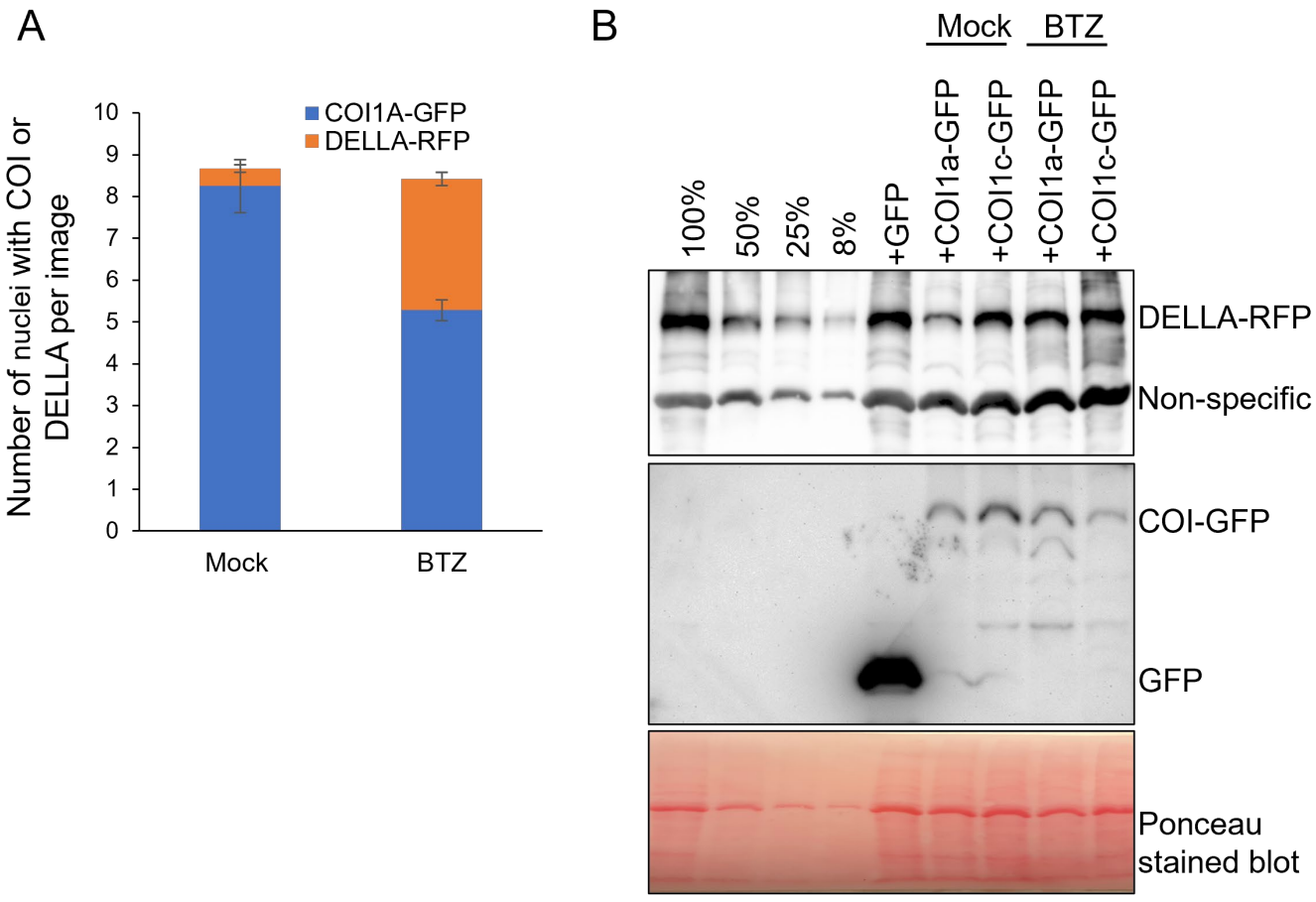

Figure 12. Expression of the maize coronatine insensitive1 (COI1) proteins leads to proteasome-dependent degradation of maize DELLA in *Nicotiana benthamiana*. (A) Nuclei showing the presence of the COI1a-EGFP (enhanced green fluorescent protein) and or DELLA-RFP (red fluorescent protein) were counted on confocal images from an experiment similar to Figure 11, with and without protease inhibitor. The bars are means +/− s.e. of N = 48 plants for the mock treatment and N = 71 plants treated with the proteasome inhibitor bortezomib (BTZ). Raw data and statistical calculations are in Supplementary Dataset S18. (B) Leaf tissue from the *N. benthamiana* plants expressing DELLA-RFP alone or with EGFP, COI1a-EGFP, or COI1c-EGFP (similar to those used in Figure 11), 48 hours after infiltration, was used for immunoblot analyses. Membranes were probed with antibodies that react with rice DELLA (SLENDER RICE 1 (SLR1)) and antibodies that react with GFP. The first membrane was stained with Ponceau S as the loading control. Non-specific binding of the SLR1 antibody to an unrelated protein was used as an extra loading control.

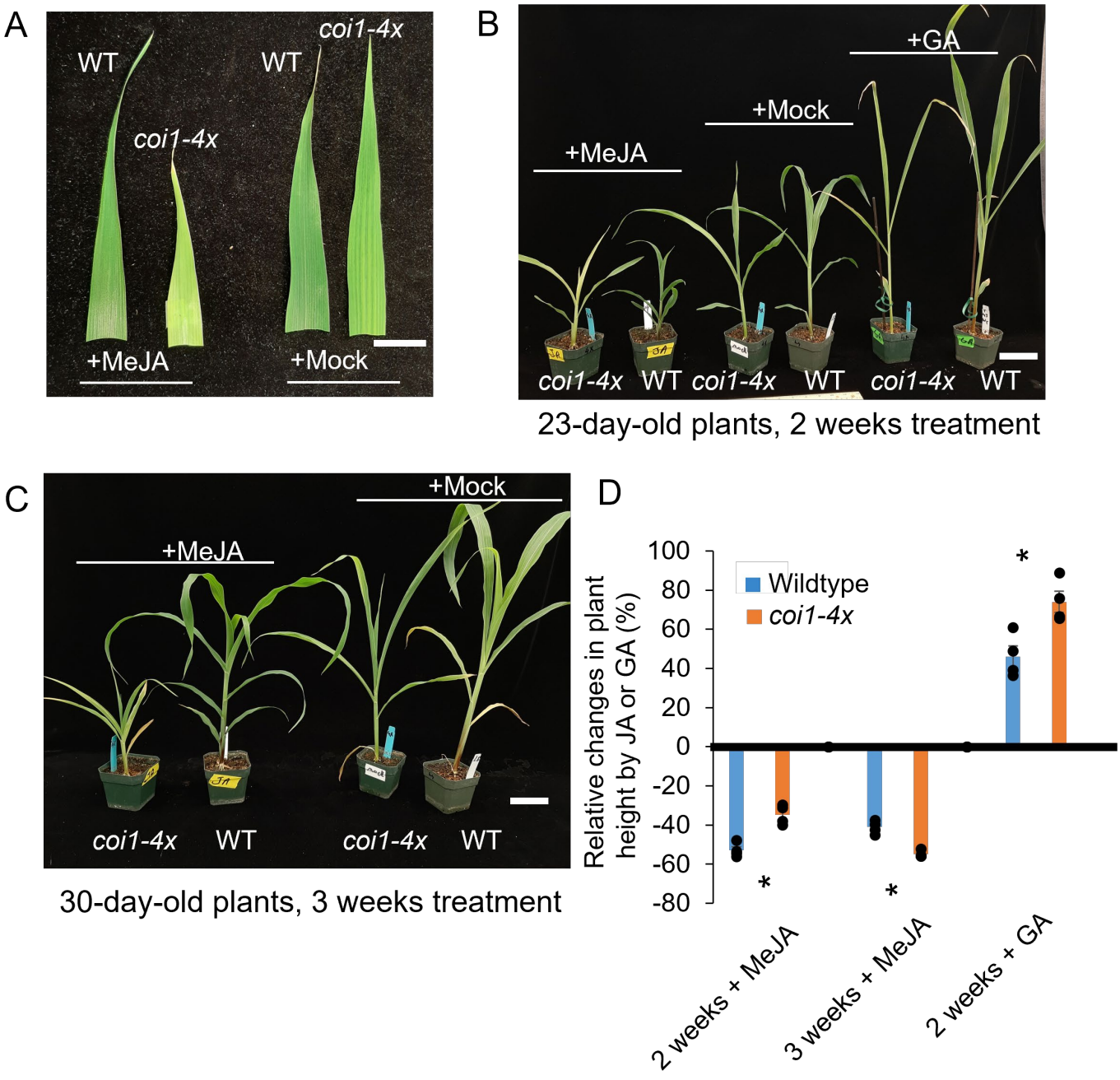

Figure 13. Effect of exogenous methyl jasmonate (MeJA) and gibberellic acid (GA) on growth of wildtype maize inbred line W22 and Plants with mutations in four maize *coronatine insensitive* (*Coi*) genes (*coi1-4x*). (A) Leaf discoloration symptoms at 30 days post-germination and after three weeks of JA treatment. Scale bar = 5 cm. (B) Plant heights at 23 days post-germination, with mock, MeJA, or GA treatments. Scale bar = 10 cm. (C) Plant heights at 30 days post-germination, with or without MeJA treatment. WT = wildtype. Scale bar = 10 cm. (D) Bar chart showing percent change in height relative to the mock-treated controls for the MeJA and GA treatments shown in panels B and C. N = 4, mean +/− s.e., two-tailed Student's *t*-test, $*P < 0.05$. Raw data and statistical calculations are in Supplementary Dataset S18.

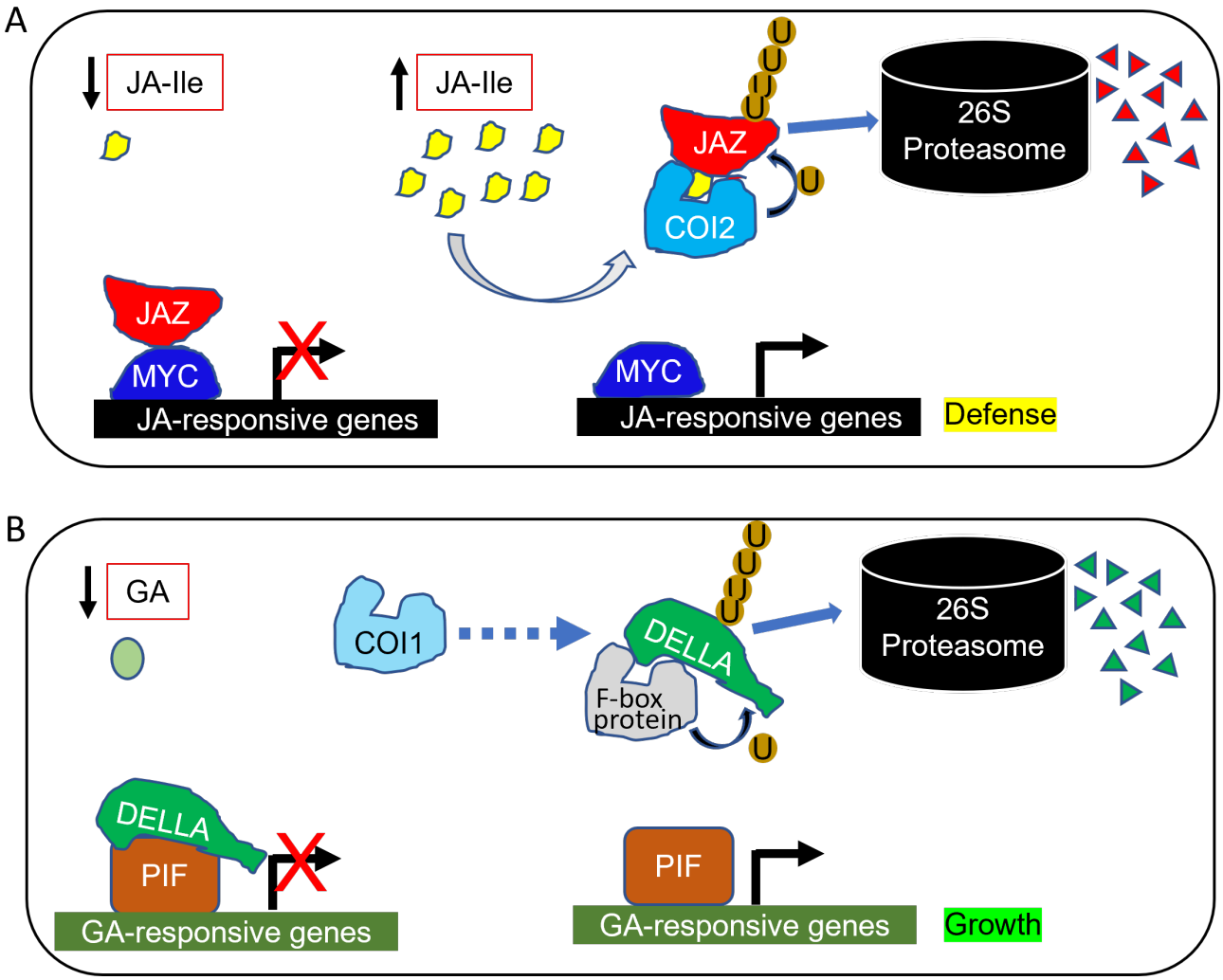

Figure 14. Model for differential functions of maize coronatine insensitive (COI) proteins in regulating growth and defense. **(**A) Maize COI2 proteins are proposed to have the classical F-box domain protein function of Arabidopsis and tomato COIs. At low jasmonate-isoleucine (JA-Ile) concentrations (black arrow pointing down), jasmonate ZIM-domain (JAZ) proteins prevent activation of JA-Ile-responsive genes by MYC transcription factor (black right-angle arrow with a red X). Higher abundance of JA-Ile (black arrow pointing up) leads to interactions between COI2 and JAZ proteins (arched gray arrow), causing addition of ubiquitin (U) to JAZ and degradation (blue arrow) by the 16S proteasome (red triangles). The absence of JAZ proteins leads to activation of transcription by MYC proteins and expression of defense-related genes (black right-angle arrow). (B) At low gibberellic acid (GA) levels (black arrow pointing down), DELLA is bound to PIF transcription factors, preventing transcription of GA-responsive genes (black right-angle arrow with a red X). At high GA levels, an as yet unknown maize F-box protein contributes to an E3 ligase complex (dashed blue arrow) that causes addition of ubiquitin (U) to DELLA and degradation (blue arrow) by the 16S proteasome, leading to activation of GA-responsive genes (black right-angle arrow). Based on the results that are presented, we propose that maize COI1 proteins directly or indirectly cause DELLA degradation (green triangles). In the *coi1-4x* mutant, there is no COI1, resulting in less DELLA degradation, less growth, and shorter stature of the maize plants.

A

		Protein identity (%)
Zm-COI1a	At-COI	58
Zm-COI1d	At-COI	58
Zm-COI1c	At-COI	57
Zm-COI1b	At-COI	58
Zm-COI2a	At-COI	56
Zm-COI2b	At-COI	55

B

		Protein identity (%)
Zm-COI1a	Zm-COI1d	94
Zm-COI1a	Zm-COI1c	79
Zm-COI1a	Zm-COI1b	78
Zm-COI1d	Zm-COI1c	80
Zm-COI1d	Zm-COI1b	80
Zm-COI1c	Zm-COI1b	93
Zm-COI1a	Zm-COI2a	60
Zm-COI1a	Zm-COI2b	61
Zm-COI1d	Zm-COI2a	60
Zm-COI1d	Zm-COI2b	60
Zm-COI1c	Zm-COI2a	60
Zm-COI1c	Zm-COI2b	59
Zm-COI1b	Zm-COI2a	61
Zm-COI1b	Zm-COI2b	60
Zm-COI2a	Zm-COI2b	95

Figure S1. In support of Figure 1. Amino acid identity of Arabidopsis and maize COI proteins. (A) Percent amino acid identity between maize CORONATINE INSENSITIVE (COI) proteins and Arabidopsis COI proteins. (B) Percent amino acid identity among the six maize COI proteins. The maize proteins are color-coded based on pairwise similarity in the phylogenetic tree in Figure 1.

Supplementary Data. Feiz et al. (2024). F-Box Protein Regulation of Growth in Maize. Plant Cell.

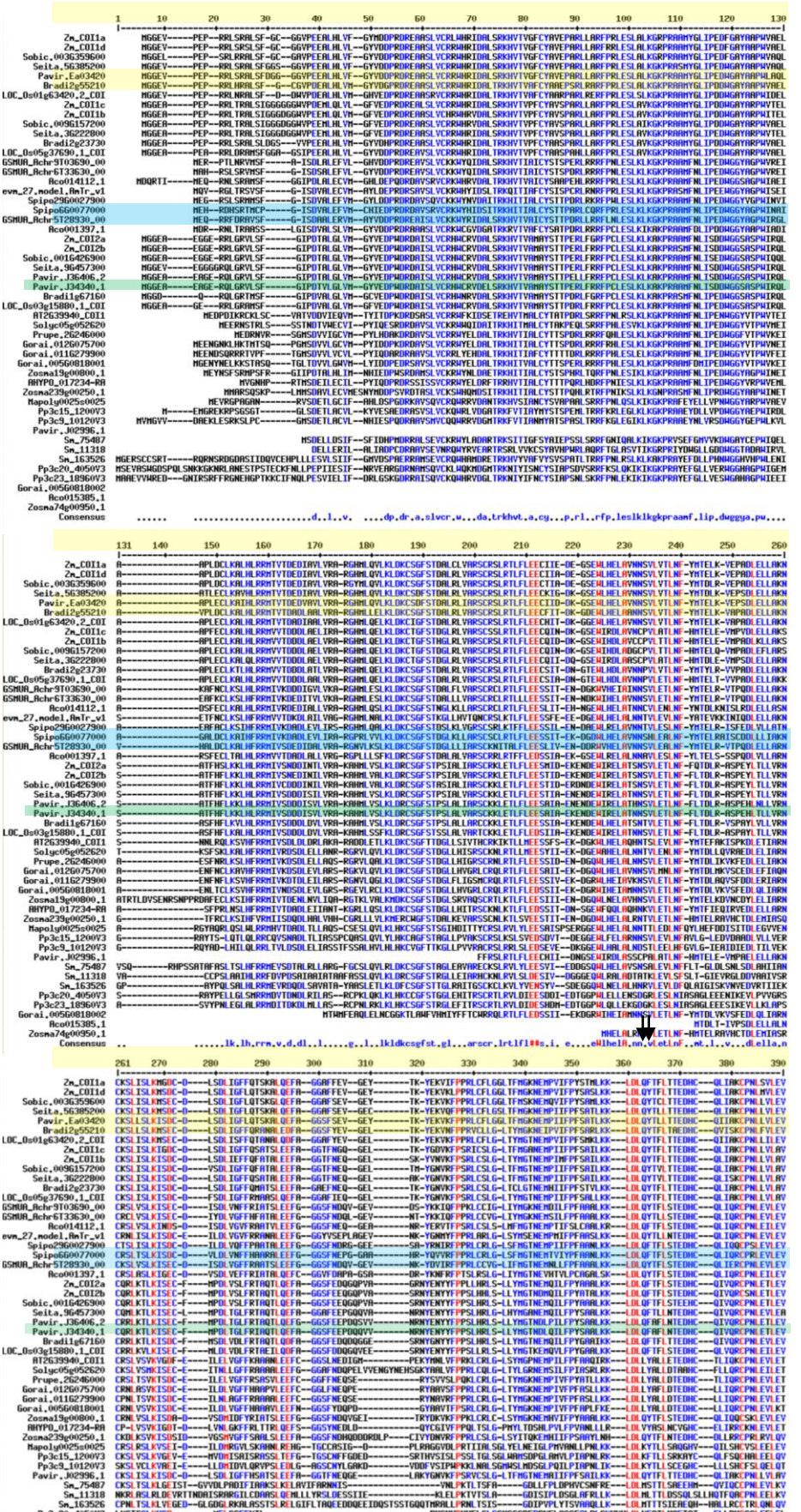

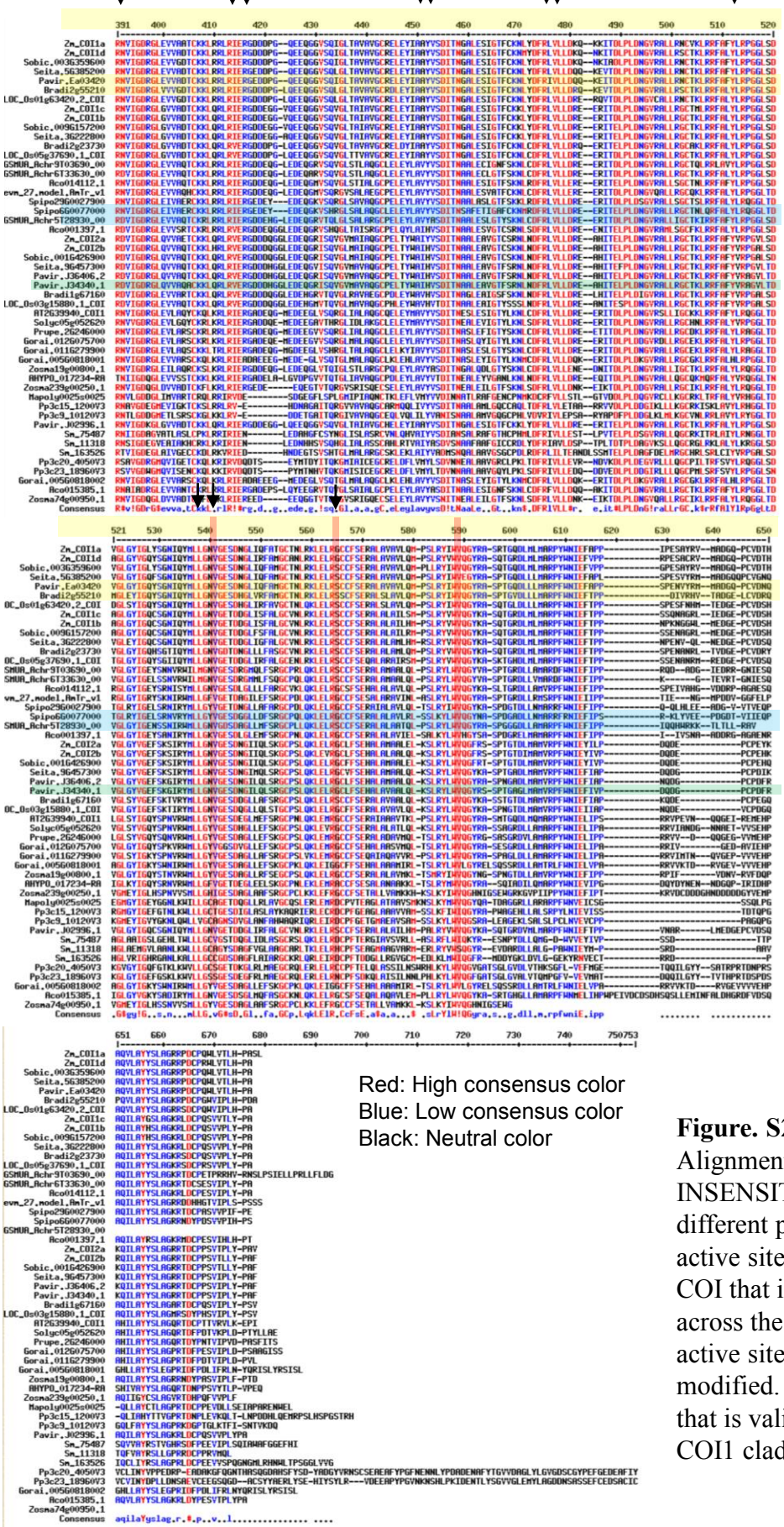

Figure. S2. In support of Figure 1. Alignment of CORONATINE INSENSITIVE (COI) proteins from different plant species. Red arrow shows the active site amino acid of the Arabidopsis COI that is modified in the COI1 clades across the Poaceae. Black arrows show the active site amino acids that are not modified. Green arrow shows an amino acid that is valine only in the C_4 type of the COI1 clade and *Marchantia polymorpha.*

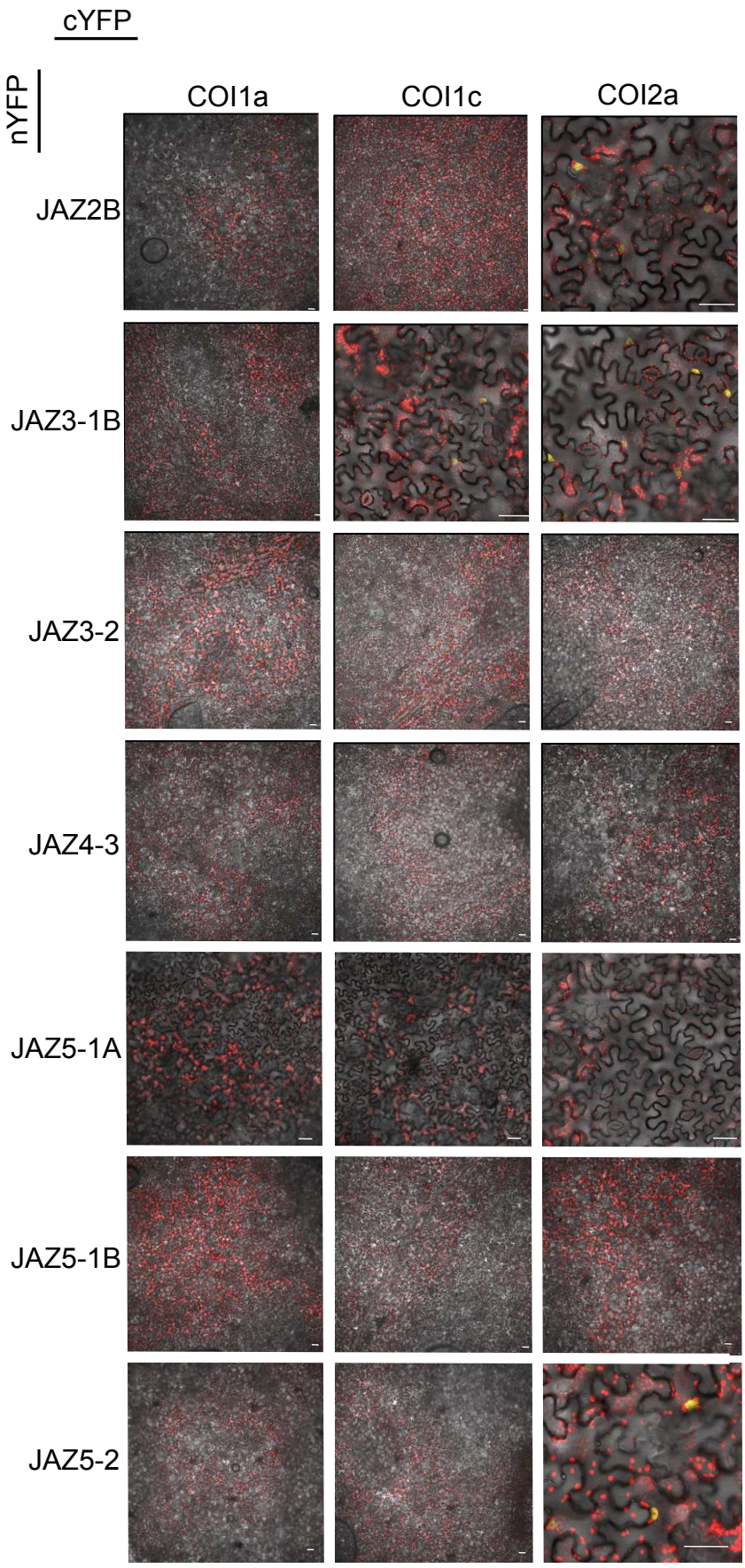

Figure S3. In support of Figure 3. Bimolecular fluorescence complementation (BIFC) between the maize coronatine insensitive (COI) proteins and severn jasmonate-ZIM domain (JAZ) proteins. COI proteins were fused to the carboxy-terminus of yellow fluorescent protein (cYFP) and JAZ proteins were fused to the amino-terminus of yellow fluorescent protein (nYFP). Shown are he maize COI1a, COI1c, and COI2c and seven JAZ proteins that did not show interactions with any of the COI proteins. Scale bars = 50 μm. JAZ protein names are as in Han and Luthe (2022).

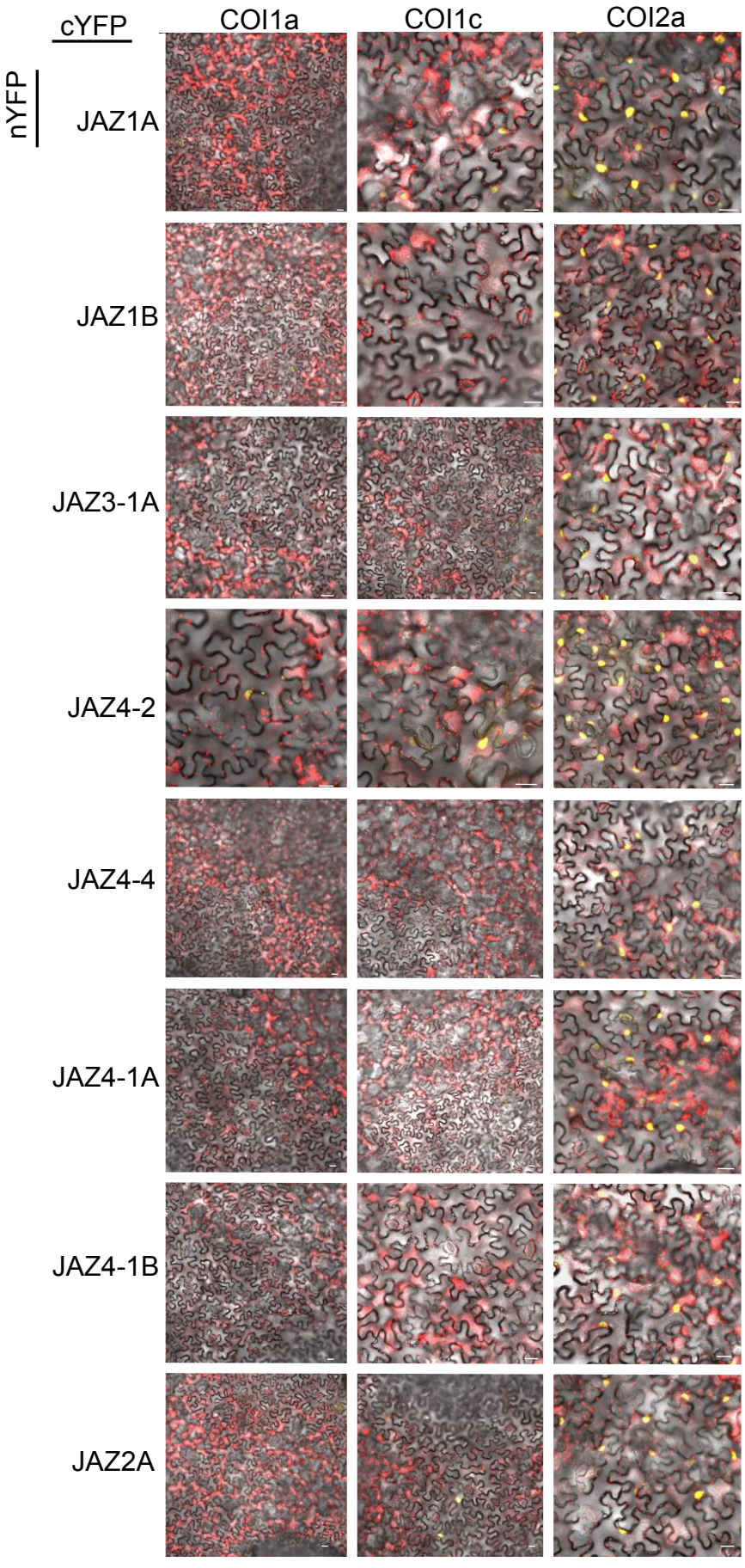

Figure S4. In support of Figure 3. An independent repeat of the COI-JAZ bimolecular fluorescence complementation (BIFC) experiment that is presented in Figures 3 and S3. Shown are interactions between the maize coronatine insensitive (COI) proteins fused to the carboxy-terminus of yellow fluorescent protein (cYFP) and jasmonate-ZIM domain (JAZ) proteins fused to the amino-terminus of yellow fluorescent protein (nYFP). Scale bars= 50 µm. JAZ protein names are as in Han and Luthe (2022).

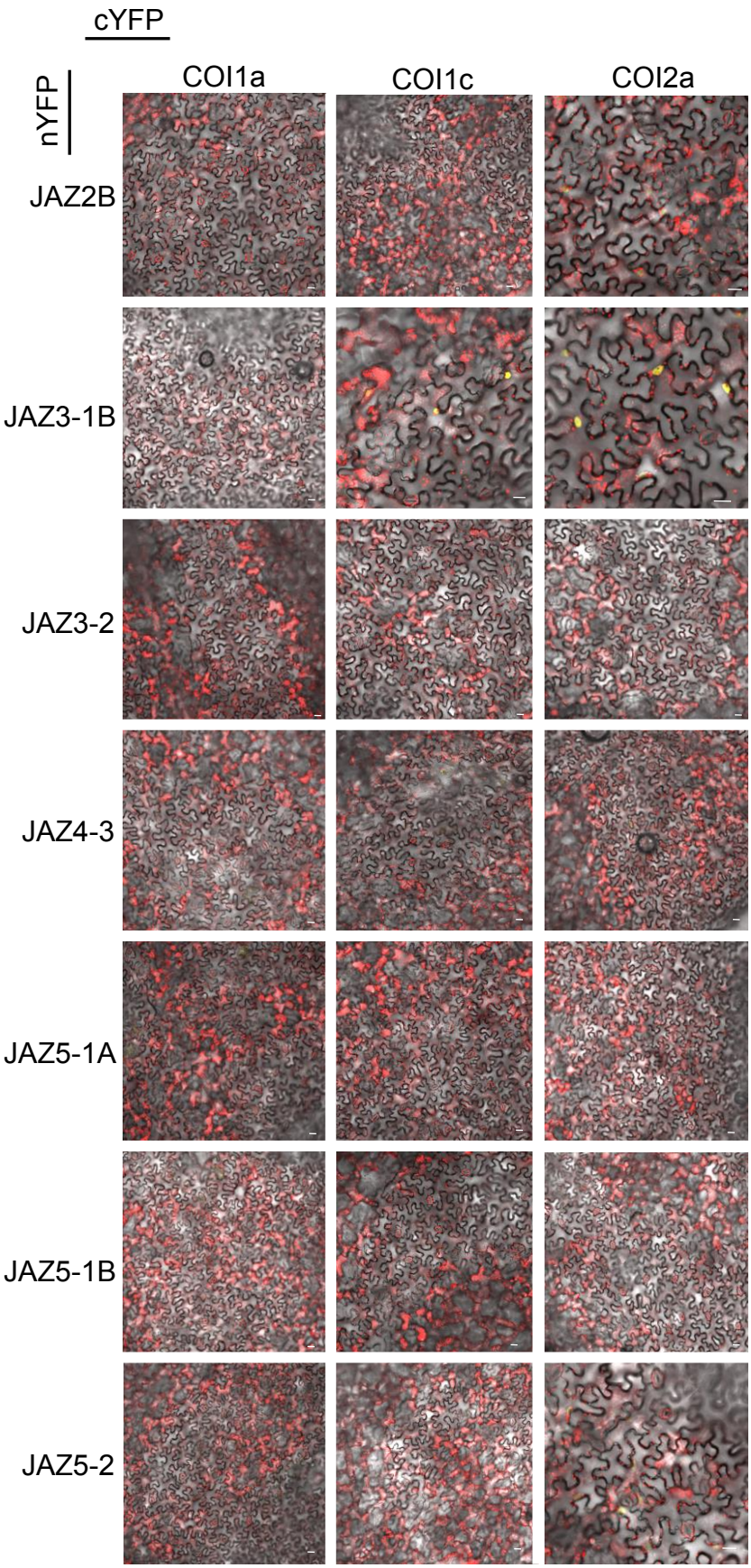

Figure S4. continued

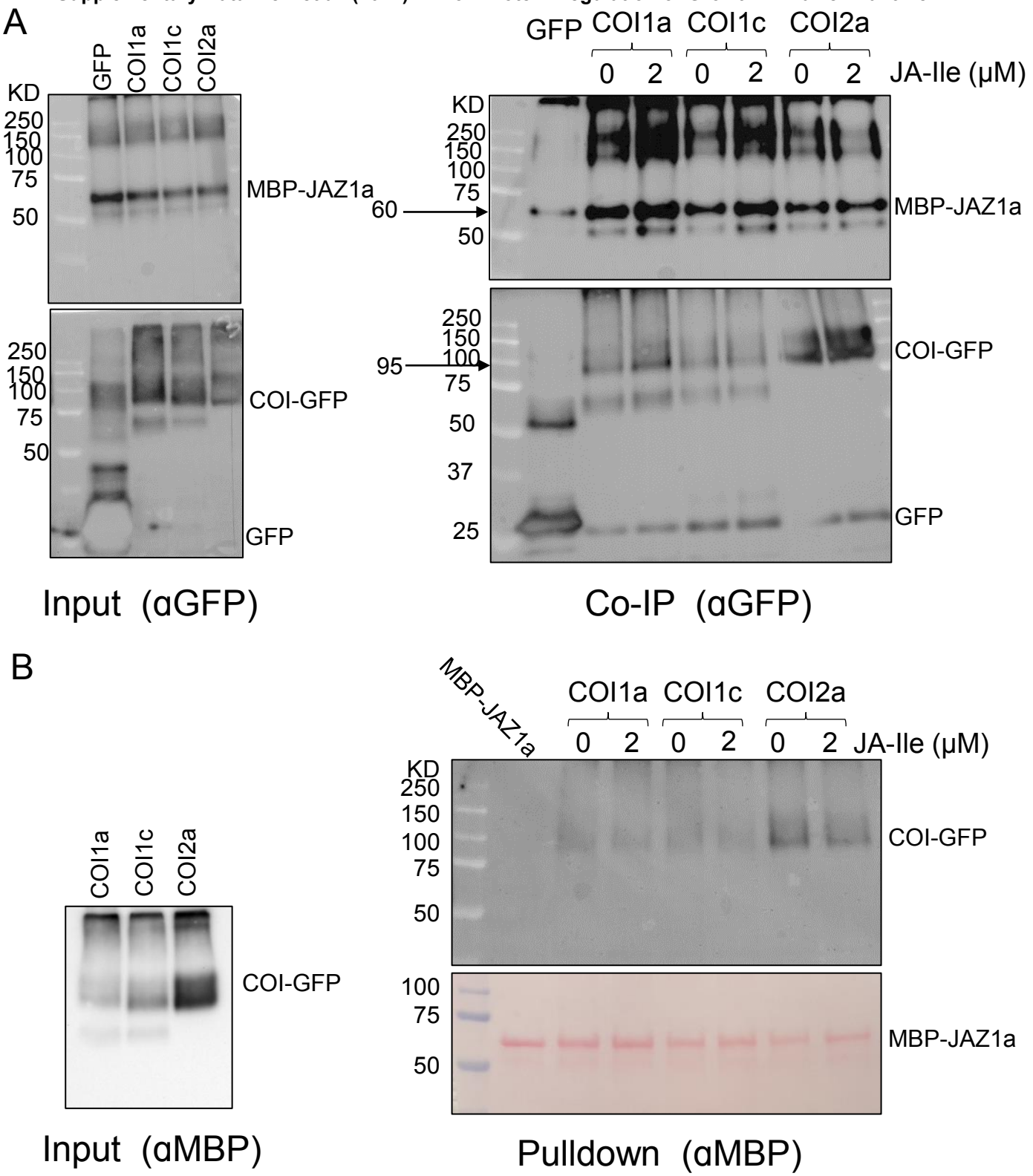

Figure S5. In support of Figure 3. Interactions between each maize COI and JAZ1a detected via coimmunoprecipitation and pulldown assays. (A) Immunoblots of the recombinant MBP-JAZ1a (with anti-MBP antibody) and COI1a, COI1c, or COI2a fused to GFP (with anti-GFP) after coimmunoprecipitation of MBP-JAZ1a (~60 kD) with COI-GFP (~95 kD) using GFP-Trap beads, with and without adding 2 μM jasmonate-isoleucine (JA-Ile). (B) Immunoblots of the COI1a, COI1c, or COI2a fused to GFP after pulldown with the MBP-JAZ1a using amylose beads, with and without adding 2 μM JA-Ile. αGFP = anti-green fluorescent protein antibodies, αMBP = anti maltose binding protein antibodies.

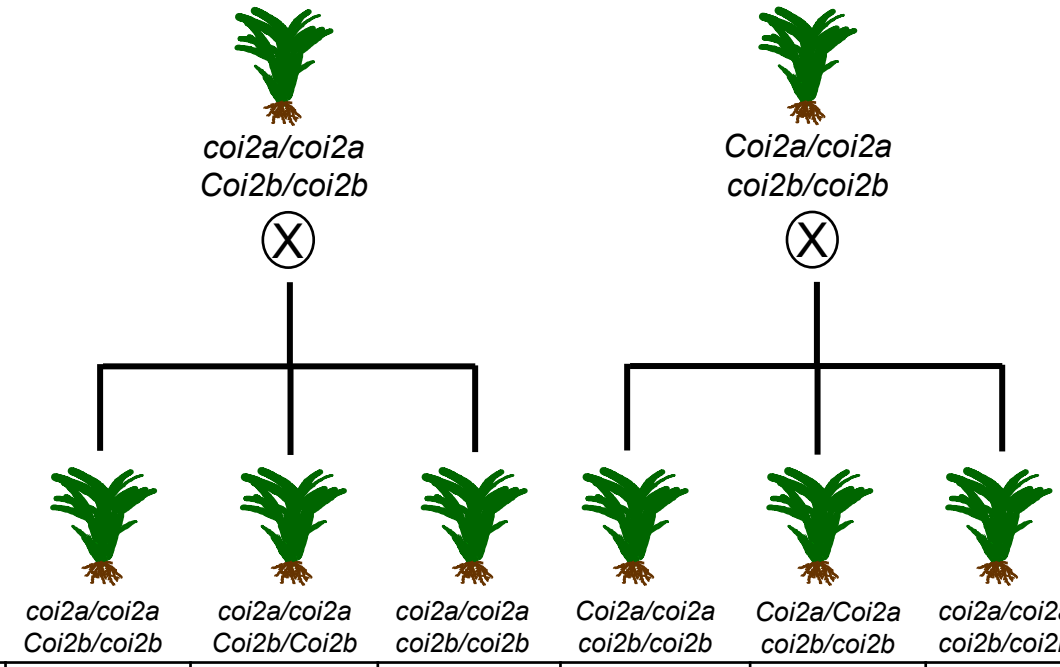

	coi2a/coi2a Coi2b/coi2b	*coi2a/coi2a Coi2b/Coi2b*	*coi2a/coi2a coi2b/coi2b*	*Coi2a/coi2a coi2b/coi2b*	*Coi2a/Coi2a coi2b/coi2b*	*coi2a/coi2a coi2b/coi2b*
Observed	42	46	0	32	42	0
Expected if *coi2a/coi2a coi2b/coi2b* is not lethal	44	22	22	37	18	19
Expected if *coi2a/coi2a coi2b/coi2b* is embryo-lethal	59	29	0	49	25	0
Expected if *coi2a coi2b* is gametophyte-lethal	44	44	0	37	37	0

Figure S6. In support of Figure 4. Segregation patterns of selfed *coi2a/coi2a Coi2b/coi2b* and *Coi2a/coi2a coi2b/coi2b* mutants. Segregation patterns show that there are no homozygous *coi2a/coi2a coi2b/coi2b* mutants among the progeny. This indicates that either male or female *coi2a coi2b* gametes do not survive.

♀ ♀

Coi2a/coi2a coi2b/coi2b X Wildtype W22

Progeny	*Coi2a/coi2a Coi2b/coi2b*	*Coi2a/Coi2a Coi2b/coi2b*
Observed	10	7
Expected if *coi2a coi2b* eggs are dead	0	17

coi2a/coi2a Coi2b/coi2b X Wildtype W22

Progeny	*Coi2a/coi2a Coi2b/coi2b*	*Coi2a/coi2a Coi2b/Coi2b*
Observed	5	12
Expected if *coi2a coi2b* eggs are dead	0	17

Wildtype W22 X *Coi2a/coi2a coi2b/coi2b*

Progeny	*Coi2a/coi2a Coi2b/coi2b*	*Coi2a/Coi2a Coi2b/coi2b*
Observed	0	58
Expected if *coi2a coi2b* pollen is dead	0	58

Wildtype W22 X *coi2a/coi2a Coi2b/coi2b*

Progeny	*Coi2a/coi2a Coi2b/coi2b*	*Coi2a/coi2a Coi2B/Coi2b*
Observed	0	20
Expected if *coi2a coi2b* pollen is dead	0	20

Figure S7. In support of Figure 4. Test crosses between *coi2a/coi2a Coi2b/coi2b* and *Coi2a/coi2a coi2b/coi2b* and the wildtype W22 maize. These crosses indicate that *coi2a coi2b* pollen is not viable.

transcriptome

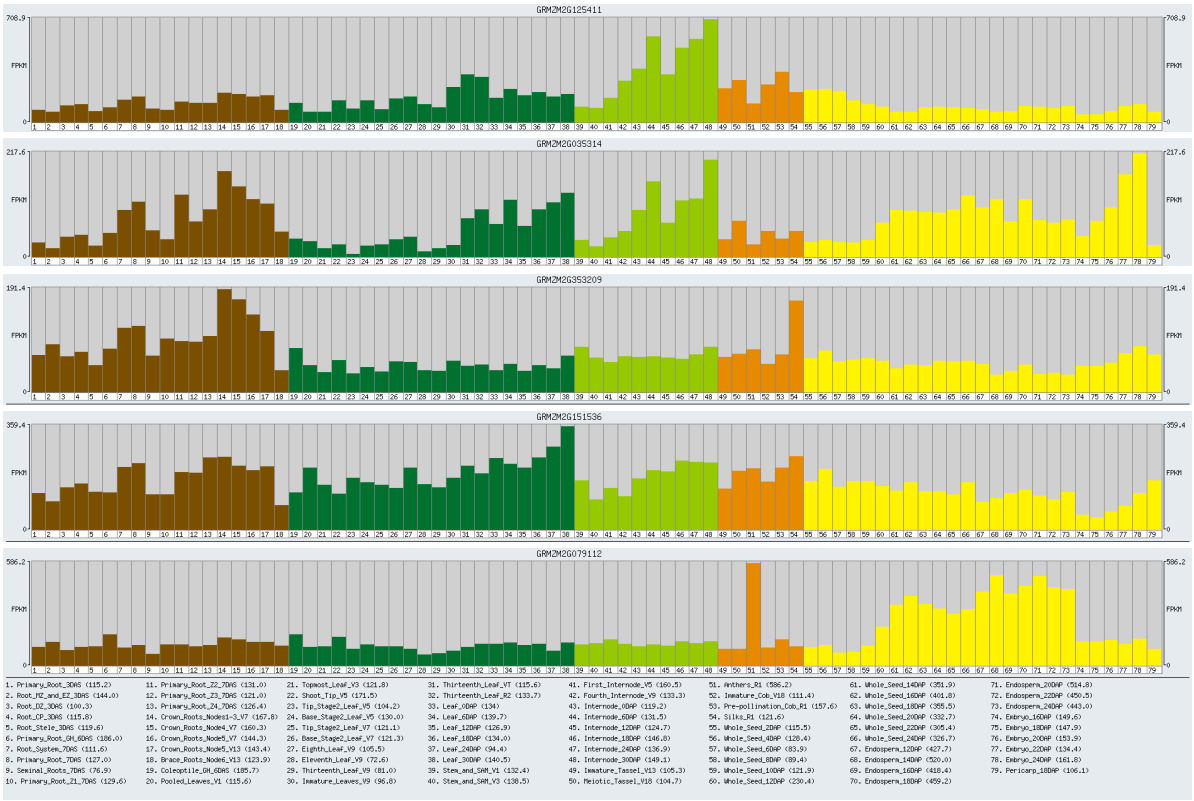

COI1a

COI1d

COI1c

COI1b

COI2a

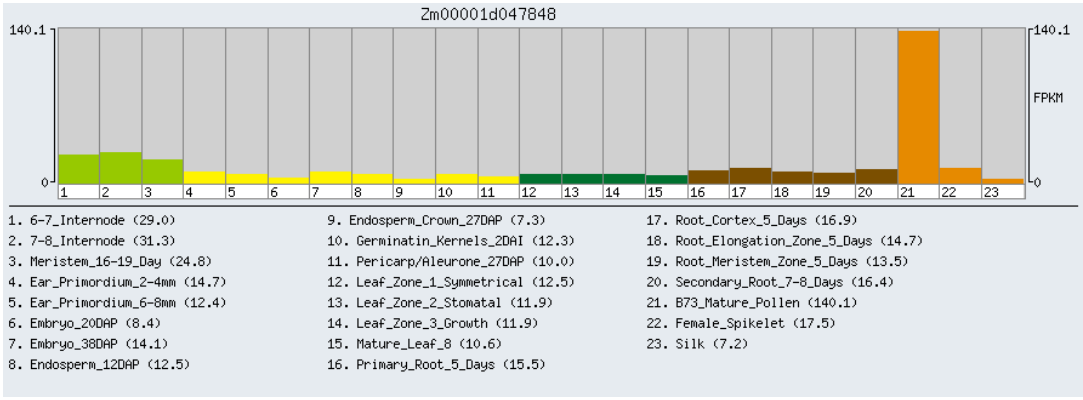

COI2b

Figure S8. In support of Figure 4. Expression of maize *Coi2* genes. Transcriptome data show highest expression of maize *Coi2* genes in anthers. Data were plotted from the Maize Genome Database (www.maizegdb.org)

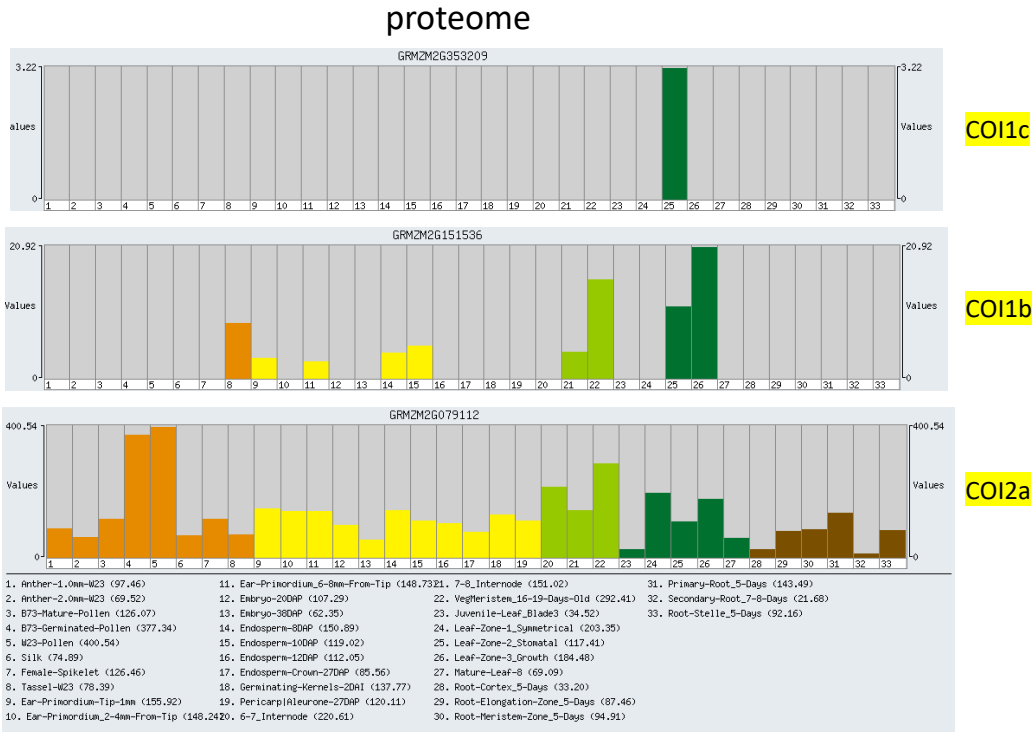

Figure S9. In support of Figure 4. Proteomics data show pollen-specific abundance of maize COI2a protein. Data are from: Walley et al (2016), Integration of omic networks in a developmental atlas of maize, *Science*, 353:814-818,

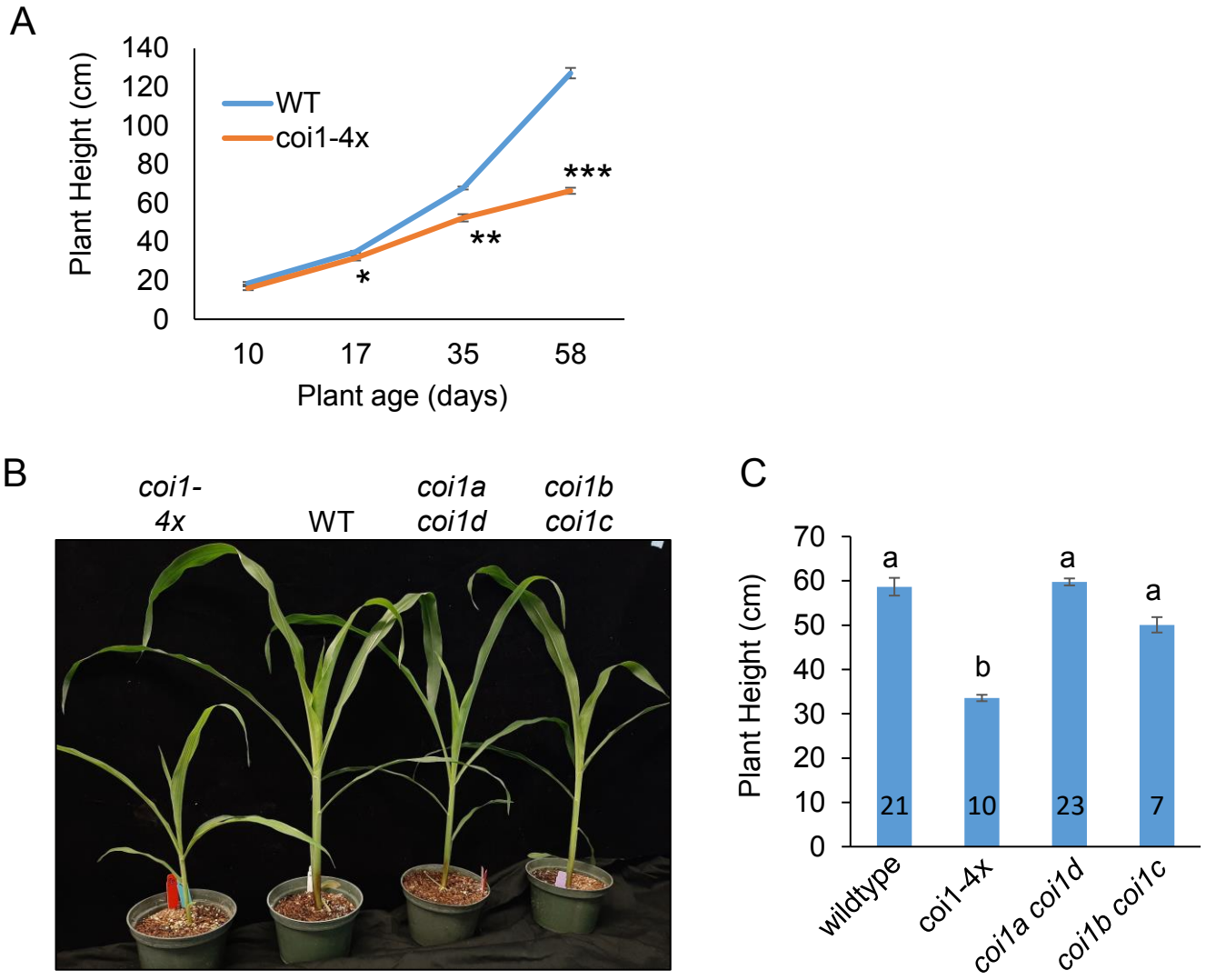

Figure S10. In support of Figure 5. Growth phenotypes of *coi1-4x* compared to wild type and double mutants. Phenotypic comparisons between the *coronatine insensitive1* (*coi1*) quadruple mutant (*coi1-4x*) and the corresponding double mutants, *coi1a coi1d* and *coi1b coi1c*, and wildtype W22 (WT). (A) plant heights were compared between *coi1-4x* and wildtype at the indicated ages. N =10 plants at 10, 17, and 35 days, and N= 6 plants at 58 days. Student's *t*-test, $*P < 0.05$, $** P < 0.01$, $*** P < 0.001$. (B, C) Plant heights at 20 days after germination. Numbers in bars = numbers of plants of each genotype, mean +/− s.e., letters indicate differences $P < 0.05$ using ANOVA followed by Tukey-Kramer test. Raw data and statistical calculations are in Supplementary Dataset S18.

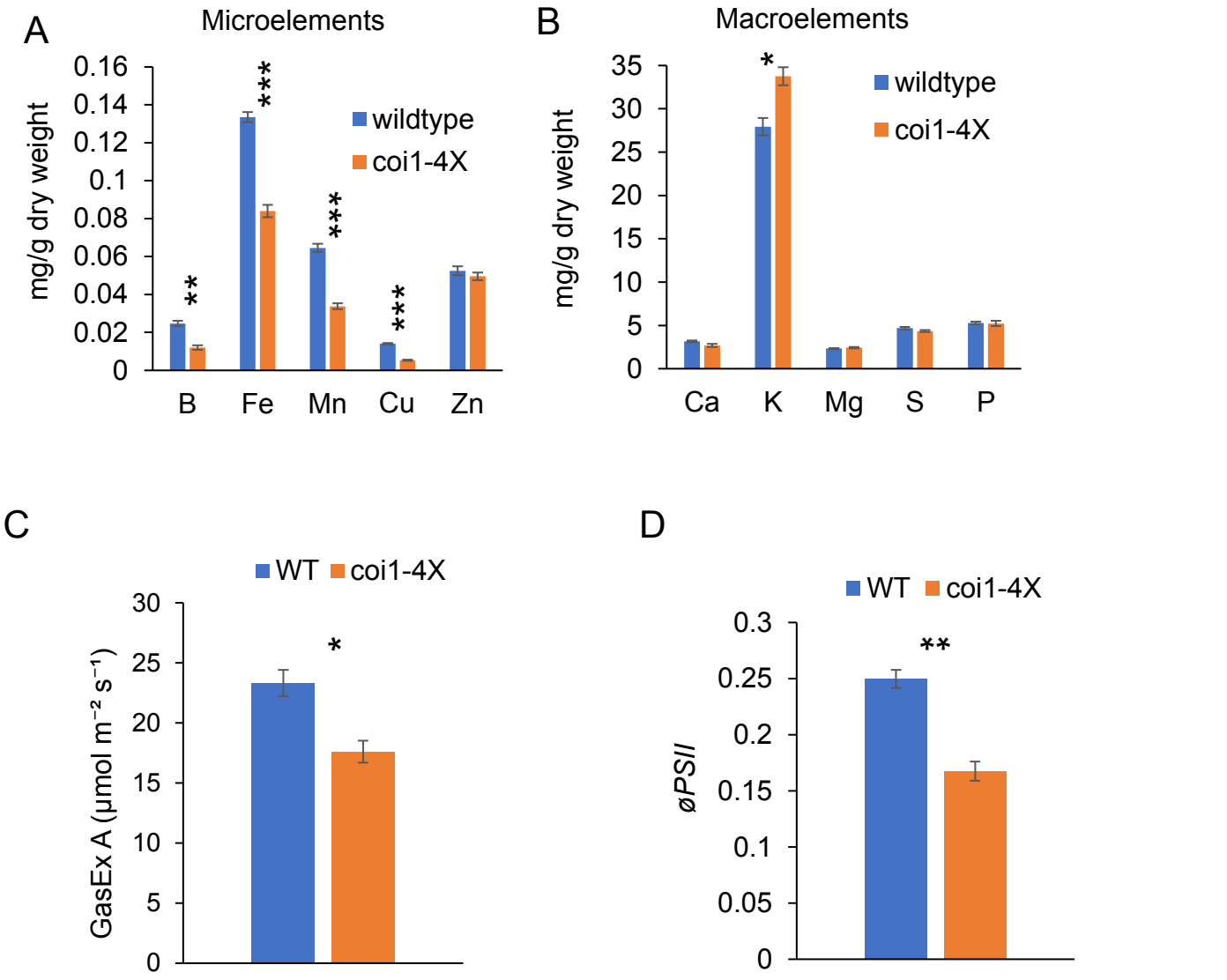

Figure S11. In support of Figure 6. Microelements, macroelements, and photosynthesis assays. (A) Microelements and (B) macroelements in 13-day-old seedlings of *coronatine insensitive1* (*coi1*) quadruple mutant (*coi1-4x*) and wildtype W22 plants, N = 5 plants, mean +/- s.e., Student's *t*-test with (* $P<0.05$, ** $P<0.01$, *** $P<0.001$). Macro and micronutrients were measured in dried tissue of the third leave by inductively coupled plasma - atomic absorption emission spectroscopy (ICP-AES). (C) Leaf CO_2 assimilation rate (GasEX A) at 400 µmol mol^{-1} CO_2 and (D) the quantum yield of the photosystem II phytochemistry (*øPSII*) at 2,000 µmol m^{-2} s^{-1} of actinic light (B) were measured at 28 days after germination, respectively. Mean +/− s.e., n = 5 plants, two-tailed Student's *t*-test , *$P < 0.05$, **$P < 0.01$, ***$P < 0.001$, WT – wildtype. Raw data and statistical calculations are in Supplementary Dataset S18.

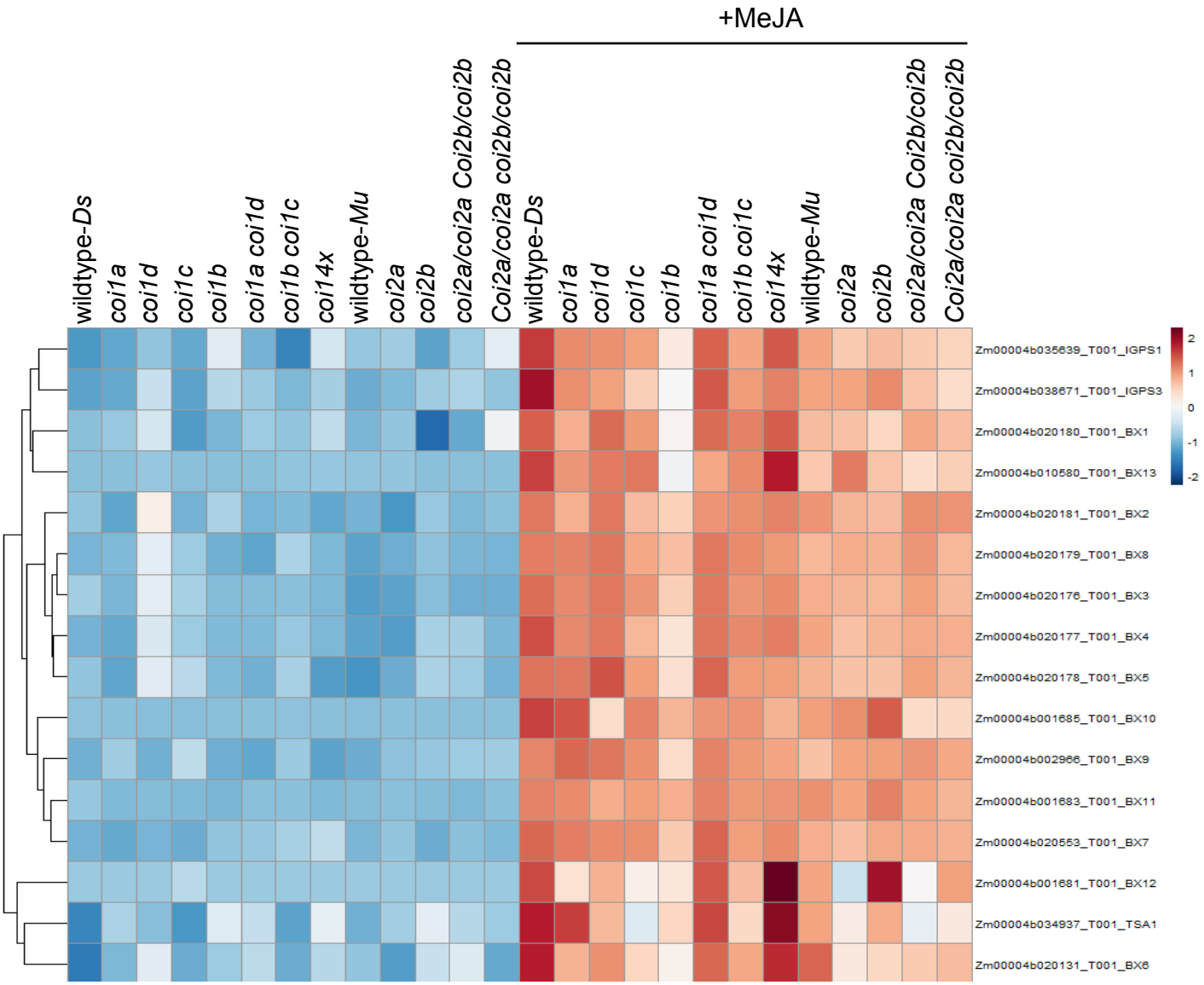

Figure S12. In support of Figure 7. Heatmap showing expression of the benzoxazinoid biosynthesis genes, with and without methyl jasmonate (MeJA) induction. The expression levels of the genes used in this heatmap are presented in Supplementary Dataset S10. Reads per million (RPM) data were transformed by log(1+RPM) prior to clustering. The color gradient in the heatmap reflects the Z scores, with red colors indicating higher-than-average expression levels (Z score > 0) and blue colors indicating lower-than-average expression levels (Z score < 0).

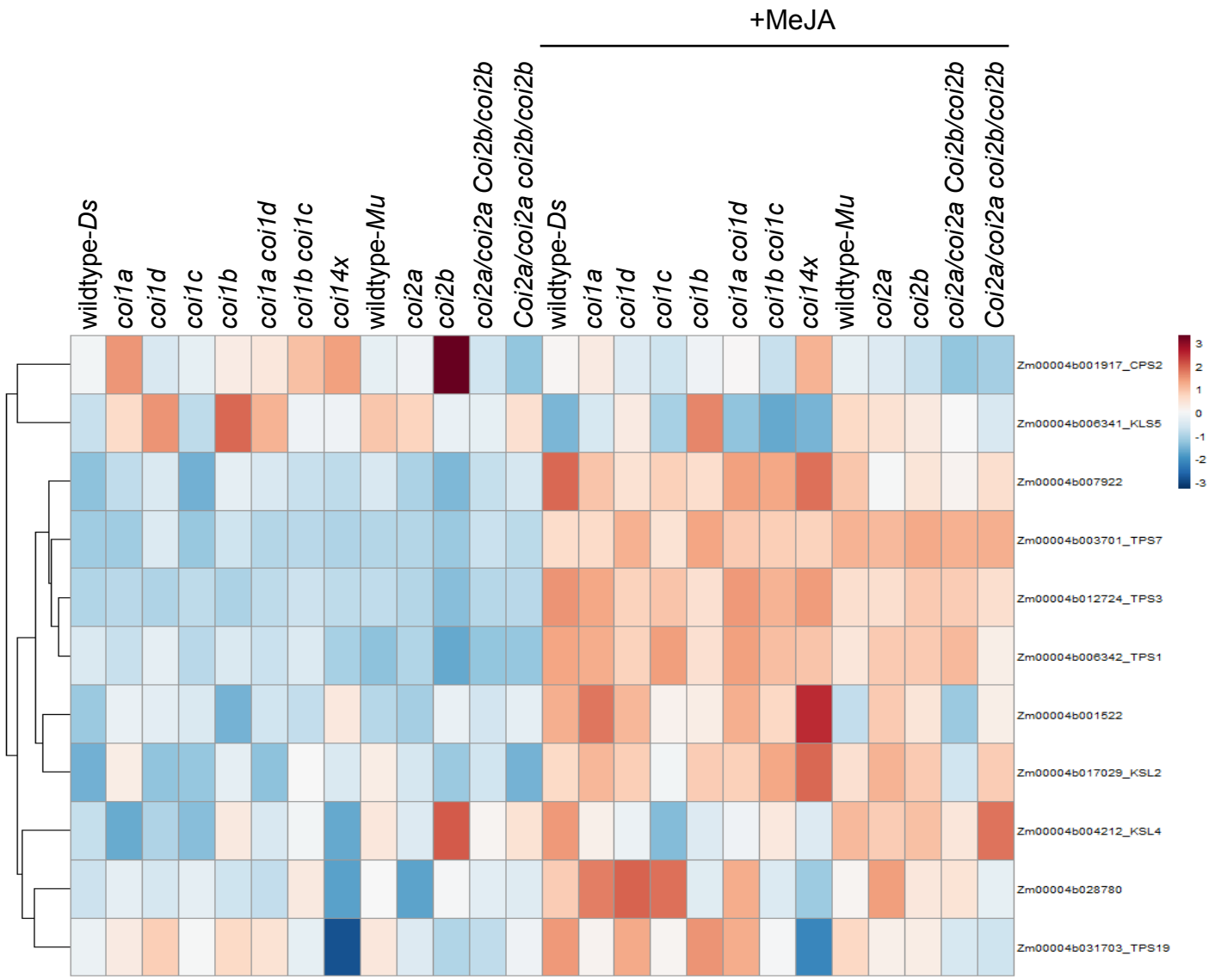

Figure S13. In support of Figure 7. Heatmap showing expression of the terpene synthase genes, with and without methyl jasmonate (MeJA) induction. The expression levels of the genes used in this heatmap are presented in Supplementary Dataset S11. Reads per million (RPM) data were transformed by log(1+RPM) prior to clustering. The color gradient in the heatmap reflects the Z scores, with red colors indicating higher-than-average expression levels (Z score > 0) and blue colors indicating lower-than-average expression levels (Z score < 0).

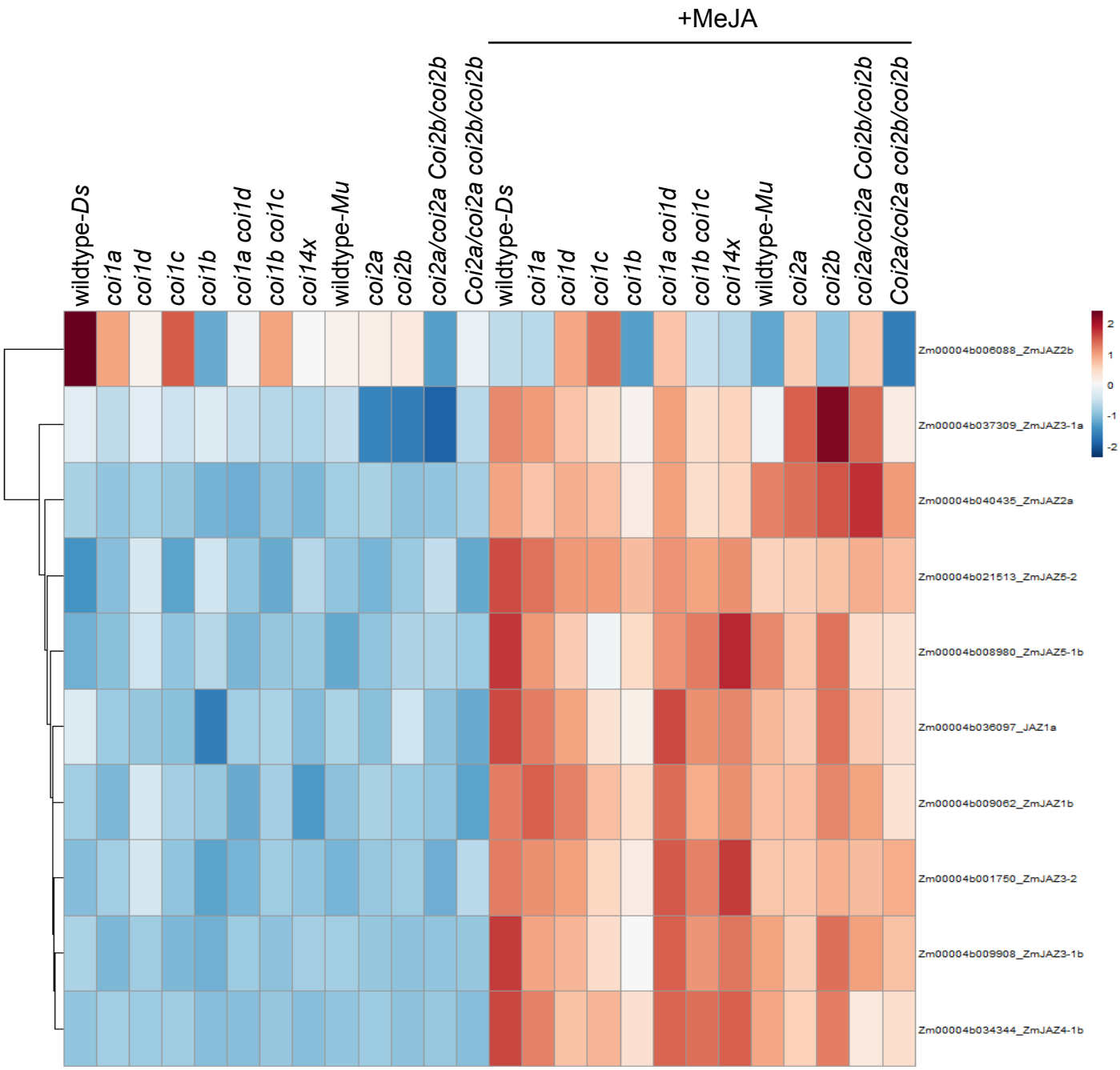

Figure S14. In support of Figure 7. Heatmap showing expression of the maize *Jaz* genes, with and without methyl jasmonate (MeJA) induction. The expression levels of the genes used in this heatmap are presented in Supplementary Dataset S12. Reads per million (RPM) data were transformed by log(1+RPM) prior to clustering. The color gradient in the heatmap reflects the Z scores, with red colors indicating higher-than-average expression levels (Z score > 0) and blue colors indicating lower-than-average expression levels (Z score < 0).

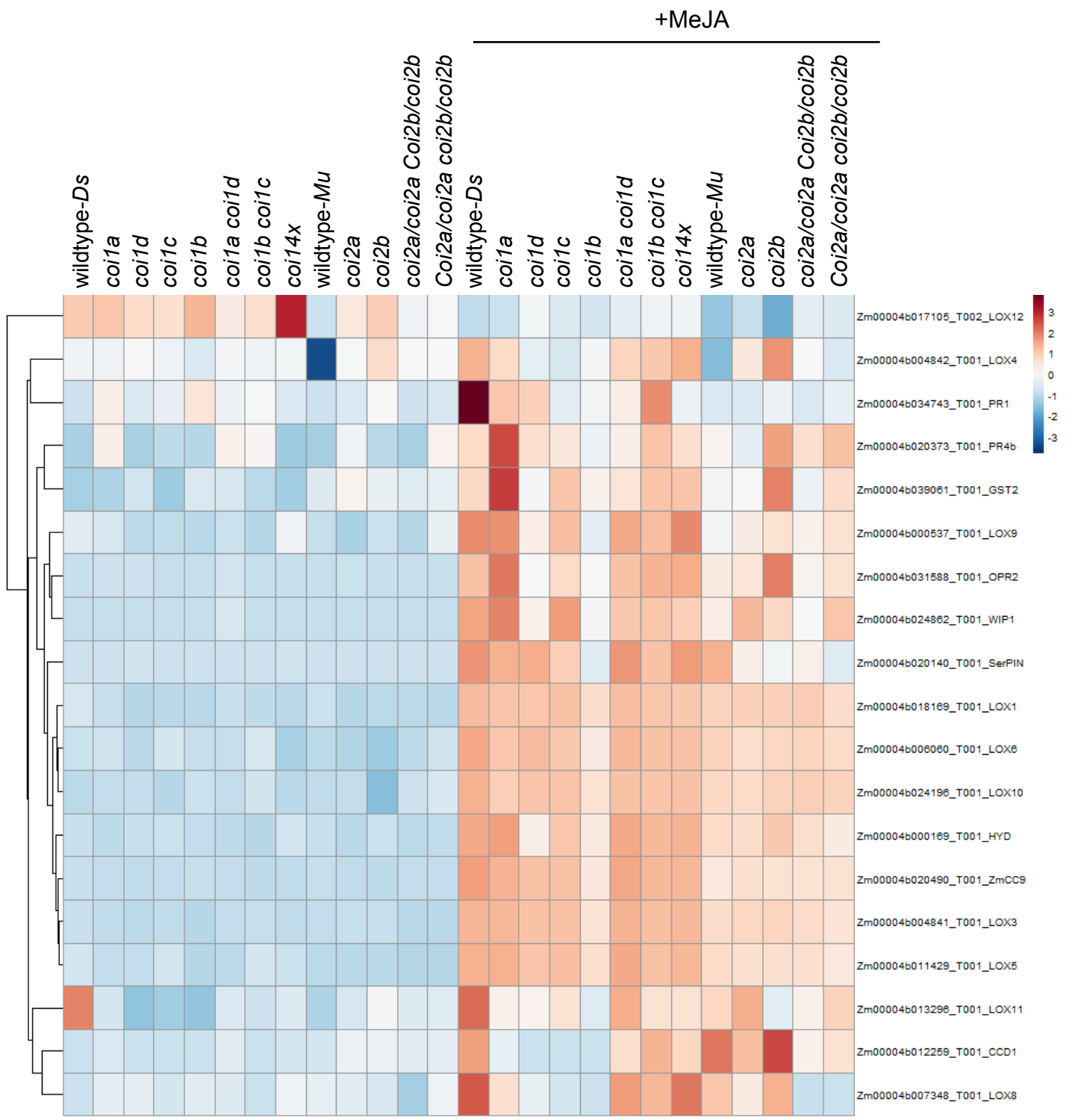

Figure S15. In support of Figure 7. Heatmap showing expression of defense and lipoxygenase (*Lox*) genes studied by Christensen et al. (2015), with and without methyl jasmonate (MeJA) induction. The expression levels of the genes used in this heatmap are presented in Supplementary Dataset S13. Reads per million (RPM) data were transformed by log(1+RPM) prior to clustering. The color gradient in the heatmap reflects the Z scores, with red colors indicating higher-than-average expression levels (Z score > 0) and blue colors indicating lower-than-average expression levels (Z score < 0).

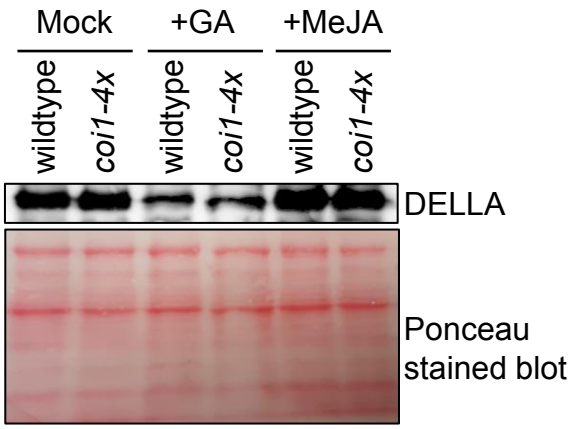

Figure S16. In support of Figure 10. DELLA protein levels decrease and increase after treatment of five-day-old seedlings with GA and MeJA, respectively. Immunoblot analyses of the maize DELLA proteins after treatment of the 5-day-old seedlings germinated in CYG germination pouches, with gibberellic acid (GA) and methyl jasmonate (MeJA) for two days. The leaf total proteins from equal surface area (similar weight) of *coi1-4x* and wildtype inbred line W22 leaves were analyzed by probing with the rice DELLA (SLENDER RICE1 (SLR1)) antibodies. The membrane was stained with Ponceau S as the loading control.

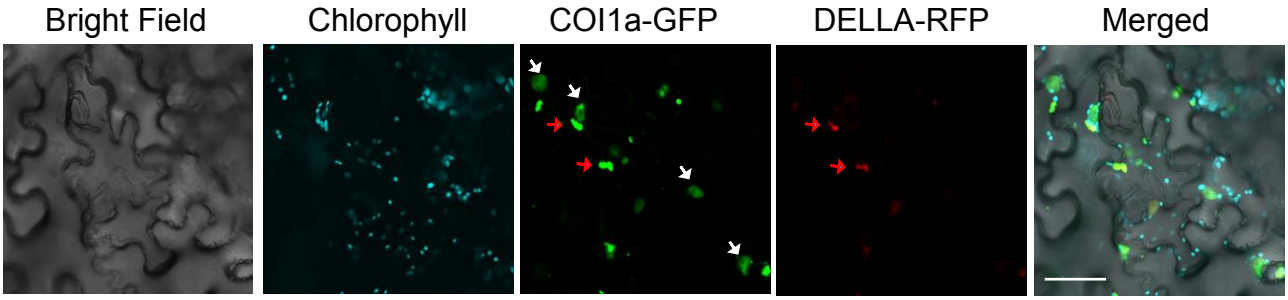

Figure S17. In support of Figure 11. Co-localization of DELLA-RFP and COI1a-EGFP in cytosolic condensates. Whereas the co-expression of the DELLA-RFP with COI1a-EGFP leads to the disappearance of nuclear-localized DELLA-RFP (Figure 11), the cytosol-localized DELLA-RFP is detectable. White and red arrows represent the nuclei and the cytosolic condensates, respectively. Scale bar = 50 μm. RFP = red fluorescent protein. GFP = green fluorescent protein. EGFP = enhanced green fluorescent protein.